METHODS OF NEUTRON FLUX DETERMINATION BY MEANS OF ORGANIC SCINTILLATOR IN NEUTRON-GAMMA RAY MIXED FIELD.

在中子-丫射線混合場中，用有机閃爍体測量中子通量的方法.

by

CHAN CHI-MING

陳志明

A Thesis submitted in Partial Fulfillment
of the Requirements for the Degree of
Master of Philosophy in Physics

The Chinese University of Hong Kong

May 1987

< TABLE OF CONTENTS >

page

Acknowledgements i

Abstract ii

Chapter 1

Introduction to Dosimetry

1.1 Activity 1

1.2 Dose 2

1.3 Dose Equivalent 7

1.4 Maximum Permissible Dose 13

Chapter 2

Introduction to Neutron Detectors

2.1 Introduction 15

2.2 Proportional Counters 16

2.3 Inorganic Scintillation Detector 19

2.4 Organic Scintillator 23

Chapter 3

Gamma Spectroscopy by NaI(Tl) Scintillation Detectors

3.1 Introduction 26

3.2 Data Smoothing 27

3.3 Peak Locating 29

3.4 Base Line Construction and Peak Area Calculation 35

3.5 Overlapping Peaks Treatment-Gaussians Fitting 37

Chapter 4

Neutron Flux and Dose Determination by Liquid Scintillator

4.1 Pulse Shape Discrimination (PSD) and Experimental Set Up 44

4.2 The Differentiation Unfolding Method for Neutron Spectroscopy 50

4.3 The Computer Program for Spectrum Unfolding 55

4.4 Modification on Neutron Spectrum Unfolding 61

Chapter 5

Neutron Spectroscopy By Subtracting Gamma-Ray Contribution

5.1 The Idea of Gamma-Ray Contribution Subtraction 73

5.2 Schemes of Gamma-Ray Response Construction 77

5.3 Scaling of Compton Distribution 81

5.4 The Fitting of Compton Distribution 84

5.5 Normalization of Counts 90

5.6 4.43 MeV Gamma-Ray Response for Plastic Scintillator 94

5.7 The Program of GSI Method for Plastic Scintillator 95

Chapter 6

Arrangements for Neutron Monitoring in a Neutron Generator Room

6.1 Construction of the Neutron Generator Room 107

6.2 The BF_3 Flux Monitor 108

6.3 Monitoring for Am-Be Source 112

6.4 Monitoring for Neutron Generator 112

Chapter 7

Results and Discussion

7.1 Performance of Liquid Scintillation Detector 114

7.2 The Performance of Plastic Scintillation Detector 123

7.3 Flux and Dose from Am-Be 129

7.4 The Neutron Flux and Fast Neutron Dose in Source Room When Neutron Generator is in Operation 132

Chapter 8

Conclusion 137

Appendix A
Cubic Spline
Interpolation 139

Reference 142

ACKNOWLEDGEMENTS

This thesis is not only done by my own effort, but entitled to the contribution of some others. The first of these is Dr. L. S. Chuang, my supervisor, who awakened me of a topic which draws the whole of my interest.

The second I am specially indebted to is Mr. K.S. Sin whose substantial technical assistance, if destitute of, would pose disastrous obstacles to the accomplishment of this thesis.

I have also profited from the earlier achievement of Mr. P.W. Li. His work on the computerization of a scintillation detector system has given me great advantages in performing experiment.

ABSTRACT

A computer program was written to unfold the neutron spectrum, by means of pulse shape discrimination (PSD) method, from the output of a liquid scintillation detector by differentiation method. A computer flow-chart is given.

Besides, a fast neutron spectrometer which utilizes the plastic scnitillator was also constructed. The gamma-ray contribution in the output of the detector was calculated from the gamma-ray response functions which were interpolated from the gamma-ray response functions of monoenergetic gamma-ray sources. Instead of the PSD, the neutron induced counts were obtained by subtracting the gamma-ray contribution from the raw output of the scintillation detector. A detail exposition of the interpolation method is given.

The dose-rate was calculated according to the neutron spectrum in the above cases.

The neutron flux and dose distribution in the neutron-generator room installed in the Chinese University of H.K. was measured by the above scintillation detectors and a paraffin covered BF_3 counter. Highly nonuniform dose distribution was detected when the neutron generator installed inside the

shielding house was in operation. The dose-rate due to the neutrons emmited from an isotope Am-Be source was also measured. The results at various locations are presented with some of them discussed in view of safty involved.

CHAPTER 1
INTRODUCTION TO DOSIMETRY

Three important quantities involved in radiation protection are activity, dose and dose equivalent.

1.1 ACTIVITY

The activity of a radiation source is defined by the number of disintergations per unit time. The historical unit of activity is Curie(Ci). One Curie, which is an estimated activity of one gram of pure Ra226 in equilibrium with its daughters, introduced in 1910 by the International Congress on Radiology and Electricity, is defined as 3.7×10^{10} disintergrations per second.

Curie is a large unit in the laboratory scale. In practice, in order to make compromise in safety and efficency, the activity in the order of milli Curie is always sufficient in general usage. One milli Curie (mCi) is 1×10^{-3} Curie.

The SI unit of activity, Becquerel(Bq), was adopted as the standard unit in 1975 by the General Conference of Weights and Measures. One Bq is defined as one disintergration per second.

Thus 1 Curie = 3.7×10^{10} Bq.

As milli curie and microcurie are more suitabe in scale than Curie, the kilo Bq and mega Bq are the more convenient unit than Bq.

In practice, the term 'activity' is always referred to the detectable particles (including photon) emitted from the source. For example, when we talk about the gamma activity of Na22, we often refer to the total photons coming from the source per unit time. Both 1.2745 Mev and 0.511 Mev photons are included in this case, although the 0.511 Mev photons are the annihiation radiation from positron.

1.2 DOSE

Compared with activity, the charge induced and energy absorbed in media , called exposure and absorbed dose respectively, relate to the radiation effect more directly.

Exposure means amount of radiation. It is defined in term of the charge induced per unit mass of air. The unit of exposure is Roentgen(R). One Roentgen is defined as the exposure due to x-rays or gamma rays radiation in 1 cm^3 of dry air, at standard temperature and pressure, generating a total charge of one esu of either sign.<1>

The fluence-exposure conversion factor of photon in $R/photon/cm^2$ for air is plotted in figure 1.1.<2>

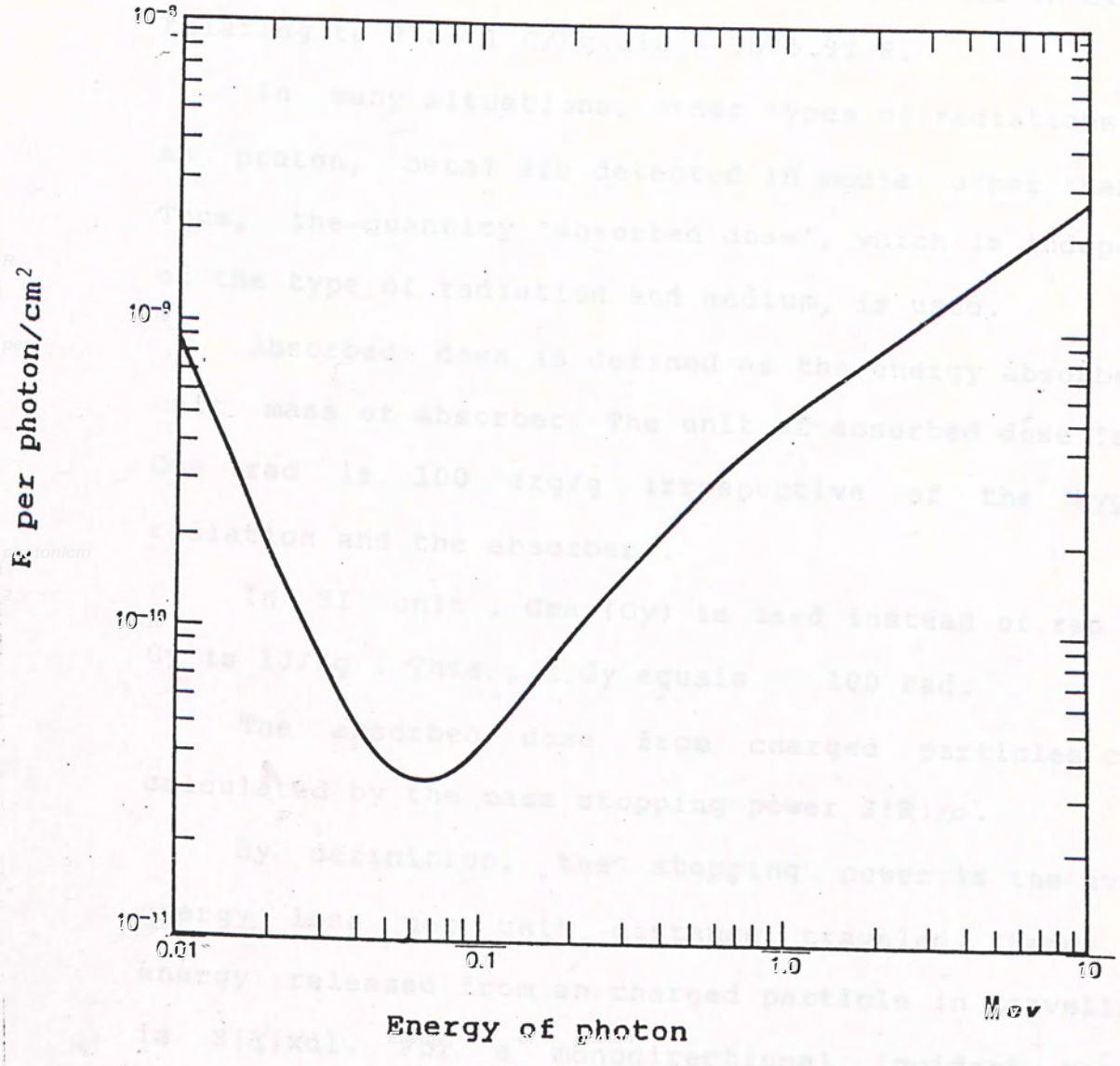

Figure 1.1 The fluence-exposure conversion factor of photon for air. (REF. 2)

Since exposure is defined in terms of charge, it can be measured by ionization chambers.

Exposure is defined by C per Kg in air in SI unit, relating to R as 1 C/Kg air = 3875.97 R.

In many situations, other types of radiations (such as proton, beta) are detected in media other than air. Thus, the quantity 'absorbed dose', which is independent of the type of radiation and medium, is used.

Absorbed dose is defined as the energy absorbed per unit mass of absorber. The unit of absorbed dose is rad. One rad is 100 erg/g irrespective of the types of radiation and the absorber .

In SI unit , Gray(Gy) is used instead of rad . One Gy is 1J/Kg . Thus , 1 Gy equals 100 rad.

The absorbed dose from charged particles can be calculated by the mass stopping power $S(E)/\rho$.

By definition, the stopping power is the average energy loss per unit distance traveled. Hence, the energy released from an charged particle in traveling dl is S(E)xdl. For a monodirectional incident beam of fluence spectrum F(r,E), the absorbed dose at a certain point r is:

$$D(r) = \frac{S(E)xdlxnumber\ of\ charged\ particles\ entering\ dA}{\rho xdAxdl}$$

$$= \frac{S(E)xdlx(F(r,E)xdAxdE)}{\rho xdAxdl}$$

$$= \frac{S(E)}{\rho} \times F(r,E) \times dE$$

The equations for calculating the stopping power of charged particles can be found in ref.1 p.118-119.

However, the absorbed dose can be estimated from the exposure when only the energy loss due to ionization is important, it is:

D = average energy reqired to create an ion pair x number of ions pairs created per unit charge x charge induced per unit mass

= average energy reqired to creat an ion pair x number of ions pairs created per unit charge x exposure

For example, if the exposure in air is N Roentgens, the corresponding absorbed dose D can be calculated as:

As the average energy required to create an ion pair is 34 ev, and the number of ion pairs created per unit charge (e) is 1, we have D = 34 x 1 x 2.58×10^{-4} J/Kg = 8.8 N mGy.

Moreover, the exposure of gamma rays with energy between 70keV and 2MeV can be approximated by[3]:

$$\text{exposure} = 0.5xE/d^2 \text{ R } h^{-1} \text{ Ci}^{-1}$$

Where E is the gamma energy in MeV and d is the distance between the source and the point of measurement in metres.

The number of incident particles and photons per cm^2 to produce one rad in soft tissue is plotted in Figure 1.2.[4]

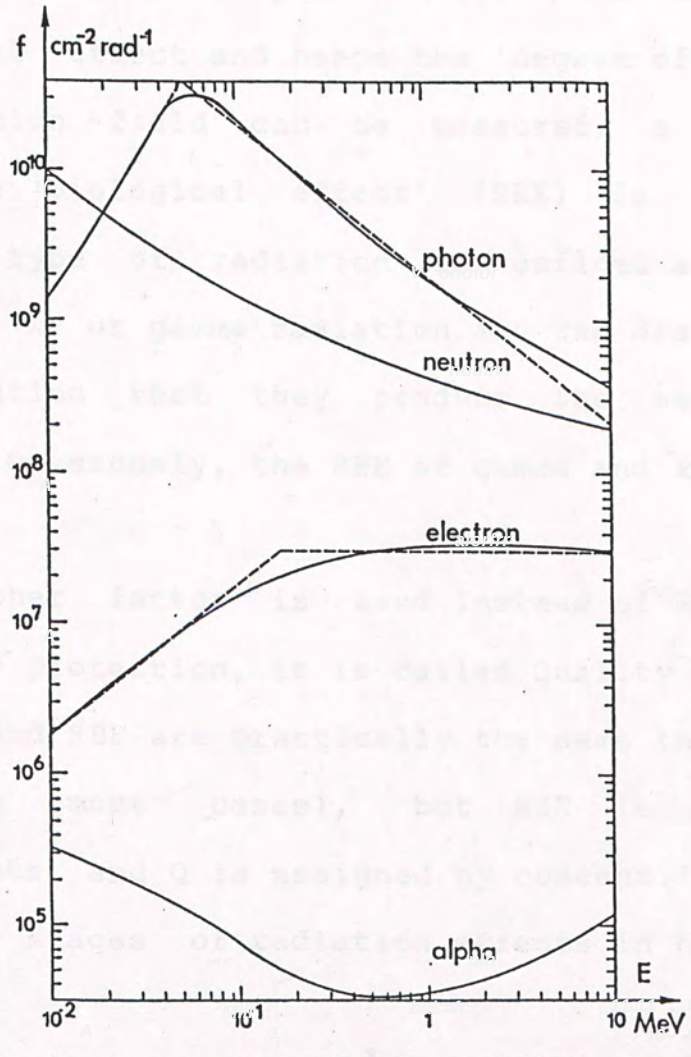

Figure 1.2 Number of incident particles and photons per cm^2 to produce 1 rad in soft tissue.(Ref.4)

1.3 DOSE EQUIVALENT

Although exposure and absorbed dose are well defined physically, they are insufficient to indicate the radiation hazard to man. Macroscopically, biological effect of radiation depends on:

1. the energy deposited in tissue,

2. the type of reaction between incident radiation and tissue, and

3. the organ irradiated.

In other words, it depends on the organ of man and the type of radiation other than the absorbed dose.

In order to operationalize the calculation of biological effect and hence the 'degree of danger ' in a radiation field can be measured, a factor called 'relative biological effect' (RBE) is used. RBE of a certain type of radiation is defined as the ratio of dose of x- or gamma radiation and the dose of that type of radiation that they produce the same biological effect. Obverously, the RBE of gamma and x- radiation is one.

Another factor is used instead of RBE nowadays in radiation protection, it is called Quality factor (Q).

Q and RBE are practically the same (numerically the same in most cases), but RBE is determined by experiments and Q is assigned by concept.[5]

The stages of radiation effects in human organ are

shown in figure 1.3 for reference.[6] The Quality factors for severl types of radiations can be found in Table 1.1.[7] The Quality factor of neutron is plotted in Figure 1.4[8].

TABLE 1.1 QUALITY FACTOR FOR SEVERAL TYPES OF RADIATION

Radiation type	Q
Gamma rays	1
X-rays	1
Beta particles	1
Positrons	1
Proton (< 11 MeV)	10
Alpha partcles (< 10 MeV)	20
Recoil nuclei (A > 4)	20

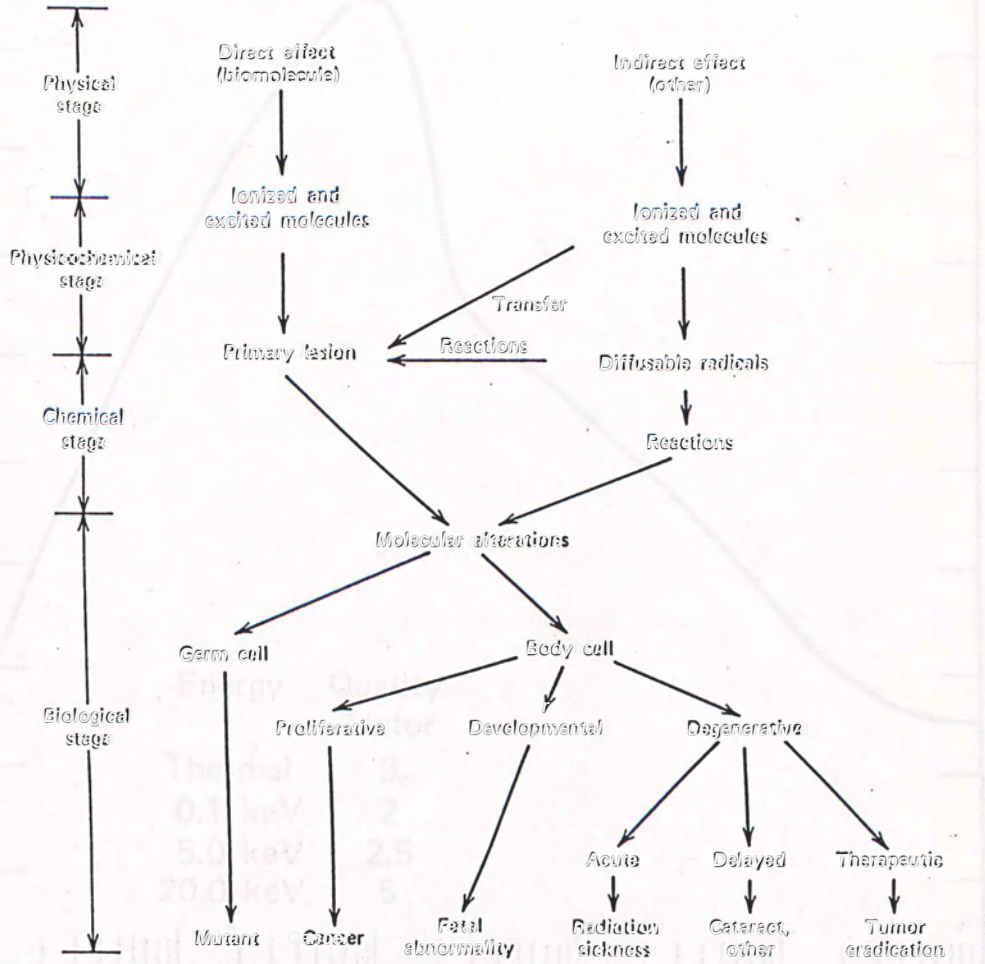

Figure 1.3 Stages of radiation effects in organisms.(Ref.6)

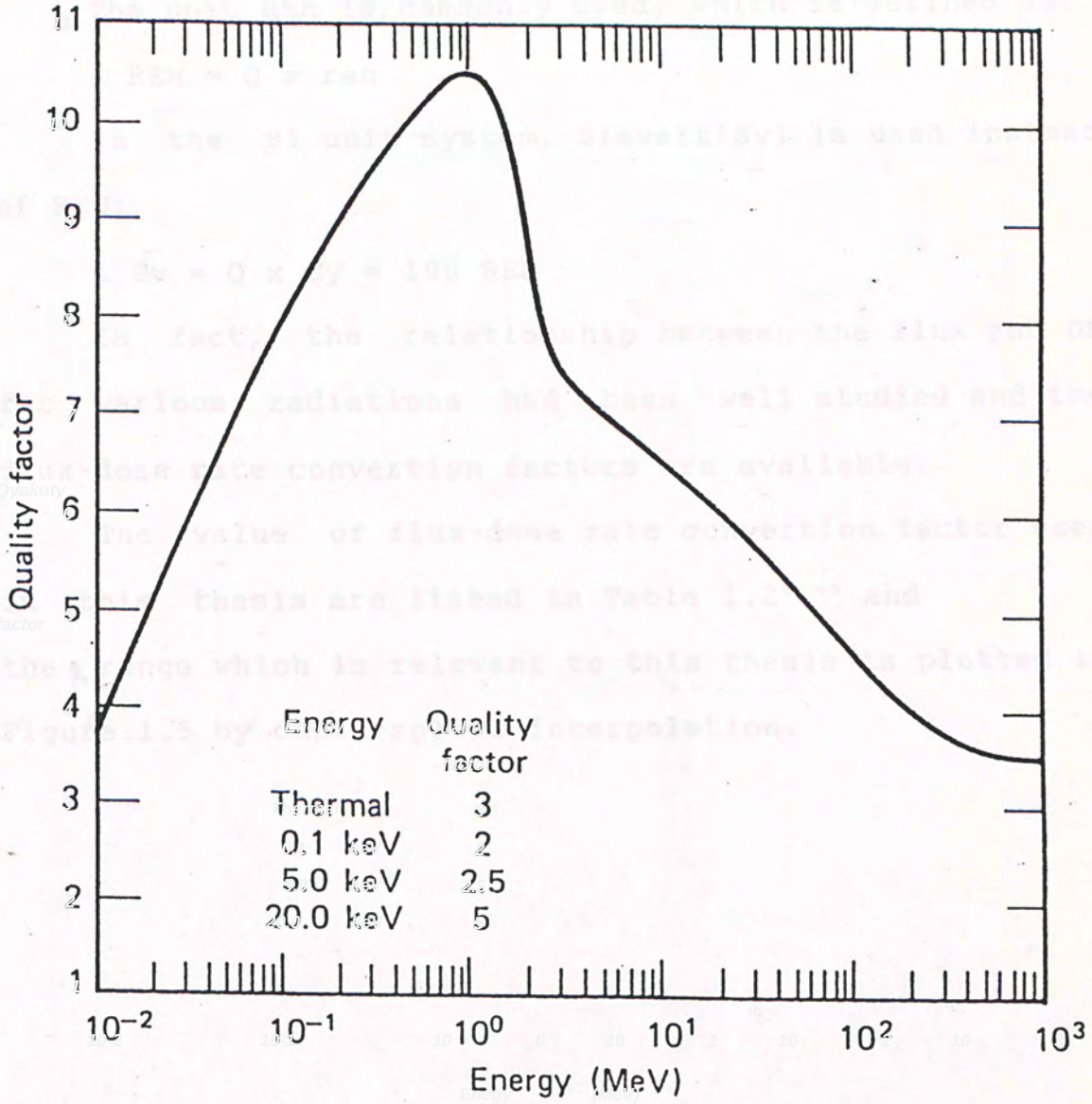

Figure 1.4 Quality factor for neutrons. (Ref.8)

Dose equivalent is simply the product of Absorbed Dose and Quality factor: Dose equivalent(DE) = D x Q.

The unit REM is commonly used, which is defined as:

1 REM = Q x rad

In the SI unit system, Sievert(Sv) is used instead of REM:

1 Sv = Q x Gy = 100 REM

In fact, the relationship between the flux and DE for various radiations had been well studied and the flux-dose rate convertion factors are available.

The value of flux-dose rate convertion factor used in this thesis are listed in Table 1.2[9] and the range which is relevant to this thesis is plotted in Figure 1.5 by cubic-spline interpolation.

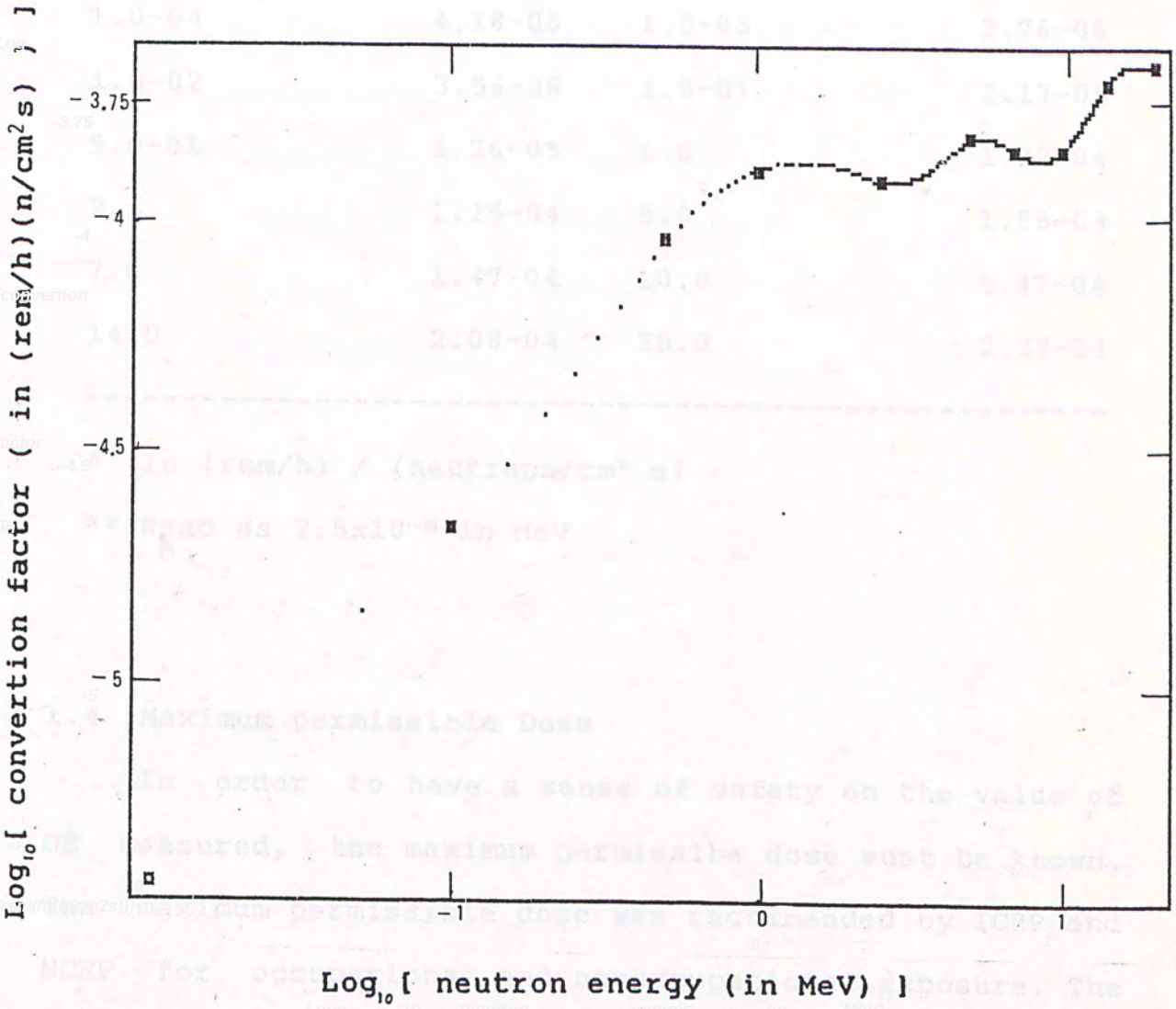

Figure 1.5 The flux-dose rate convertion factor. The curve is obtained by cubic spline interpolation. The points show the data from ref. (9).

TABLE 1.2 Neutron flux to dose rate factors

Neutron energy	factor	Neutron energy	factor
2.5-08	3.67-06	1.0-07	3.67-06
1.0-06	4.46-06	1.0-05	4.54-06
1.0-04	4.18-06	1.0-03	3.76-06
1.0-02	3.56-06	1.0-01	2.17-05
5.0-01	9.26-05	1.0	1.32-04
2.5	1.25-04	5.0	1.56-04
7.0	1.47-04	10.0	1.47-04
14.0	2.08-04	20.0	2.27-04

* In (rem/h) / (neutrons/cm^2 s)

** Read as 2.5x10^{-8} in MeV

1.4 Maximum permissible Dose

In order to have a sense of safety on the value of DE measured, the maximum permissibe dose must be known. The maximum permissible dose was recommended by ICRP and NCRP for occupational and nonoccupational exposure. The standard is summarized in Table 1.3.[10] Occupational exposure is based on 8 working hour per day and 40 working hour per week.

TABLE 1.3 MAXIMUM PERMISSIBLE DOSE

Organ	REM / YEAR
A. Occupation exposure	
1. Whole body; head and trunk, active blood-forming organs, lens of eye, or gonads	5*
2. Hands and forearms, feet, ankles	75
3. Skin of whole body	30
B. Nonoccupational exposure	
1. Whole body	0.5
2. Skin, thyroid	1.5
3. Bone	0.1 of occupational

* not to exceed 3 rem per calender quarter, fertile women should be exposed to less than 0.5 rem in gestation period.

CHAPTER 2
INTRODUCTION TO NEUTRON DETECTORS

2.1 INTRODUCTION

Since neutron don't directly ionize atoms, they are detected by the charged partcles or photons which are the products of reactions between neutron and nucleus.

If the mechanism of reaction is known, certain information can be extracted from this indirect measurement. In fact, the amount of obtainable information (flux, energy spectrum, distribution etc.) is limited by the type of reaction and the products to be detected. This raise many problems in neutron detection.

Obviously, counting efficiency depends on the cross section of reaction that the detectable products can be formed. Hence, the efficiency varies for different neutron energy. Thus, different types of detector performs different purpose.

In measuring neutron energy spectrum , the signal measured is only the message from the product of neutron-nucleus reaction. The recorded signal spectrum must be unfolded to obtain the original neutron spectrum. Many unfolding codes had been established today.

The properties of some commonly used neutron detectors are summarized here. The passive method (neutron activation, threshold detector), moderator detectors, ionization chamber and time-of-flight method are not included. However, Firk had given a comprehensive review for time-of-flight spectometers.[11]

Moderator detector detects neutrons after moderation by proportional counter, inorganic scintillator or neutron activiation method. A short introduction about moderator detectors can be found in ref. 12.

Only the basic properties of detectors are described below. The detailed measurement techniques can be found from a brief and well organized introduction in ref. 35.

2.2 PROPORTIONAL COUNTERS

2.2.1 BF_3 counter [13][14]

Basic reaction: $^{10}_{5}B + n \rightarrow {}^{4}_{2}He + {}^{7}_{3}Li + 2.78$ MeV

Particles to be detected: Alpha, $^{7}_{3}Li$

advantages: 1. The gamma discrimination property is good.

2. Reaction cross section with thermal neutron is large.

3. The reaction cross section is a function of energy following 1/v variation.

Application: Thermal neutron detection

Sensitivity: 0.3c/s per n/cm² s for counters with diameter 2.5 cm and active length 12cm. 1.5c/s per n/cm² s can be achived when Boron10 is enriched to 90%.

Remarks:

1. The wall effect exist. It is caused from partial energy deposition of Li and Alpha particles which are produced near the wall. There are two methods to suppress the wall effect, namely, 1) enlarge the diameter, 2) increasing the gas pressure such that the range of charged particles are shortened.

2. A BF_3 counter with a Cadmium coating can be used to measure the dose rate from intermediate energy neutrons.

FIGURE 2.1 is a typical spectrum from a BF_3 counter.

2.2.2 He counter [18]

Basic reaction: $^{3}_{2}He + n \rightarrow {}^{1}_{1}H + {}^{3}_{1}H + 765$ KeV

Particles to be detected: proton, triton

Advantages: 1. Gamma discrimination power is good but not as good as a BF_3 counter.

2. The reaction cross section for thermal

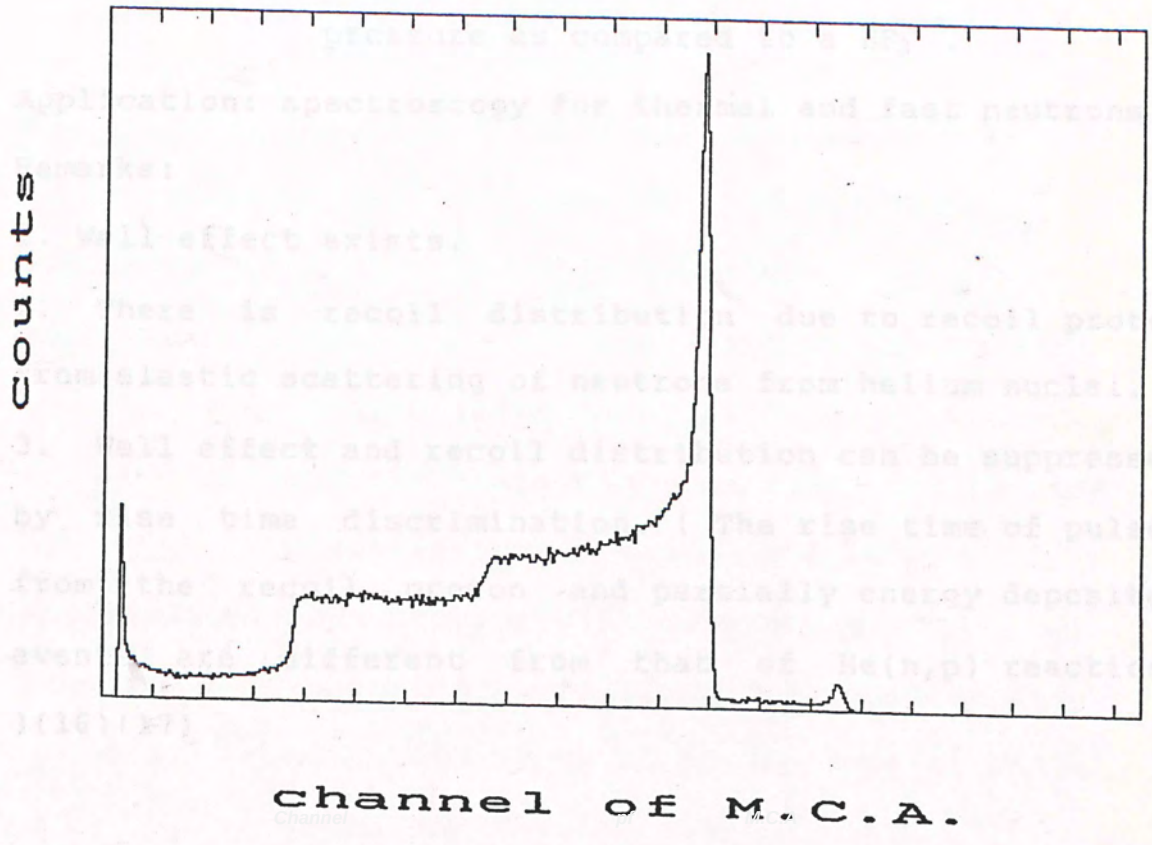

Figure 2.1 A typical spectrum from a BF_3 counter.

neutrons is large.

3. The reaction cross section varies as 1/v from 0.001ev to 0.04ev.

4. It can be operated with higher gas pressure as compared to a BF_3 .

Application: spectroscopy for thermal and fast neutrons

Remarks:

1. Wall effect exists.

2. There is recoil distribution due to recoil proton from elastic scattering of neutrons from helium nuclei.

3. Wall effect and recoil distribution can be suppressed by rise time discrimination. (The rise time of pulses from the recoil proton and partially energy deposited events are different from that of He(n,p) reaction.)(16)(17)

2.3 INORGANIC SCINTILLATION DETECTOR

2.3.1 Zinc Sulphide + hydrogeneous material

Basic reaction: Elastic scattering of fast neutrons from hydrogen nuclei

Particles to be detected: Recoil protons

Advantages: Gamma counts can be rejected by pulse height discrimination.

Application: Fast neutron flux monitoring

Sensitivity: Up to 5% for NE451

Remark:

1. Counting efficiency is low compared to a organic scintillator.

2. They are not used in research today.

2.3.2 Zinc Sulphipe + ^{6}Li (LiF mixture)[18]

Basic reaction: $^{6}_{3}Li + n \rightarrow {}^{4}_{2}He + {}^{3}_{1}H + 4.78MeV$

Particles to be detected: Alpha, Triton

Advantages: 1. Gamma sensitivity is very low because the Q-value is high.

2. Pulse shape discrimination may be used for very high gamma intensity.

Application: Slow neutron flux monitoring

Sensitivity: About 25% - 30% for 0.1 ev neutron and 50% - 60% for 0.01 ev neutron for MB421 (^{6}Li enriched to 96%).

Remark:

1. Boron (^{10}B) can be used instead of ^{6}Li.

2. Modification with two layers design was reported.[19] LiF layer is coated on ZnS(Ag) scintillator. The gamma sensitivity is neligible. Since the detector is extremely thin, it is suitable for time-of-flight measurement.

2.3.3 LiI(Eu) Crystal

Basic reaction: For thermal neutron

$$^{6}_{3}Li + n \rightarrow {}^{3}_{1}H + {}^{4}_{2}He + 4.78MeV$$

For fast neutron

$$^{6}_{3}Li + n \rightarrow n' + {}^{2}_{1}H + {}^{4}_{2}He + -1.47MeV$$

Particles to be detected: Alpha, Triton

Advantages: 1. Free of wall effect as the ranges of the charged particles are small in the crystal.

2. The reaction cross section between n in thermal energy range and Li is large.

Application: Thermal neutron flux measurement and fast neutron spectroscopy

Sensitivity: Counting efficiency is larger than 90% for thermal neutron for a 10mm thick crystal.

Remark:

1. Because the range of secondary electrons in crystal is small, it would deposit all of its energy and cause large light output. Hence, the gamma ray discrimination is inferior than the proportional counter.

2. LiI(Eu) must be cooled to liquid nitrogen temperature in fast neutron spectroscopy. Otherwise, the nonlinear response of tritons and alpha particles will severely broaden the respose function. The energy resolution of full-energy peak is about 20% at liquid nitrogen temperature.

3. LiI is not used in fast neutron reseach today.

2.3.4 Li glass scintillation detector :

(Cerium activated silicate glasses)

Basic reaction: $^{6}_{3}Li + n \rightarrow {}^{4}_{2}He + {}^{3}_{1}H + 4.78MeV$

Particles to be detected: Alpha, Triton

Advantages: 1. Cross section is large for low energy neutron.

2. It is inefficient for gamma rays. The high Q-value (4.78MeV) of reaction can produce pulse height larger than that of 1 MeV gamma.

3. Cross section of $^{6}Li(n,\alpha)T$ is in 1/v type for low energy neutron.

4. The decay time of light pulse can be fast as in nanosecond order.

5. Large area detector can easily be fabricated.

Application: Low energy neutron beam monitoring and time-of-flight measurement

Sensitivity: Depends on the concentration of Cerium and Lithum. For example, the efficiency of 1 inch thick NE905 (6.6% Li, enriched in ^{6}Li to 95%) is 19%.[21]

Remark:

1. Li glass scintillator is the most widly used inorganic scintillator in neutron detection.

2. The light output for charged particles is small

compare with electrons. The reaction products with Q-value 4.78MeV only produce light output equivalent to 1.2 MeV gamma ray. Hence, the gamma discrimination power is weaker than many other detectors.

2.4 ORGANIC SCINTILLATOR

The basic theory and applications of the organic scintillators had been well discussed and developed by Birks.[22] Numerous reviews and detail studies (elementary process, light response, light collection, time response etc.) had been reported and published.[23-28]

In practice, the important conditions for organic scintillator used in neutron spectroscopy are:

1. High hydrogen content is needed. Since the recoil protons from n-p scattering are detected in organic scintillator, high hydrogen content can increase the counting efficiency.
2. The cross section of reactions between neutron and nuclei inside the scintillator must be accuratly known. The value of cross section is needed in efficiency calculation and spectrum unfolding.
3. The light output as a function of proton energy

must be known, unless the scintillator is used in the time-of-flight measurement.

4. The decay time of light pulse should be short in time-of-flight measurement(in nano second order) .Pulse shape discrimination property is required to discriminate the gamma background.

The properties of some commercially available organic scintillators are listed in Table 2.1 .[29]

The counting efficiency depends on the type of scintillator, the energy of neutron, the geometry of scintillator and the energy threshold. Many measurements and calculations (usually by Monte Carlo method) had been reported.[30-34]

There are some examples in Table 2.2 .

TABLE 2.1 THE PROPERTIES OF SOME COMMERCIALLY AVAILABLE ORGANIC SCINTILLATORS

Scintillator	Type	Density kg/m	Light output (relative)	Decay-constant for main component micro second	no.of H atoms/ no.of C atoms
anthracene	crystal	1.25	100	30	0.715
stilbene	crystal	1.16	50	4.5	0.858
NE102	plastic	1.032	65	2.4	1.104
NE110	plastic	1.037	46	3.3	1.104
pilot B	plastic	1.032	68	1.8	1.100
pilot Y	plastic	1.032	60	3.1	1.102
NE213	liquid	0.874	78	3.7	1.213
NE224	liquid	0.877	80	2.6	1.33

TABLE 2.2 EFFICIENCY OF SOME ORGANIC SCINTILLATORS

Scintillator	thickness in cm	diameter in cm	neutron energy in MeV	threshold energy in MeV	efficiency %
NE102A	2.5	7.1	9.5	1.0	34.8 [31]
NE102A	2.5	7.1	9.5	4.2	3.9 [31]
NE213	5	12.7	10	2.5	15 [33]
NE213	10	3.8	10	0.81	32 [33]

CHAPTER 3

GAMMA SPECTROSCOPY BY NaI(Tl) SCINTILLATION DETECTORS

3.1 INTRODUCTION

It is necessary to measure the gamma energy and photopeak area (absolute activity would not be reqired) of the pulse height spectrum from NaI(Tl) scintillation detector in measuring the neutron flux, in neutron-gamma ray mixed field, using the method developed in chapter 5. In fact, there are continuous works on gamma spectroscopy. Peak locating and area determination are two basic aims of spectrum analysis.

Two principal methods are used in peak locating. The first one uses the first or second derivative of the pulse height spectrum to locate the peak position. The sign of the first derivative would changes from positive to negative and the second derivative would show a minimum at a peak. The second method fits the data by one or more gaussians. The centroid of the gaussian is considered to be the peak position.

There are also two principal methods to determine the peak area. One of them is to contruct a baseline of the peak by a polynomial. This baseline is a background of the peak, and [illegible] the peak area is obtained by

subtracting the area under the baseline in the peak region from the area under the peak. The other one is to fit the peak by gaussian as well as baseline curve. The peak area is determined analytically.

All these methods except peak locating by second derivative are used in the present work.

The main difficulty of gamma spectroscopy by NaI(Tl) scintillation detector is the poor energy resolution power. Figure 3.1 illustrates the resolution power of NaI(Tl) scintillator and Ge(Li) semiconductor detector.[36]

3.2 DATA SMOOTHING

The signal from NaI(Tl) scintilator is collected with a 1024—channel multichannel analyser (M.C.A) and then sent to a microcomputer.

The data must be smoothed before the peaks are sought. A simple smoothing process is used. Each point of the raw data is approximated by a polynomial which is fitted to 2m points around that point by least square method.[37] The smoothed value at channel i is expressed as :

$$Y_m(i) = (1/K_m) \sum_{k=-m}^{m} C_{k,m}\, y(i+k)$$

Where $y(i+k)$ is the raw counts at channel i+k. $C_{k,m}$ and K_m are constants independent of the spectrum. 2m+1

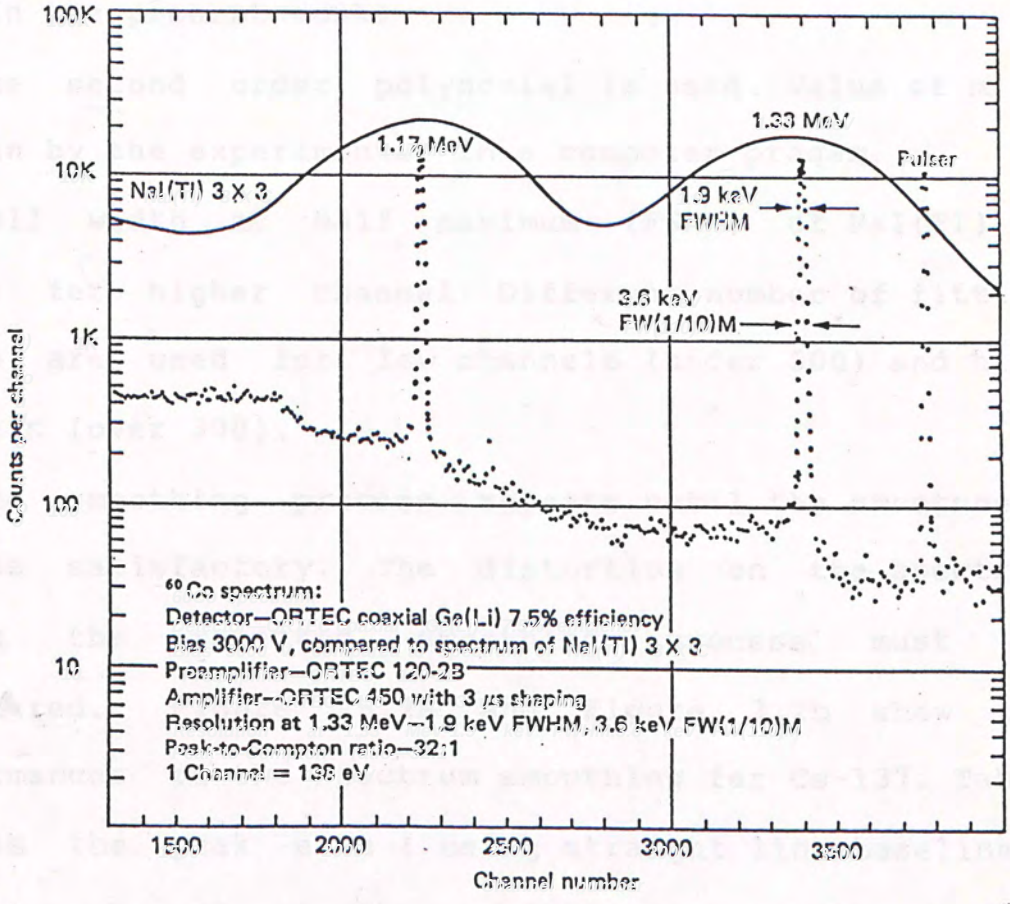

Figure 3.1 The Co-60 spectrum obtained with a NaI(T1) scintillator and a Ge(Li) detector. (Ref.36)

points are used in least square fitting. The value of 2m+1 should be just less than the half width of the peaks.

In the present work:

1. The second order polynomial is used. Value of m is choosen by the experimenter in a computer progam.
2. Full width at half maximum (FWHM) of NaI(Tl) is larger for higher channel. Different number of fitting points are used for low channels (under 300) and high channels (over 300).
3. The smoothing process repeats until the smoothness becomes satisfactory. The distortion on the spectrum during the repeated smoothing process must be considered. Figure 3.2a and Figure 3.2b show the performances of the spectrum smoothing for Cs-137. Table 3.1 is the peak area (using straight line baseline) and the channel of the maximum of the photopeak from Cs-137 after the smoothing process repeats 2, 5, 10 and 20 times. It is found that the distortion on the peak area and peak location is negligiable.

3.3 PEAK LOCATING

The M.C.A is calibrated before the spectrum is analysed. Energy as a function of the channel number is in the form:

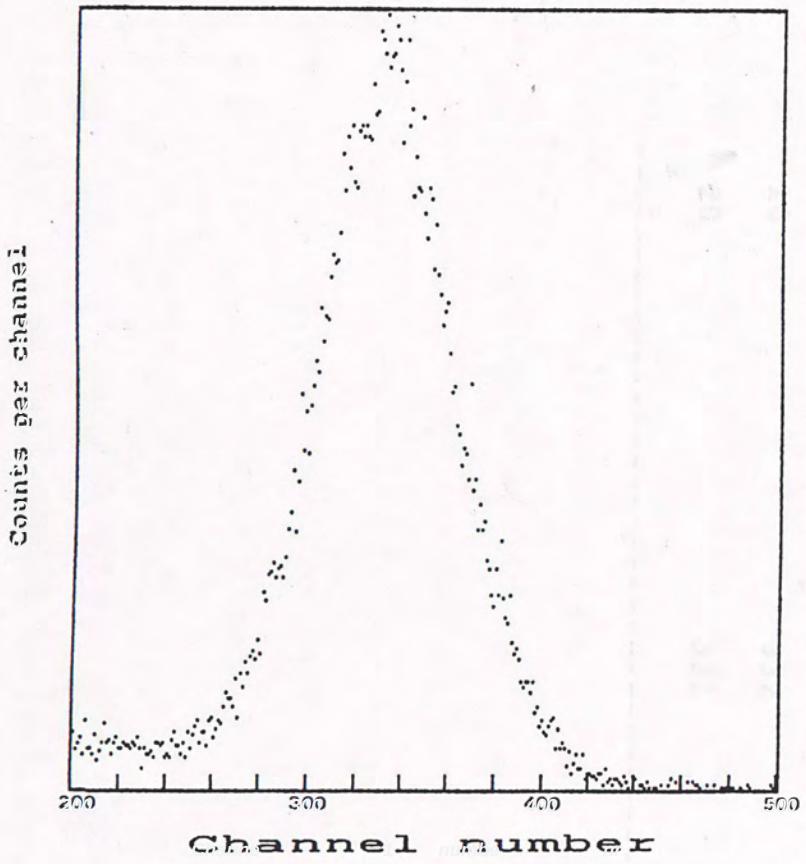

Figure 3.2a The photopeak of Cs-137 detected by a NaI(Ti) scintillator.

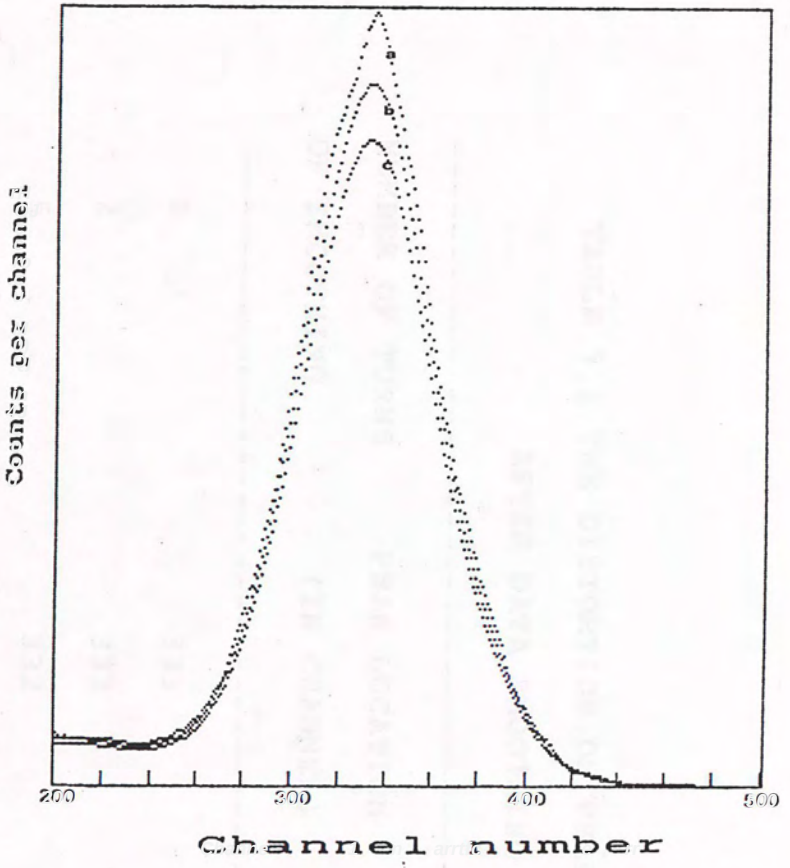

Figure 3.2b The photopeak of Cs-137 after smoothing. Curve a, b, c have been smoothed 2, 10, 20 times, repectively.

TABLE 3.1 THE DISTORTION ON PEAK AREA AFTER DATA SMOOTHING

NUMBER OF TURNS OF SMOOTHING	PEAK LOCATION (IN CHANNEL)	PEAK AREA (IN COUNTS)
1	333	21863
2	333	21680
5	332	21118
10	332	20313
20	331	18733

$$E = a + bC + cC^2$$

Where C is the channel number, a, b, c are constants. These constants are obtained by least square fit on the data of E and C from standard calibration sources. The typical order of C is 10^{-7}.

The peak is located by checking the change of slope channel by channel. If y'(i) is the first derivative at channel i, then channel i is considered to be a peak when:

$$y'(i-3)>0 \ , \ y'(i-2)>0 \ , \ y'(i-1)\geqslant 0,$$

$$y'(i+1)\leqslant 0 \ , \ y'(i+2)<0 \ , \ y'(i+3)<0.$$

The first derivative is calculation by least square method as described in ref.36.

If second order polynomial is used, the first derivative of channel i is:

$$y'(i) = \{ 3/[m(m+1)(2m+1)] \} \sum_{j=-m}^{m} jy(i+j)$$

for 2m+1 points fitting.

Peaks can also be located by checking the maximum counts within the region of interest, but the derivative method would be more accurate. The counts within the region of a peak as a function of the channel number can be approximated as:

$$y(i) = A\,G(p-i) + B + Ci + Di^2 + Ei^3$$

Where G is a Gaussian function centred at channel p and A is the height of the peak. The cubic represent the background. Then:

$$y'(i) = A\,G'(p-i) + C + 2Di + 3Ei^2$$

$$y''(i) = A\,G''(p-i) + 2D + 6Ei$$

The values of C, D and E calculated by nonlinear least square fit described in section 3.4 are found to decrease rapidly. For example, the order of C, D, E for 1.17 and 1.33 MeV peaks of Co-60 is 10^{-1}, 10^{-5} and 10^{-7}, respectively.

It means that the background dependence of derivative is small. The derivative method suppresses the background and gives a more accurate peak location.

The first and second derivatives of Na22 is shown in Figure 3.3.

After the peak is located, the left and right boundaries of the peak are sought. Channel i is the right or left boundary when :

1. $y(i) \leqslant y(i+1)$, $y(i) < y(i+2)$, $y(i) < y(i+3)$

   $y(i) \leqslant y(i-1)$, $y(i) < y(i-2)$, $y(i) < y(i-3)$

or 2. $y'(i-1) \leqslant 0$, $y'(i-2) < 0$

   $y'(i+1) \geqslant 0$, $y'(i+2) > 0$

or 3. $|y'(i)| \leqslant 0.00001$, $|y'(i+1)| \leqslant |y'(i)|$

   $|y'(i+2)| \leqslant |y'(i+1)|$, $|y'(i+3)| \leqslant |y'(i+2)|$

The condition 3 treats the right boundary for the peaks at the right end of the spectrum. It often shows no minimum at right boundary in this case.

The right boundary is sometimes located too far out, so a subroutine suggested by H.P.Yule is used to

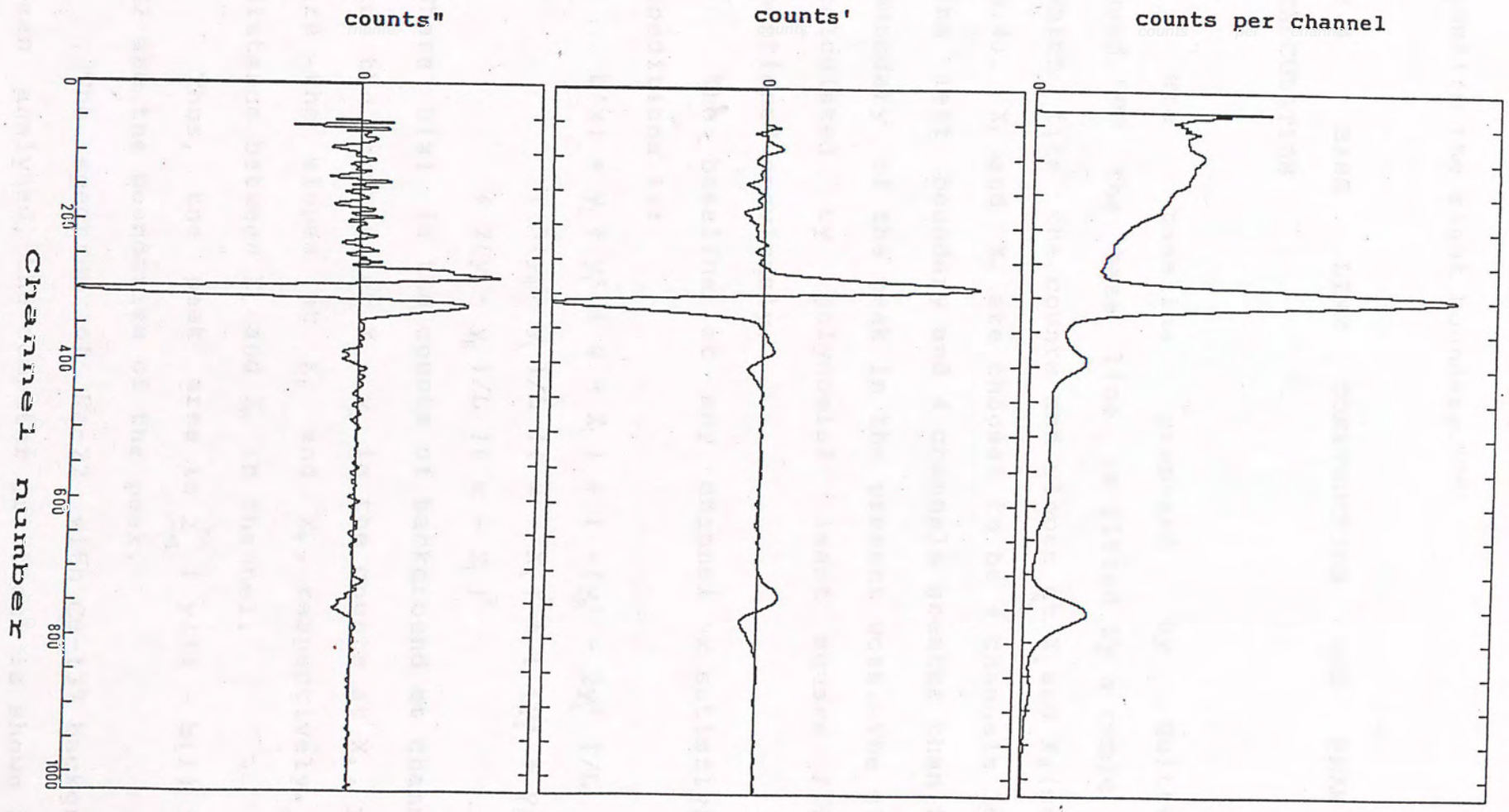

Figure 3.3 The derivatives of the spectrum of Na-22.
Figure a is the raw pulse height spectrum. Figure b and c are the first derivative and second derivative of the spectrum in Figure a, repectively. The heights in the figures are only relative.

comfirm the right boundary.[38]

3.4 BASE LINE CONSTRUCTION AND PEAK AREA CALCULATION

The baseline proposed by Quittner is used.[38] The base line is fitted by a cubic which fits the counts and slopes at X_L and X_R (see Figure 3.4). X_L and X_R are choosen to be 4 channels lower than the left boundary and 4 channels greater than the right boundary of the peak in the present work. The slopes are calculated by polynomial least square fitting as mentioned previously.

The baseline at any channel x satisflying these conditions is:

$$b(x) = y_L + y_L' (x - X_L) + [-(y_R' - 2y_L')/L + 3(y_R - y_L)/L](x - X_L)^2 + [(y_L' + y_R')/L + 2(y_L - y_R)/L](x - X_L)^3$$

Where b(x) is the counts of background at channel x, y_L is the counts at X_L, y_R is the counts at X_R, y_L' and y_R' are the slopes at X_L and X_R, respectively. L is the distance between X_L and X_R in channel.

Thus, the peak area is $\sum_{i=x1}^{x2} [y(i) - b(i)]$. X1 and X2 are the boundaries of the peak.

The spectrum of Na-22 with Cs-137 background has been analysed, the computer print out is shown in Figure

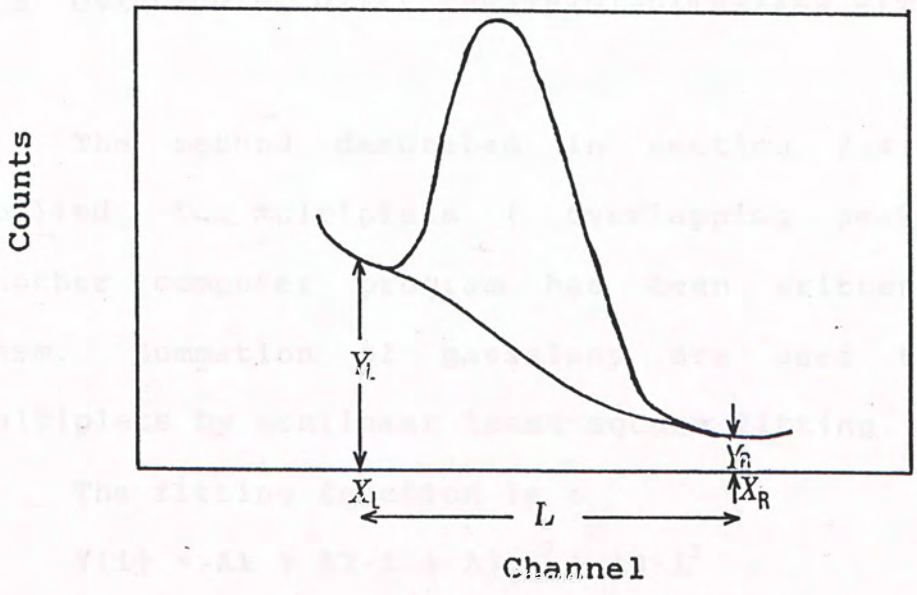

Figure 3.4 Base line construction by Quittner method

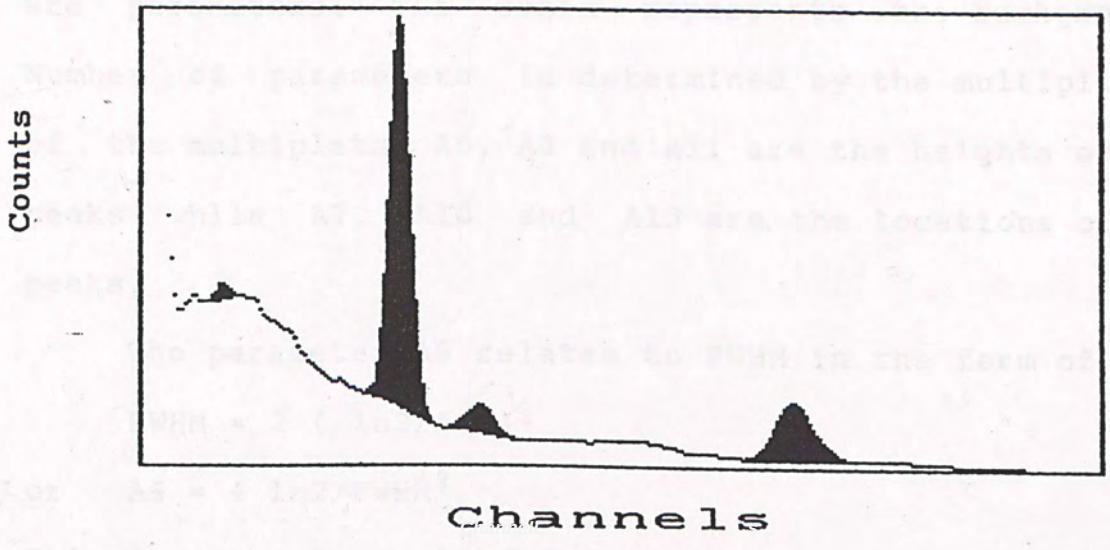

Figure 3.5 The computer print out of the gamma spectrum analysing program, the black regions show the peaks. The source is Na-22.

3.5.

3.5 OVERLAPPING PEAKS TREATMENT-GAUSSIANS FITTING

The method described in section 3.4 cannot be applied to multiplets (overlapping peaks). Thus another computer program has been written to resolve them. Summation of gaussians are used to fit the multiplets by nonlinear least square fitting.

The fitting function is :

$$Y(i) = A1 + A2 \cdot i + A3 \cdot i^2 + A4 \cdot i^3 + A5 \exp[-A6 (i-A7)^2] + A8 \exp[-A9 (i-A10)^2] + A11 \exp[-A12 (i-A13)^2]$$

Where Y(i) is the fitted counts at channel i. A1 to A13 are parameters. The cubic represents the background. Number of parameters is determined by the multiplicity of the multiplets. A5, A8 and A11 are the heights of the peaks while A7, A10 and A13 are the locations of the peaks.

The parameter A6 relates to FWHM in the form of

$$FWHM = 2 (\ln 2/A6)^{1/2}$$

or $A6 = 4 \ln 2/FWHM^2$

This form is also valiad for A9 and A12.

The area of gaussians is given by $A5(\pi /A6)^{1/2}$, $A8(\pi /A9)^{1/2}$ and $A11(\pi/A12)^{1/2}$.

Iterative method is used in the nonlinear least square fitting.[40] The quantity to be minimized is :

$$\sum_{i=x1}^{x2} W_i \; (\; y(i) - Y(i) \;)$$

where y(i) is the experimental counts at channel i, X1 and X2 are the boundaries of the peaks, and W_i is the weighting factor. W_i is chosen to be the reciprocal of variance of the counts at channel i. Hence, $W_i = 1/y(i)$ according to Poisson distribution.

It is important to choose suitable initial values of parameters in the iterative method. In the present work, the initial value of A1 and A2 are set to zero. A3 and A4 are calculated by joining a straight line from the left valley to the right valley of the peaks. A5, A8 and A11 are approximated by the maxima of the peaks before they are resolved. A7, A10 and A13 are approximated by locations of the maxima. A6, A9 and A12 are calculated by equation $4\ln2/FWHM^2$. The value of FWHM in terms of channel number can be determined experimentally using calibration sources.

Figure 3.6 shows the peaks of Co-60. Figure 3.6a is the spectrum seen in M.C.A. Figure 3.6b shows the raw data, the fitting curve and background. Figure 3.6c shows the resolved peaks.

The 0.3029 and 0.356 MeV peaks of Ba-133 are also resolved and plotted in Figure 3.7a to 3.7b. Since there

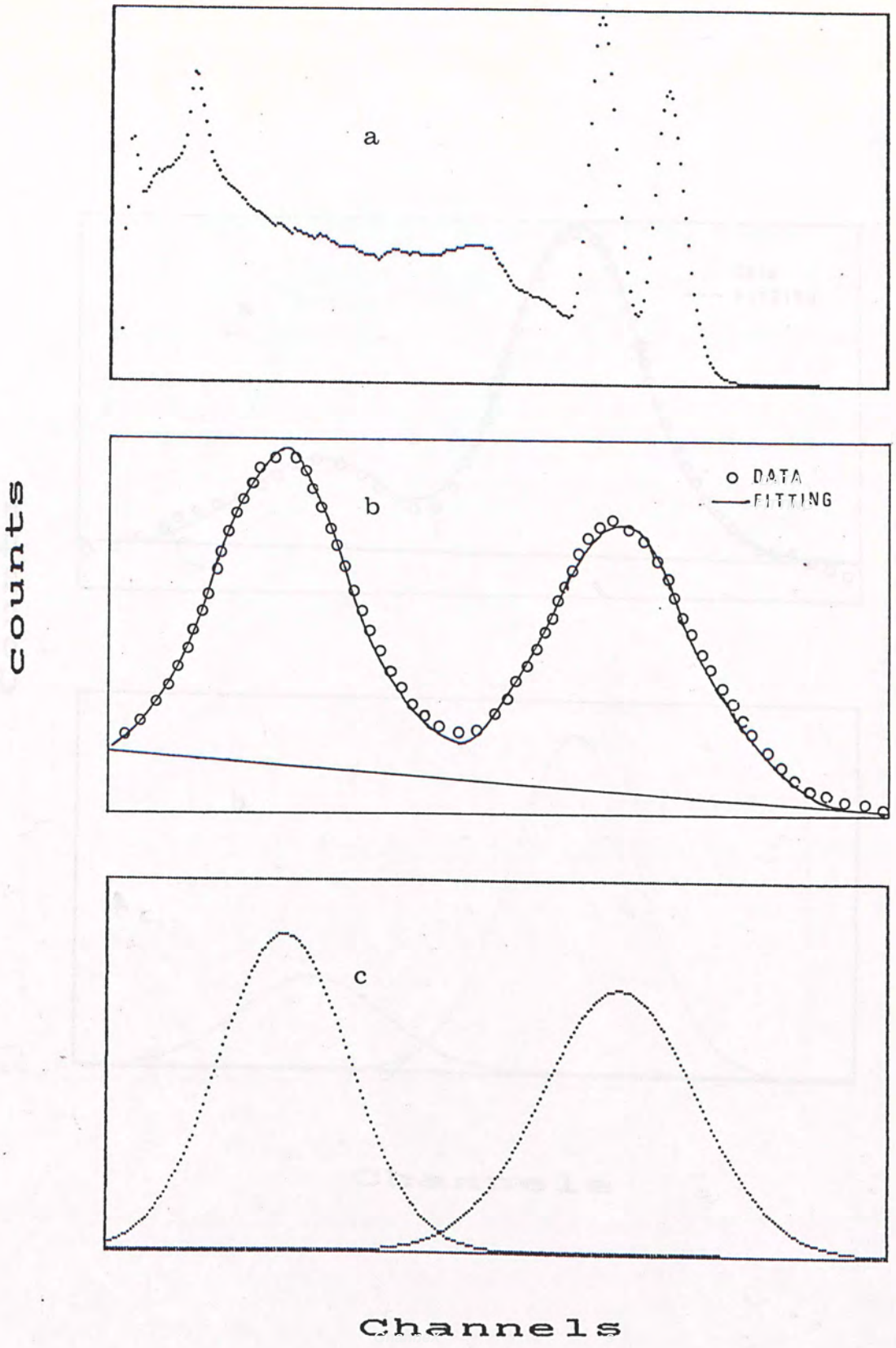

Figure 3.6 The photopeaks of Co-60. Figure a is the raw spectrum seen in the M.C.A. Figure b shows the result of the gaussian fitting program. The peaks are resolved and plotted in Figure c.

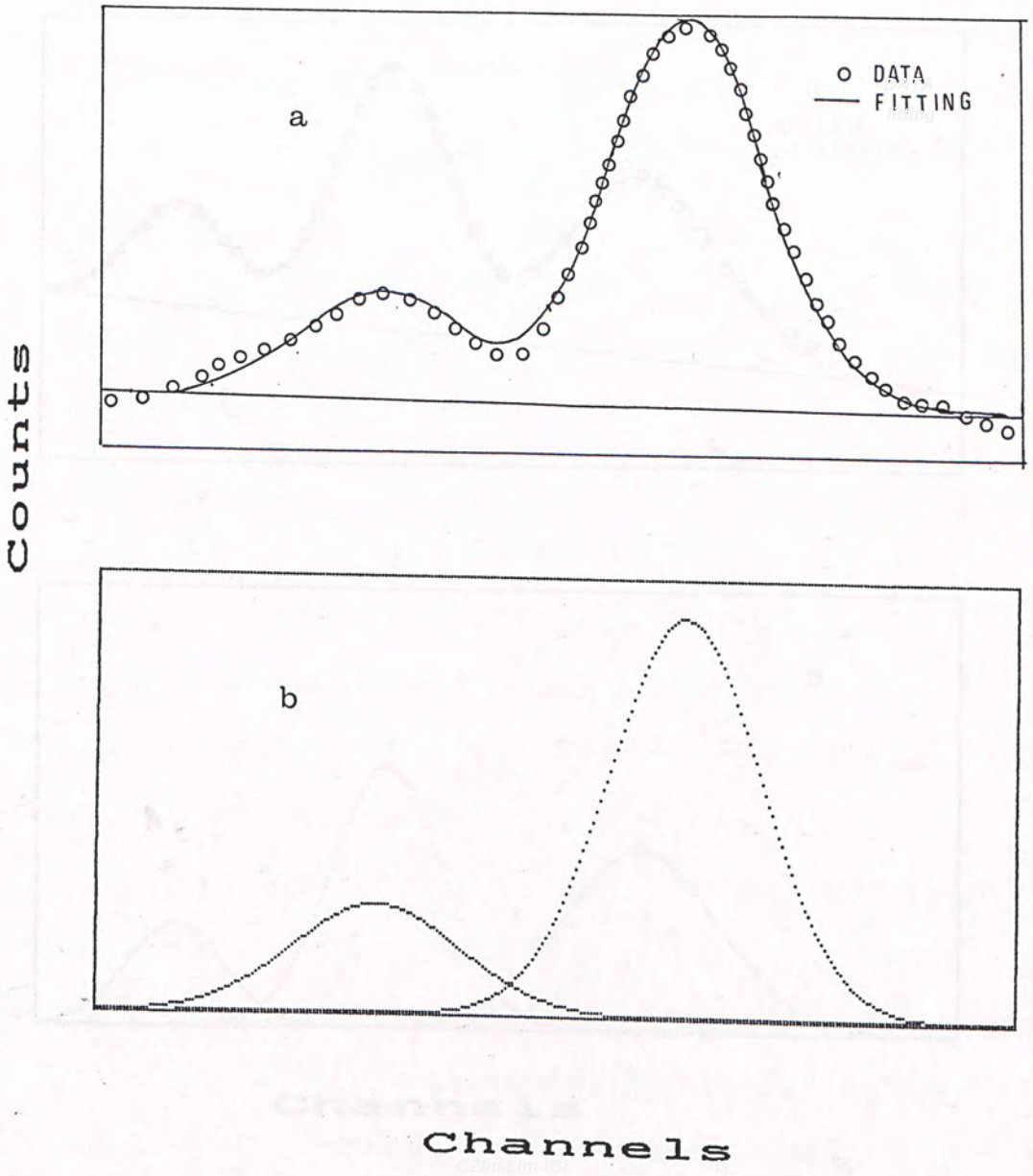

Figure 3.7 Figure a is the raw spectrum of Ba-133 detected by NaI(Ti) scintillator, and the fitting curve. Figure b is the photopeaks resolved by gaussians fitting.

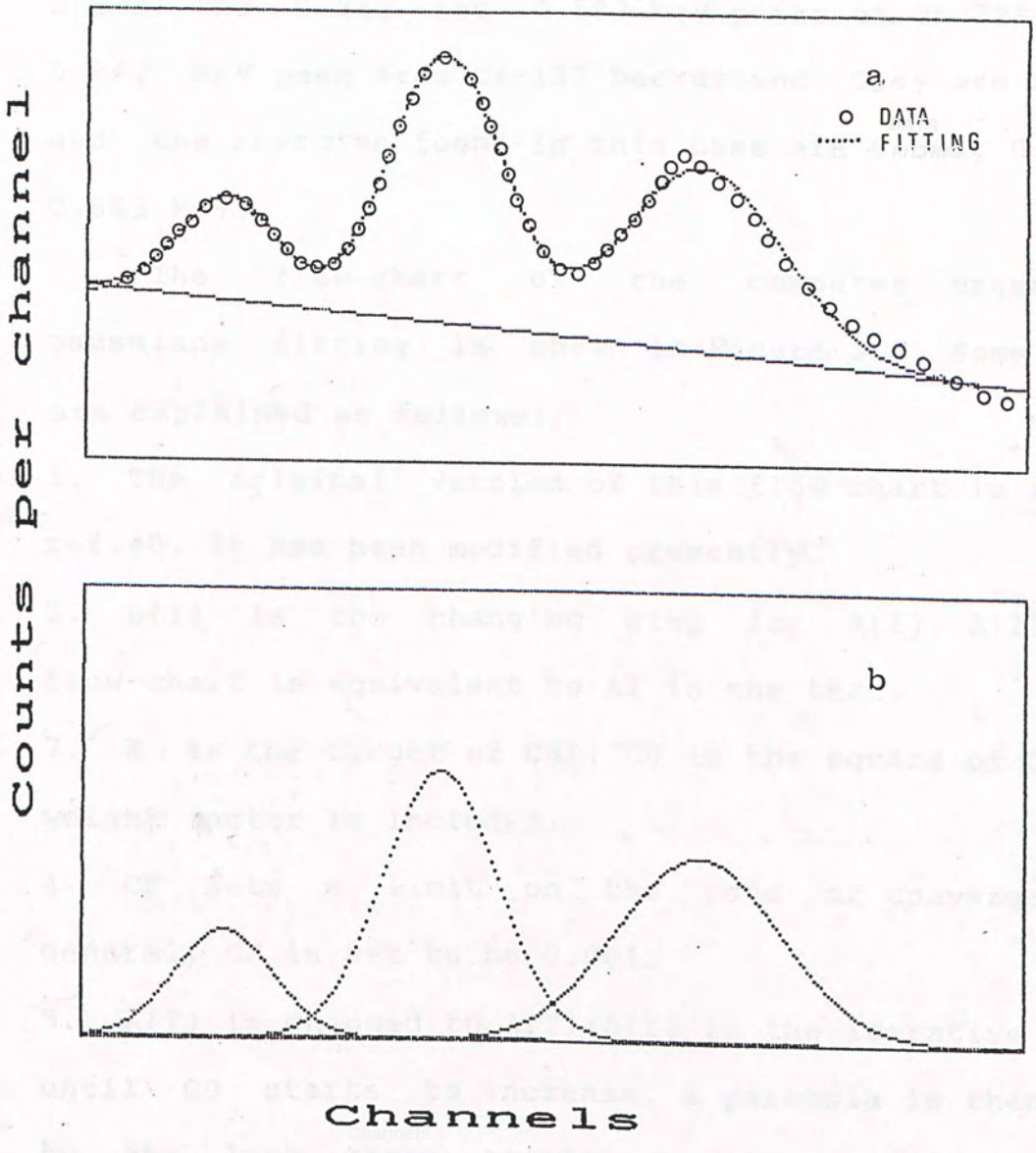

Figure 3.8 Figure a is the raw spectrum of the 0.511 and 0.583MeV gamma-rays from Th-228. The fitting curve is also shown in the same figure. The peak at the right side of the Figure is produced by Cs-137 background. Figure b shows the peaks after resolved.

are small peaks with energy 0.2764 and 0.3838 MeV, the fitting is not as good as Co-60. Figure 3.8a to 3.8b shows the 0.511 and 0.583 MeV peaks of Th-228 and the 0.662 MeV peak from Cs-137 background. They are resolved and the energies found in this case are 0.508, 0.580 and 0.663 MeV.

The flow-chart of the computer program for gaussians fitting is shown in Figure 3.9. Some details are explained as follows:

1. The original version of this flow-chart is found in ref.40. It has been modified presently.

2. D(I) is the changing step for A(I). A(I) in the flow-chart is equivalent to AI in the text.

3. E is the target of CHI. C0 is the square of CHI, the weight factor is included.

4. CF sets a limit on the rate of convergence. In general, CF is set to be 0.001.

5. A(I) is changed to A(I)+D(I) in the iterative process until C0 starts to increase. A parabola is then fitted to the last three points, namely , (A(I)-2D(I),C1), (A(I)-D(I),C2) and (A(I),C3). The minimum of the parabola gives the new value of A(I).

6. The statement D(J)=D(J)xN7/D7 can increase the size of step when many steps are required to get the minimum, and decreases the size of step when approaching the minimum.

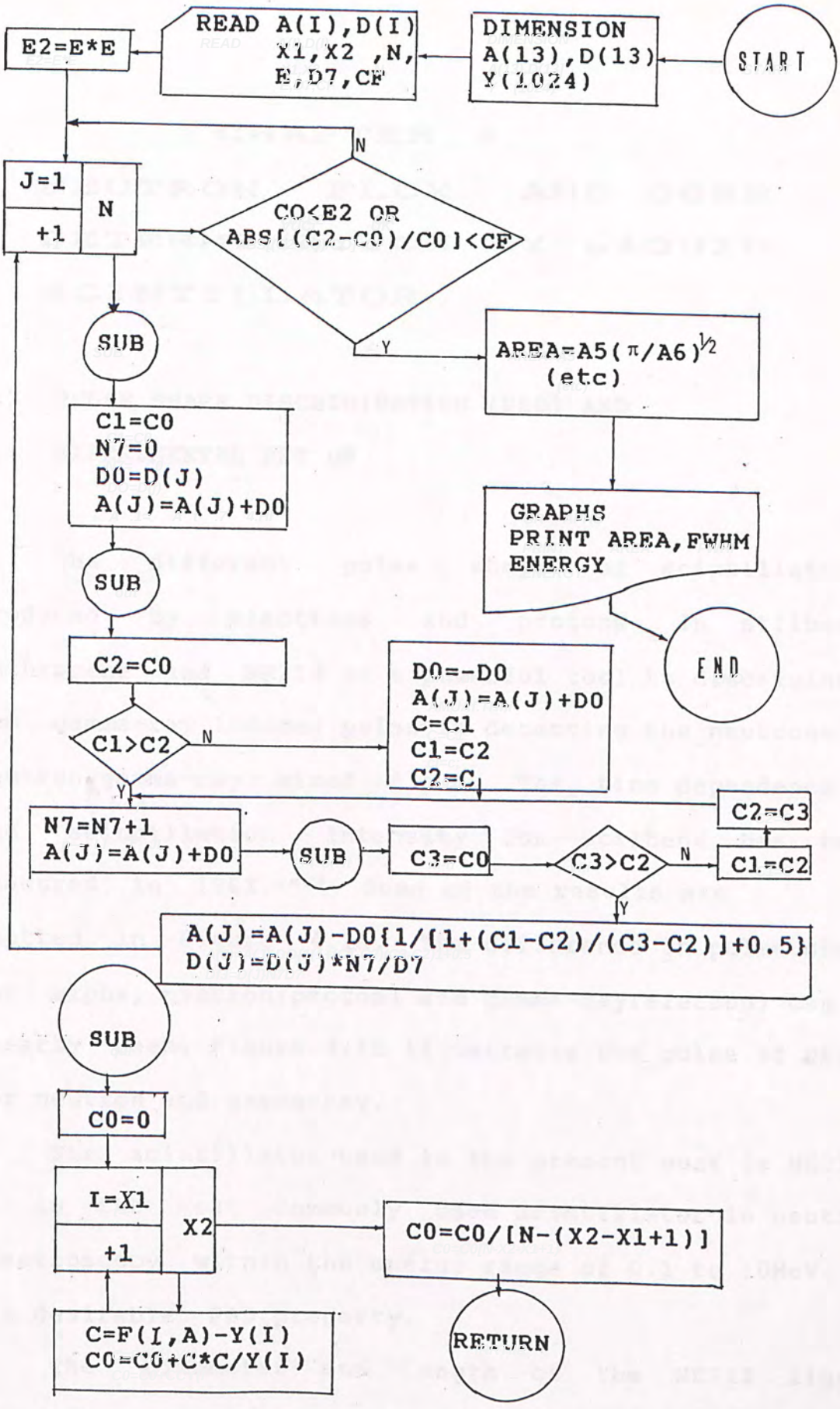

Figure 3.9 The flow-chart of the computer program for gaussians fitting.

CHAPTER 4

NEUTRON FLUX AND DOSE DETERMINATION BY LIQUID SCINTILLATOR

4.1 PULSE SHAPE DISCRIMINATION (PSD) AND EXPERIMENTAL SET UP

The different pulse shape of scintillations produced by electrons and protons in stilbene, anthracene and NE213 is a powerful tool to discriminate the gamma-ray induced pulse in detecting the neutrons in neutron-gamma-ray mixed field. The time dependence of the scintillation intensity for stilbene has been measured in 1961.[41] Some of the results are plotted in Figure 4.1a. The difference in pulse shape for alpha, neutron(proton) and gamma-ray(eletron) can be clearly seen. Figure 4.1b illustrates the pulse of NE213 for neutron and gamma-ray.

The scintillator used in the present work is NE213. It is the most commonly used scintillator in neutron spectroscopy within the energy range of 0.1 to 10MeV. It has desirable PSD property.

The diammeter and length of the NE213 liquid scintillator, which couples to the photomultiplier tube

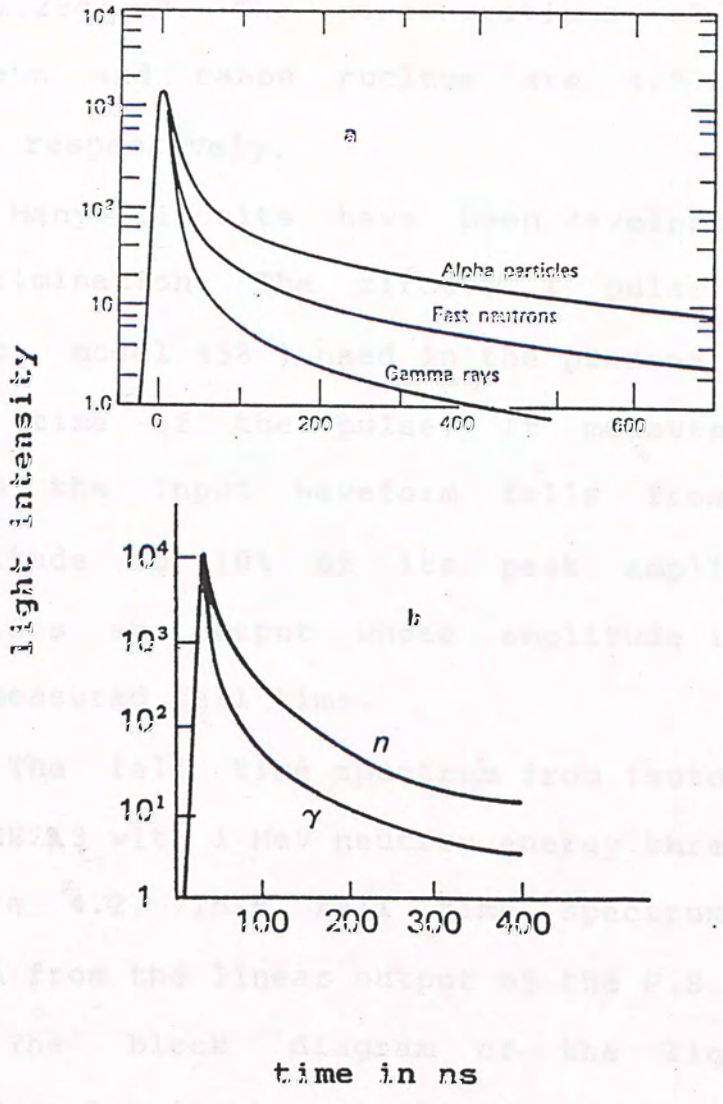

Figure 4.1 Time dependence of scintillation intensity for organic scintillator exited by difference types of charged particles. Figure a (ref. 41) shows the result for stilbene. Figure b (ref. 1) shows the result for NE213.

RCA8587, is 4.45cm and 5.08cm, respectively. Its density is 1.23g/cm^3. The concentrations of hydrogen nucleus and cabon nucleus are 4.87x10 and 4.01x10 cm^{-3}, respectively.

Many circuits have been developed for pulse shape discrimination. The circuit (pulse shape analyzer, ortec, model 458) used in the present work measures the fall time of the pulse. It measures the time during which the input waveform falls from 90% of its peak amplitude to 10% of its peak amplitube , and then provides an output whose amplitude is proportional to the measured fall time.

The fall time spectrum from isotope Am-Be recorded by NE213 with 1 MeV neutron energy threshold is shown in Figure 4.2. This fall time spectrum is collected by M.C.A from the linear output of the P.S.A.

The block diagram of the liquid scintillator spectrometer is shown in Figure 4.3.

The performance of this PSD system has been checked by comparing the counts from co-60 with and without gating. The ratio of counts before the amplifier is gated by PSA to the counts after the amplifier is gated is 272 : 1 . Figure 4.4 illustrates the effect of PSD on gamma-rays.

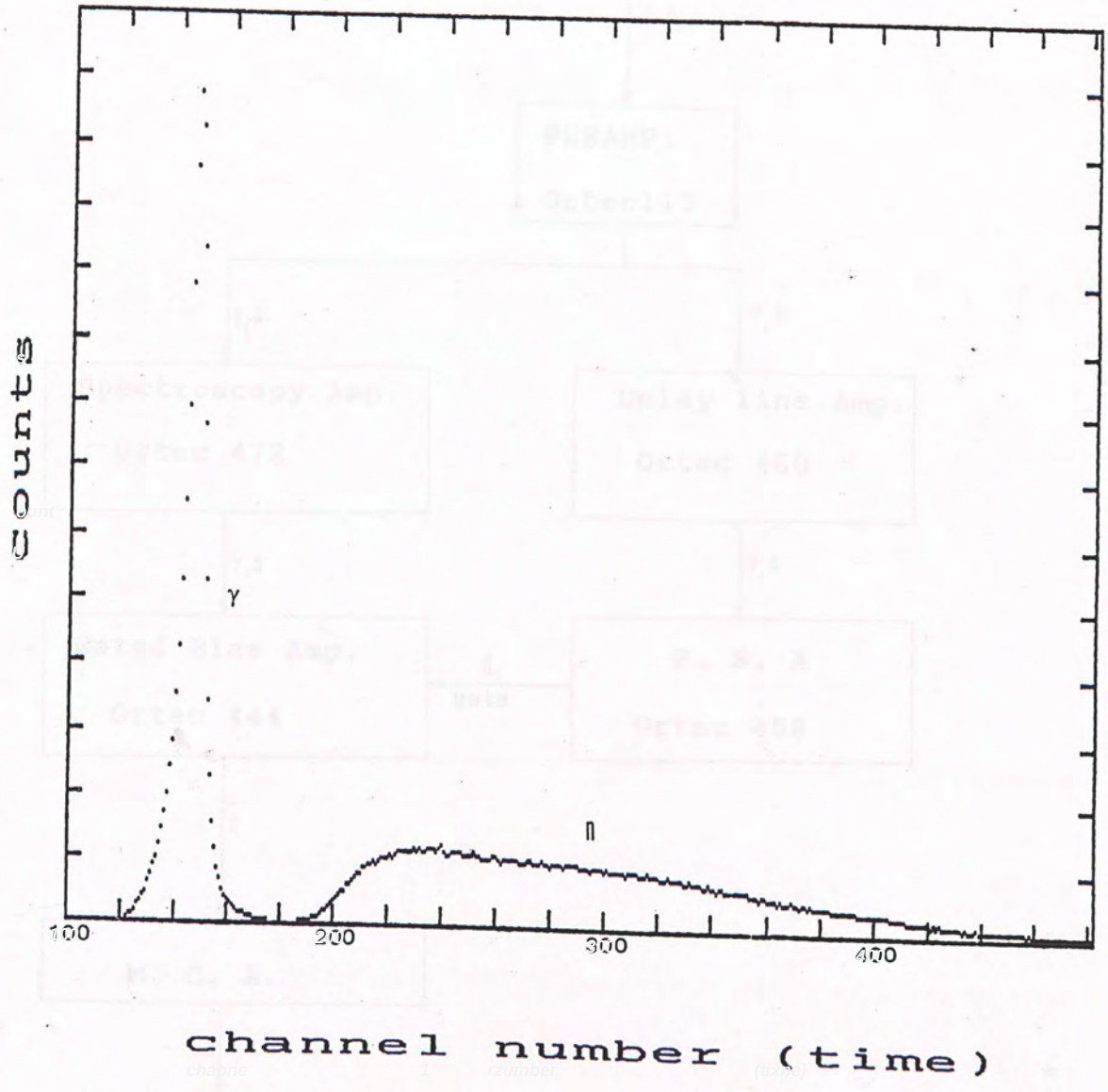

Figure 4.2 The fall time spectrum of Am-Be source. The Energy threshold is 1 MeV.

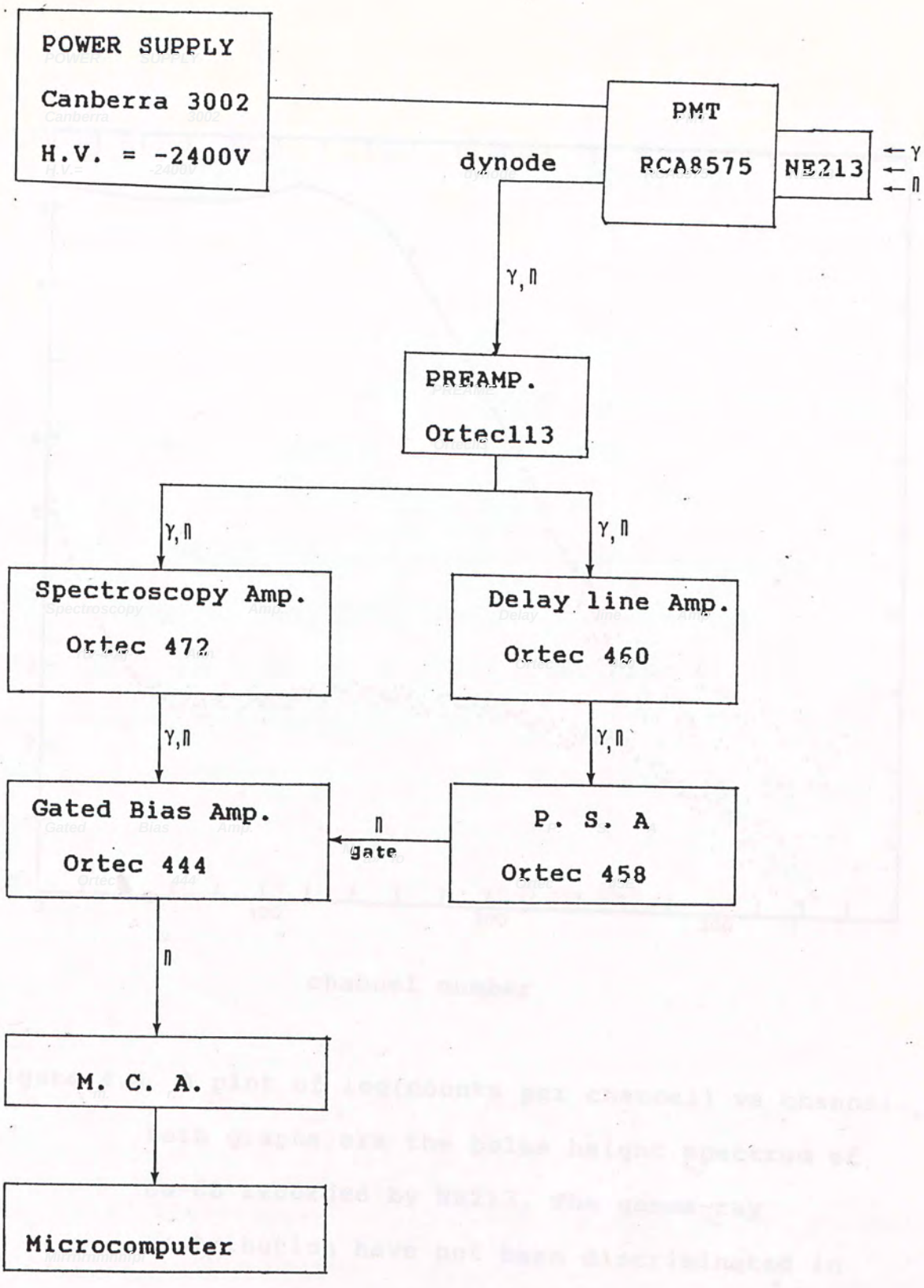

Figure 4.3 Block diagram of the liquid scintillation spectrometer

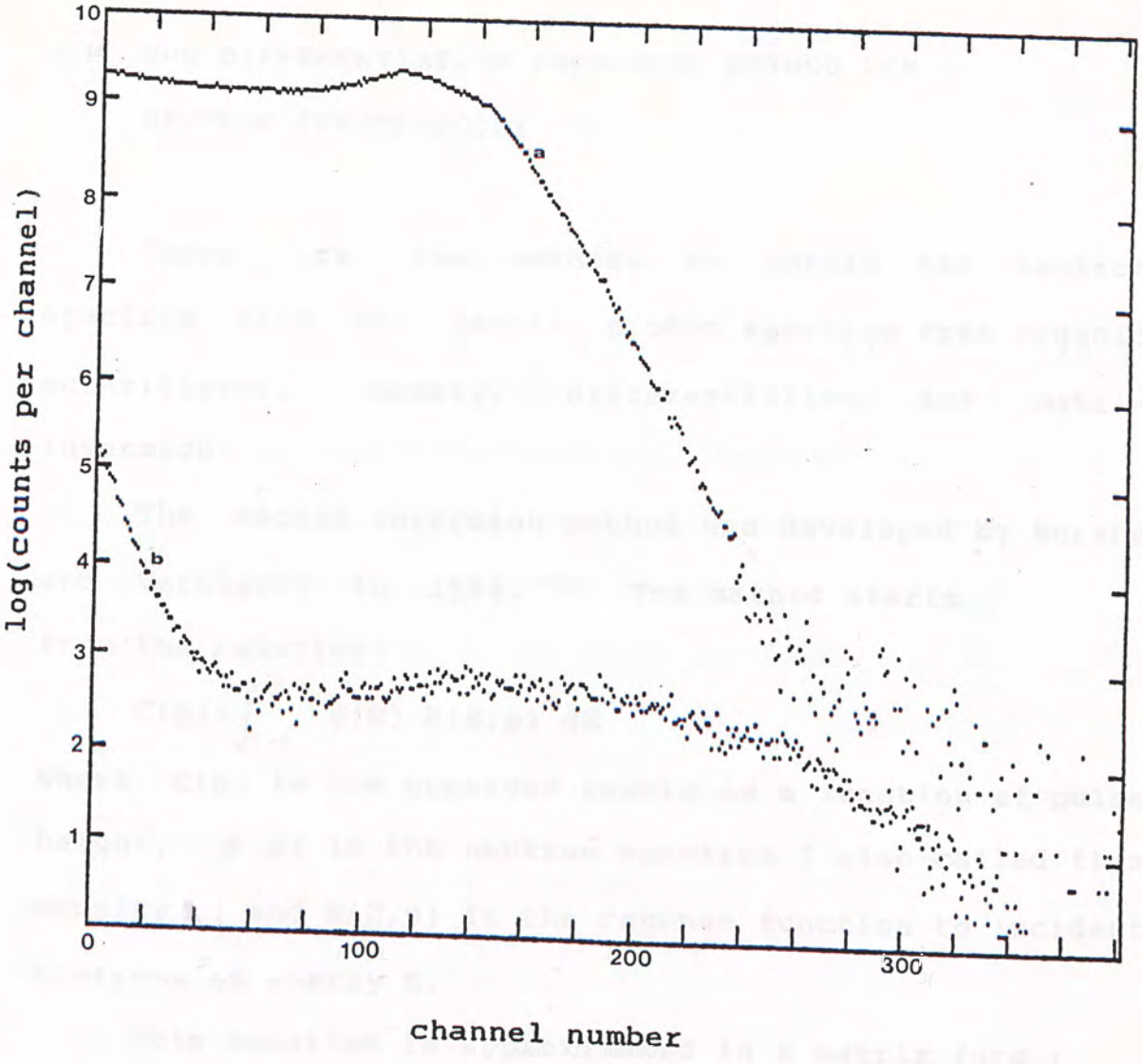

Figure 4.4 A plot of log(counts per channel) vs channel. Both graphs are the pulse height spectrum of Co-60 recorded by NE213. The gamma-ray contribution have not been discriminated in graph a. When PSD is in use, graph b is obtained. Note that the semi-log scale is used.

4.2 THE DIFFERENTIATION UNFOLDING METHOD FOR NEUTRON SPECTROSCOPY

There are two methods to unfold the neutron spectrum from the recoil proton spectrum from organic scintillator, namely, differentiation and matrix inversion.

The matrix inversion method was developed by Burrus and Verbinski in 1968.[42] The method starts from the relation:

$$C(p)=\int_{E=0}^{\infty} \Phi(E)\, R(E,p)\, dE$$

Where C(p) is the observed counts as a function of pulse height. $\Phi(E)$ is the neutron spectrum (also called flux density) and R(E,p) is the reponse function to incident neutrons of energy E.

This equation is approximated in a matrix form :

$$C_i = \sum_{j=1}^{J} \Phi_j\, R_{ij}\, \Delta E_j$$

Where Φ_j is then obtained by minimizing the quantity :

$$\sum_{i=1}^{I} W_i \left(C_i - \sum_{j=1}^{J} \Phi_j R_{ij}\, \Delta E_j \right)^2$$

The differentiation method is used in the present work and is formulated as below.[43] [44]

The total number of protons (P) produced by neutrons of energy E' is :

$$P = \Phi\, A \in (E',L) \qquad (4.1)$$

Where Φ is the incident neutron flux. A and L are the area and thickness of the scintillator, repectively.

$\in(E',L)$ is the efficiency for detecting neutrons by single scattering on hydrogen nucleus and is griven by eq. (4.2) as follows.

$$\in(E,L) = n_h \delta_h L(1-e^{a})/aL$$

$$= n_h \delta_h L\ f(aL) \qquad (4.2)$$

Where $a = n_h \delta_h + n_c \delta_c$, n_h and n_c is the concentration of hydrogen nucleus and carbon nucleus, respectively. δ_h and δ_c is the neutron-proton scattering cross-section and the neutron-carbon reaction cross-section, repectivly.

Since the recoil proton is isotropic in c.m. system for neutron energy under 10 MeV, the number of recoil proton would equally distribute in the energy range from 0 to E' and form a retangular reponse function, as shown in Figure 4.5.

Hence, the number of proton per unit energy interval is given by :

$$P(E) = A \in(E,L)/E$$

If incident neutrons are not monoenergetic, all incident neutons of energy greater than E can contribute to P(E), hence,

$$P(E) = \int_E^{\infty} [\ A \in(E',L)/E'\ ]\ (d\Phi/dE')\ dE' \qquad (4.3)$$

Differentiating both side of eq.4.3 with respect to energy gives:

$$\Phi(E) = -\frac{dP(E)}{dE} \times \frac{E}{A \in(E,L)} \qquad (4.4)$$

There are four factors which can distort the

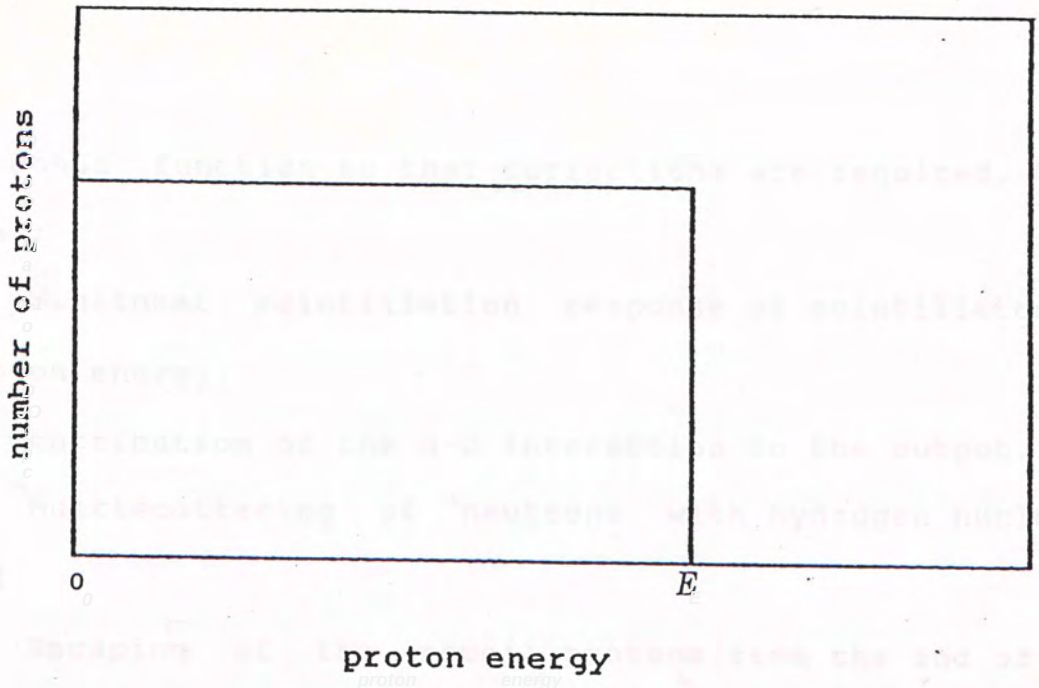

Figure 4.5 The energy distribution of recoil protons produced by neutrons of energy E in the ideal case.

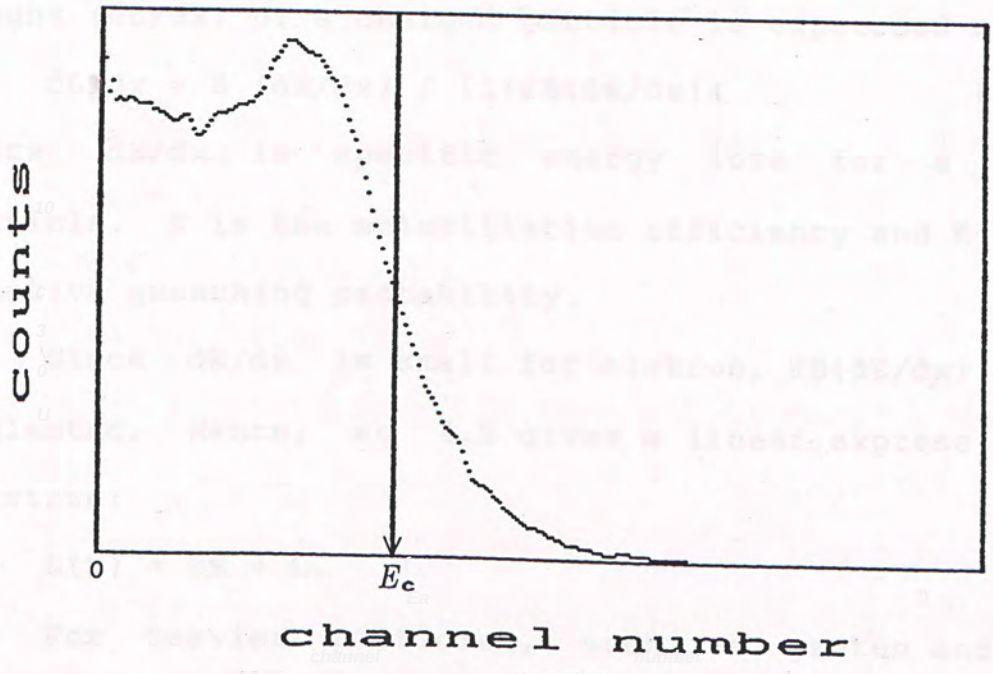

Figure 4.6 The compton edge of Cs-137. The arrow locates the channel corresponding to the half height of the compton edge.

response function so that corrections are required. They are :

1. Nonlinear scintillation response of scintillator to proton energy.

2. Contribution of the n-C interaction to the output.

3. Multiscattering of neutrons with hydrogen nucleus, and

4. Escaping of the recoil protons from the end of the scintillator (the wall effect).

The successful formula in describing the scintillation reponse is proposed by Birks.[22]
The flourescence light energy emitted per unit path lenght (dL/dx) of a charged particle is expressed as:

$$dL/dx = S\,(dE/dx) \,/\, [1+KB(dE/dx)] \qquad (4.5)$$

Where dE/dx is specific energy loss for a charge particle. S is the scintillation efficiency and K is the relative quenching probability.

Since dE/dx is small for eletron, KB(dE/dx) can be neglected. Hence, eq 4.5 gives a linear expression for electron:

$$L(E) = SE + L_o$$

For heavier particles, such as proton and alpha particle, KB(dE/dx) cannot be neglected, hence, L(E) is not directly proportional to energy loss of the particle.

However, the response due to proton can be given in

terms of electron equivalence. The relation between the electron energy E_e and the proton energy E_p for equal light output can be approximated by:

$$E_e = \alpha E_p^{\beta} \qquad (4.6)$$

The data within proton energy range 0.1 to 13 MeV from Verbinski[30] are used to determine α and β by least square method . α and β are found to be 0.1505 and 1.4746, repectively.

The electron energy versus channel number relation is obtained from the compton eletrons produced by monoenergetic gamma-ray sources. Then the proton energy as a function of channel number can be found from eq.4.6.

The maximum energy of the compton electron from gamma-ray of energy E have energy E_c which refers to compton edge in M.C.A. The simple relation of E and E_c is expressed as:

$$E_c = E / (1+0.511/2E)$$

where E is expressed in MeV.

The half height of the drop off of compton edge is taken to be the channel number corresponding to the electron enegry E_c . Figure 4.6 is the compton edge of Cs-137, the channel corresponding to the half height of the edge is marked.

Double scattering from hydrogen nucleus moves the counts from low pulse height region to the higher pulse

height region. The wall effect plays the opposite role of double scattering, it removes the counts in high pulse height region and creates counts with lower pulse height. These two effects can be crudely correctd by a shape correcting factor S(E). It is given by the semiempirical relation proposed by Broek.(43)

$$S(E) = 1 - 0.780(R/L) + 0.090 n_h \delta_h L + 0.077 n_h \delta_h' r \qquad (4.7)$$

Where $\delta_h' = \delta_h(0.068E)$. R is the range of proton at energy E and equals to $1.78(E-0.119)^{1.615}$ mg/cm^2 for NE213. r is the radius of the scintilator.

From eq.4.4 and eq.4.7, we get :

$$\Phi(E) = -\frac{dP(E)}{dE} \times \frac{E}{A\, S(E) \in (E,L)} \qquad (4.8)$$

4.3 THE COMPUTER PROGRAM FOR SPECTRUM UNFOLDING

The electron energy verus channel number relation is obtained by gamma sources before the spectrum is unfolded. The calibration sources used in the present work are listed in Table 4.1.

The relation $E = a + bx + cx^2$ is used. Where a, b, c are determined by least square method.

The values of $\in$ and S are independent of the neutron field. Their values were calculated by eq.4.2 and eq4.7 in 0.05 MeV energy interval within the energy

TABLE 4.1 GAMMA SOURCES FOR ENERGY VERSUS CHANNEL NUMBER CALIBRATION

SOURCE	ENERGY (MeV)	ELECTRON ENERGY (MAXIMUM) (MeV)
Ba-133	0.356	0.20725
Cs-137	0.662	0.47732
Mn-54	0.835	0.63920
Na-22	1.275	1.06167
Th-228	2.614	2.38172
AMBE	4.43	4.18843

range from 0.05 to 16 MeV. The values were stored in the floppy disk.

The cross section was obtained from the appendix of ref.(44). The values which are not included in ref.(44) were interpolated by Newton's method and were checked by the graph in ref.(45).

The neutron-proton scattering cross section is given by Swartz:[46]

$$\delta_h(E) = \frac{5.603\,\pi}{1+7.417E+0.1105E^2} + \frac{0.8652\,\pi}{1+0.2427E+0.0028E^2}$$

Besides, the flux-dose equivalent convertion factors described in chapter 1 were calculated by cubic-spline interpolation method in 0.05MeV energy interval and were stored in the floppy disk.

Data in M.C.A are transferred to a microcomputer by a RS232 interface card. The data is firstly grouped according to eq.4.6 such that each channel represents 0.05 MeV energy increments of the raw data. If the channel corresponding to the upper bound of an energy interval (say I+r, 0<r<1) lies between two channel A, B, then the counts of channel B (C(B)) would be divided into two parts, rC(B) and (1-r)C(B). Counts rC(B) would be included in this energy interval and (1-r)C(B) would be counted into the next energy interval. The effect of grouping is equivalent to construct a multichannel raw spectrum that the channel number is linear with the

energy. Thus, the spectrum so grouped is the recoil proton spectrum.

Secondly, the value of $\Phi(E)$ is calculated by smoothed derivative described in chapter 3. Normally, 19 points are used in the least square fitting to obtain the smoothed derivative. Then, the neutron spectrum can easily be calculated by eq 4.8 after values of S and have been read from the floppy disk.

Lastly, the counts of each energy interval of the neutron spectrum is multiplied by the corresponding flux-dose equivalent convertion factor. The summation of the products gives the dose rate of the neutron field.

However, there are many factors which affect the absolute efficiency of the system. Thus, the system was calibrated by an isotope Am-Be. The background had been subtracted before the efficiency was calculated. The background was taken by placing a paraffin cone between the source and the detector, so that the neutrons come from the source were removed and only the counts induced by the neutrons scattered from the surroundings were recorded. The energy threshold was set to be 2MeV during calibration. The fraction of neutron emission above 2MeV is estimated by the spectrum from a theoretical calculation by Vander Zwan.[49]

The simplified flow chart of this program is given in Figure 4.7. The spectrum of isotope Am-Be with

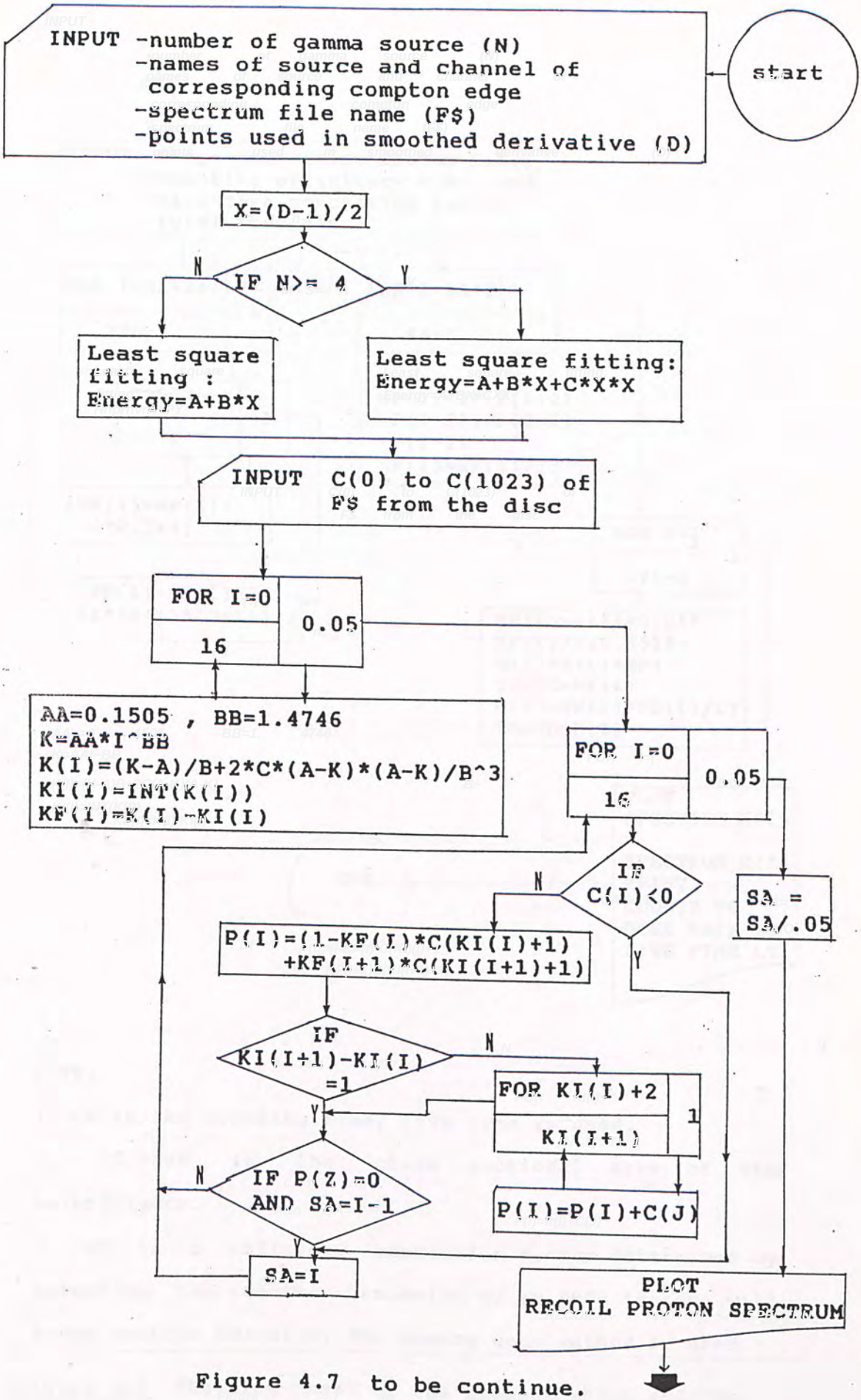

Figure 4.7 to be continue.

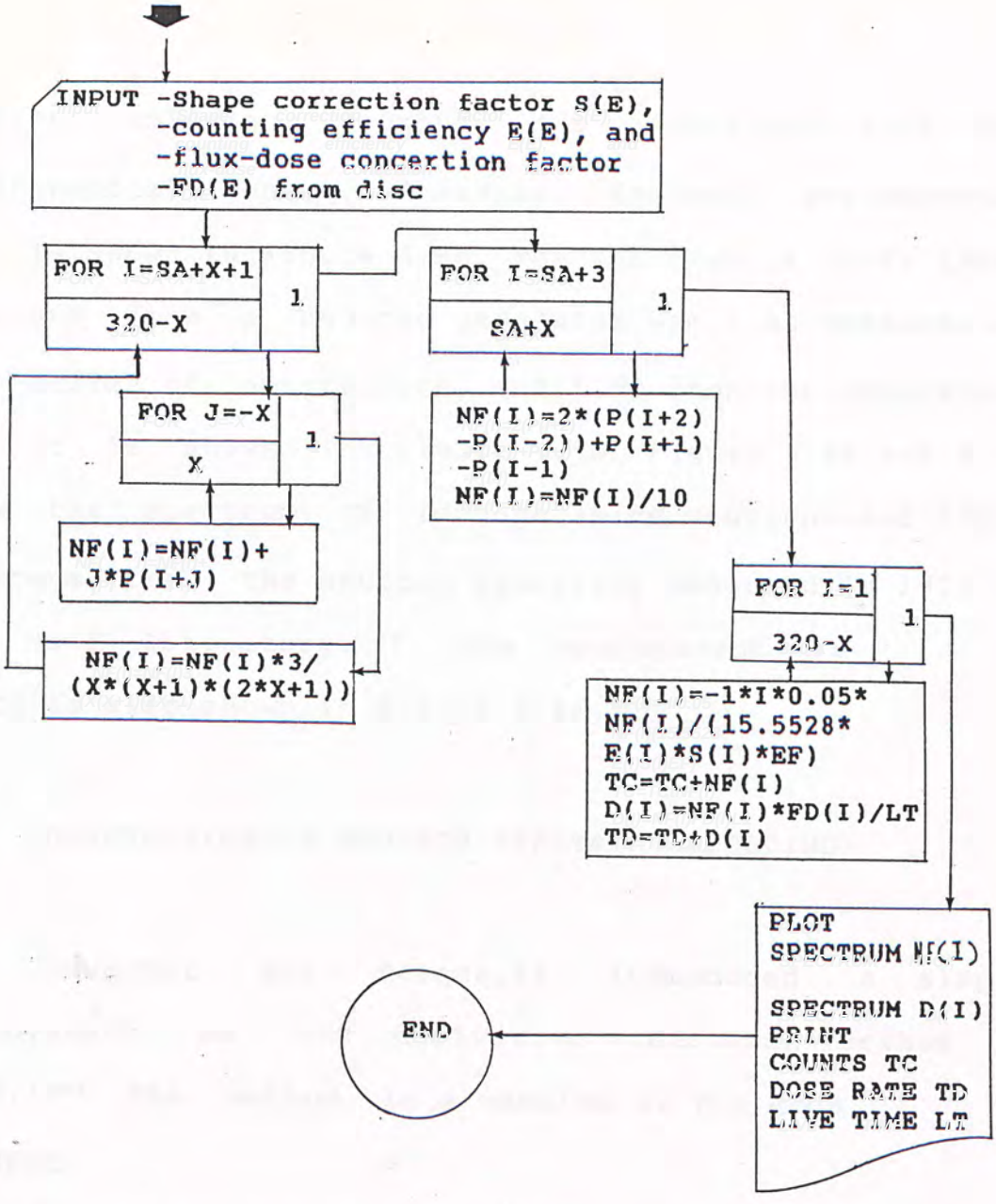

NOTE:

1. LT is the counting time, live time is used.

2. 15.5528 is the cross sectional area of the scintillator.

3. EF is a efficiecy correction factor determined by measuring the neutron emission of an AMBE isotope with known neutron emission. The shadow cone method is used.

Figure 4.7 The flow-chart of the program which unfolds the neutron spectrum by differentiation method.

neutron emission 2.5×10^6 n/s (obtained from the radiochemical centre, Amershan, England) was measured and is shown in Figure 4.8b. The spectrum of (D+T) 14MeV neutrons from a neutron generator was also measured at 135 angle of observation and 1.5m from the generator, and it is shown in Figure 4.9b. Figure 4.8a and 4.9a show the spectrum of isotope Am-Be neutrons and 14MeV neutrons from the neutron generator measured in 1979 in the same laboratory.[47] The measurement of Lorch is also shown in Figure 4.8a.[48]

4.4 MODIFICATION ON NEUTRON SPECTRUM UNFOLDING

Slaughter and Stront,II introduced a simple improvement on the derivative unfolding method in 1982.[50] The method is a version of the code FLYSPEC.

Now, a modified derivative unfolding method is developed based on the work of Slaughter and Stront,II. In deed, it is only a improved version of the method described in section 4.3.

Let us start with eq 4.8 in section 4.3,

$$\Phi(E) = - \frac{dP(E)}{dE} \times \frac{E}{A\, S(E) \in (E,L)} \qquad (4.8)$$

The detector pulse height, x, can be expressed in terms of light output as follows:

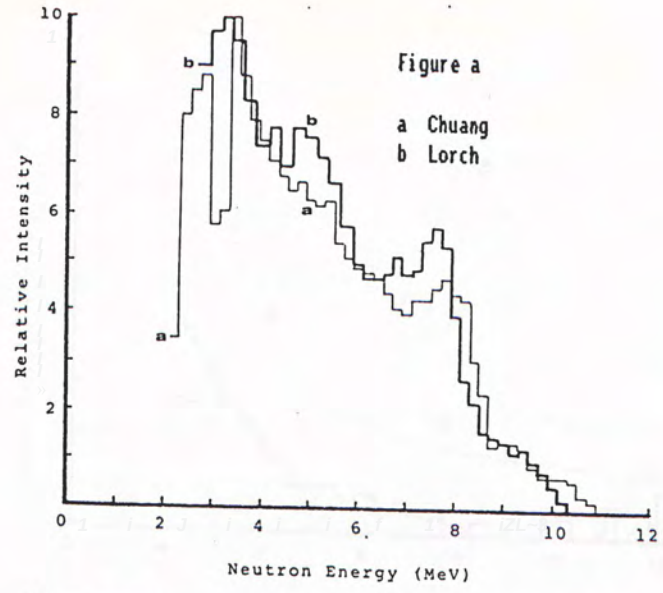

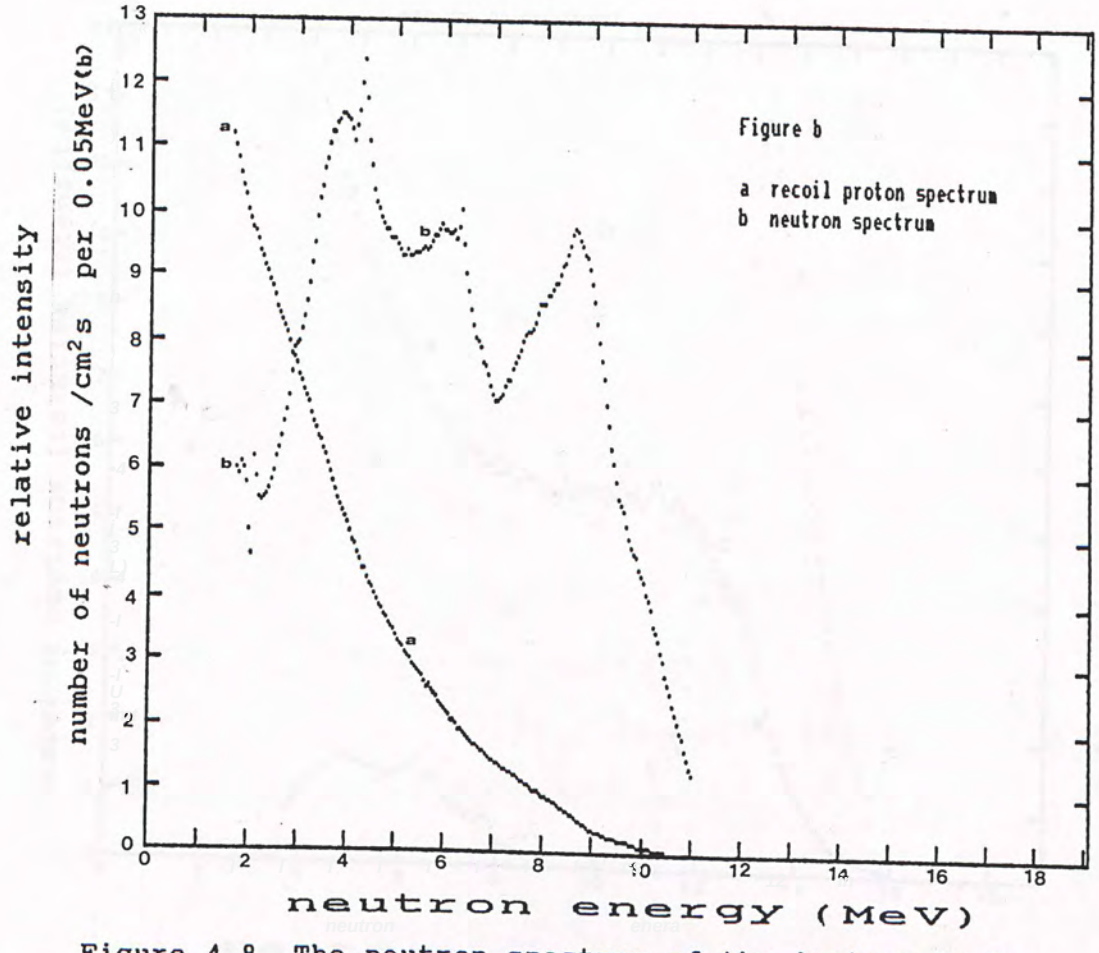

Figure 4.8 The neutron spectrum of the isotope Am-Be. Figure 4.8a is taken from ref.(47). It shows the result taken in 1979 and the result given by Lorch. Figure 4.8b is the present result.

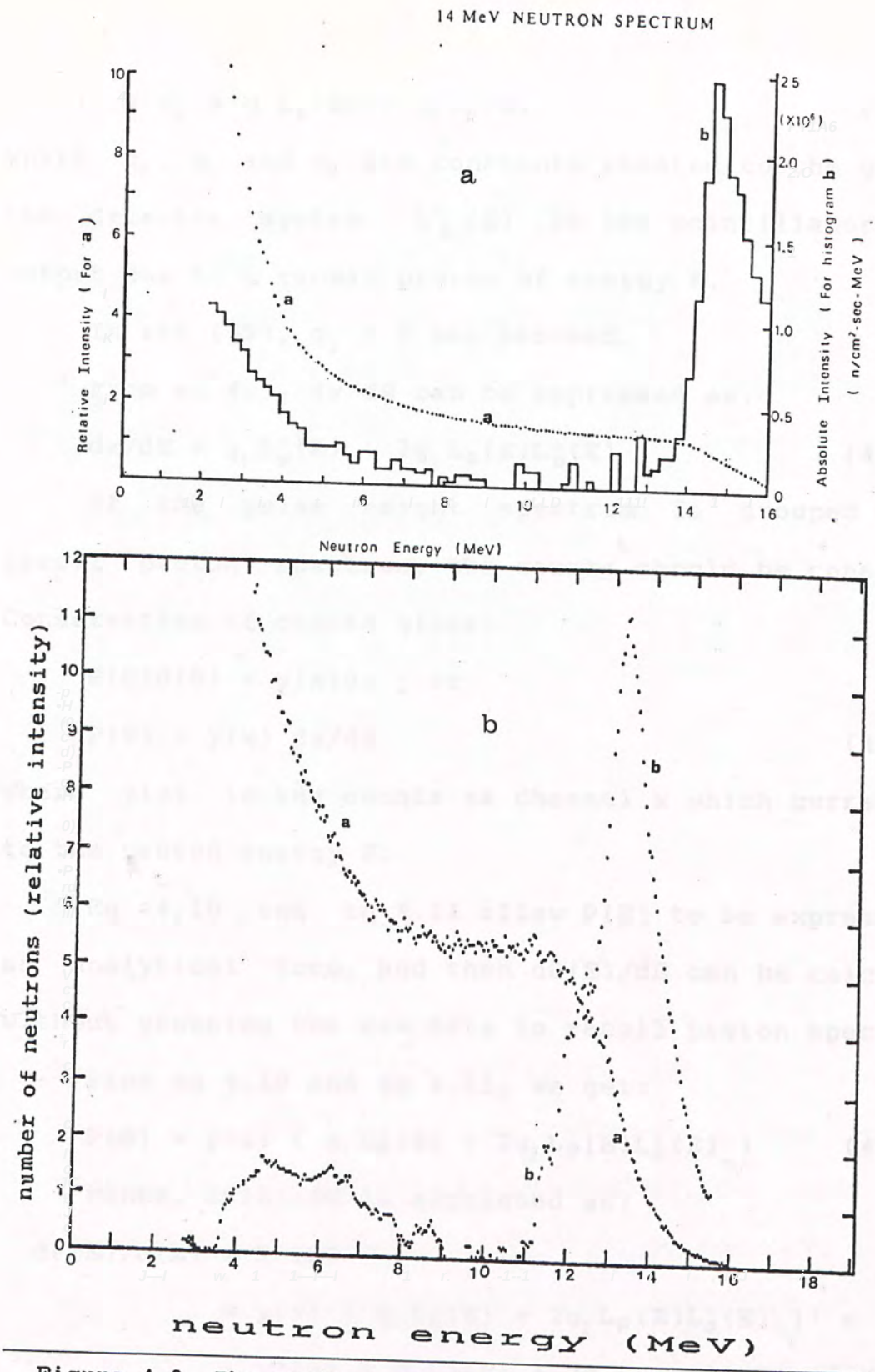

Figure 4.9 The neutron spectrum of the (D+T) reaction.
Figure a shows the result measured in 1979.
The present result is shown in figure b.

$$x = g_0 + g_1 L_p(E) + g_2 L_p(E)^2 \qquad (4.9)$$

Where g_0, g_1 and g_2 are constants related to the gain of the detector system. $L_p(E)$ is the scintillator light output due to a recoil proton of energy E.

In ref (49), $g_2 = 0$ was assumed.

From eq 4.9, dx/dE can be expressed as:

$$dx/dE = g_1 L_p'(E) + 2g_2 L_p(E) L_p'(E) \qquad (4.10)$$

If the pulse height spectrum is grouped to the recoil proton spectrum, the counts should be conserved. Conservation of counts gives:

$$P(E)d(E) = y(x)dx \text{ , or}$$

$$P(E) = y(x)\, dx/dE \qquad (4.11)$$

Where y(x) is the counts at channel x which corresponds to the proton energy E.

Eq 4.10 and eq 4.11 allow P(E) to be expressed in an analytical form, and then dP(E)/dE can be calculated without grouping the raw data to recoil proton spectrum.

From eq 4.10 and eq 4.11, we get:

$$P(E) = y(x) \left(g_1 L_p'(E) + 2g_2 L_p(E) L_p'(E) \right) \qquad (4.12)$$

Hence, dP(E)/dE is expressed as:

$$\begin{aligned} dP(E)/d(E) &= P'(E) \\ &= y(x) \left(g_1 L_p'(E) + 2g_2 L_p(E) L_p'(E) \right)' + \\ &\quad y'(x) \left(g_1 L_p'(E) + 2g_2 L_p(E) L_p'(E) \right) dx/dE \\ &= y(x) \left(g_1 L_p''(E) + 2g_2 L_p'(E)^2 + \right. \\ &\quad \left. 2g_2 L_p(E) L_p''(E) \right) + y'(x) \left(g_1 L_p'(E) + \right. \\ &\quad \left. 2g_2 L_p(E) L_p'(E) \right)^2 \end{aligned} \qquad (4.13)$$

Hence , eq 4.8 becomes:

$$\Phi(E) = - E/(A\, S(E) \in(E,L)) [\, y(x) (g_1 L_p''(E) + 2g_2 L_p'(E) + 2g_2 L_p(E) L_p''(E)) + y'(x) (g_1 L_p'(E) + 2g_2 L_p(E) L_p'(E))^2] \quad (4.14)$$

Just like the smoothed derivative method used in chapter 3, $y'(x)$ is also calculated by representing the pulse height data by piece-wise polynomials. Then $y'(x)$ can be expressed as:

$$y'(x) = 3/[\, m(m+1)(2m+1)] \sum_{i=-m}^{m} i y(i+x) ,$$

if 2m+1 points are involed in least square fitting.

If $g_2 = 0$, eq 4.14 reduce to the form:

$$\Phi(E) = - E/(A\, S(E) \in(E,L)) [\, y(x)\, g_1 L_p''(E) + y'(x) (g_1 L_p'(E))^2] \quad (4.15)$$

It is equivalent to the equation derived by Slaughter and Strout,II.

$L_p(E)$, $L_p'(E)$ and $L_p''(E)$ at various energy can be interpolated from the data of Verbinski.(30) However, $L_p(E)$, $L_p'(E)$ and $L_p''(E)$ must be continuous in such interpolation method, otherwise, the unfolded neutron spectrum would be distorted. The cubic spline interpolation can satisfly these conditions. It fits the data by cubics such that the first derivative and second derivative at each point within the range bounded by given data are continuous.(see Appendix A)

Values of $L_p(E)$, $L_p'(E)$ and $L_p''(E)$ are stored in floppy disc. They are read at the beginning of the

unfolding program. The values of $L_p(E)$, $L_p'(E)$ and $L_p''(E)$ are plotted in Figure 4.10a to 4.10c. The raw data from Verbinski are listed in Table 4.2.

The channel versus light output calibration is required in this method. The detector is calibrated by standard gamma-ray source. One light is defined as 1.13 times the electron energy corresponding to the half height of the compton edge produced by the 1.275MeV gamma-ray from Na-22. After the data of light unit and corresponding channel are found and read by the microcomputer, g_0 , g_1 and g_2 can be calculated by least square method.

The error due to poisson distribution of data can be estimated for each data point in the neutron spectrum as follows:

$$\Delta\Phi(E) = [\ (\Delta y(x)\ \partial\Phi(E)/\partial y(x)\ ) + (\Delta y'(x)\ \partial\Phi(E)/\partial y'(x)\ )^2\ ]^{1/2} \qquad (4.16)$$

where $(\Delta y(x))^2 = y(x)$, and

$$(\Delta y'(x))^2 = 3/[\ m(m+1)(2m+1)\ ] \sum_{i=-m}^{m} i^2 y(i+x)\ ,$$

if 2m+1 points are involved in the least square fitting.

According to eq. 4.14, we get:

$$\partial\Phi(E)/\partial y(x) = -\ (E/AS\in)\ (\ g_1 L_p''(E) + 2g_2 L_p'(E)^2 + 2g_2 L_p(E) L_p''(E)\ )\ ,\ \text{and}$$

$$\partial\Phi(E)/\partial y'(x) = -\ (E/AS\in)\ (\ g_1 L_p'(E) + 2g_2 L_p(E) L_p'(E)\ )^2$$

This method has two advantages in comparison with

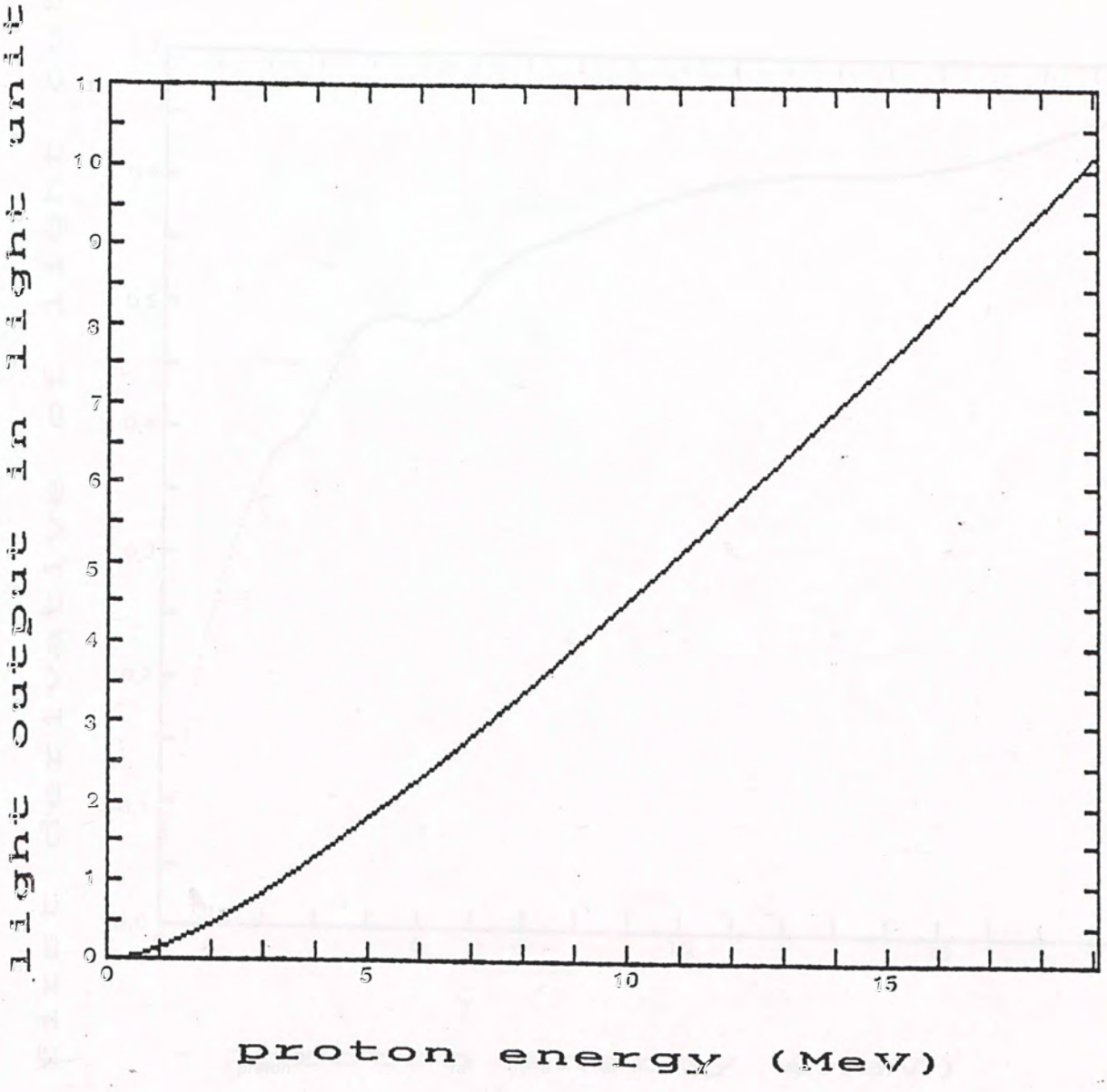

Figure 4.10a The proton energy dependence of the light output of NE213 ($L_p(E)$). Data is taken from ref. (30).

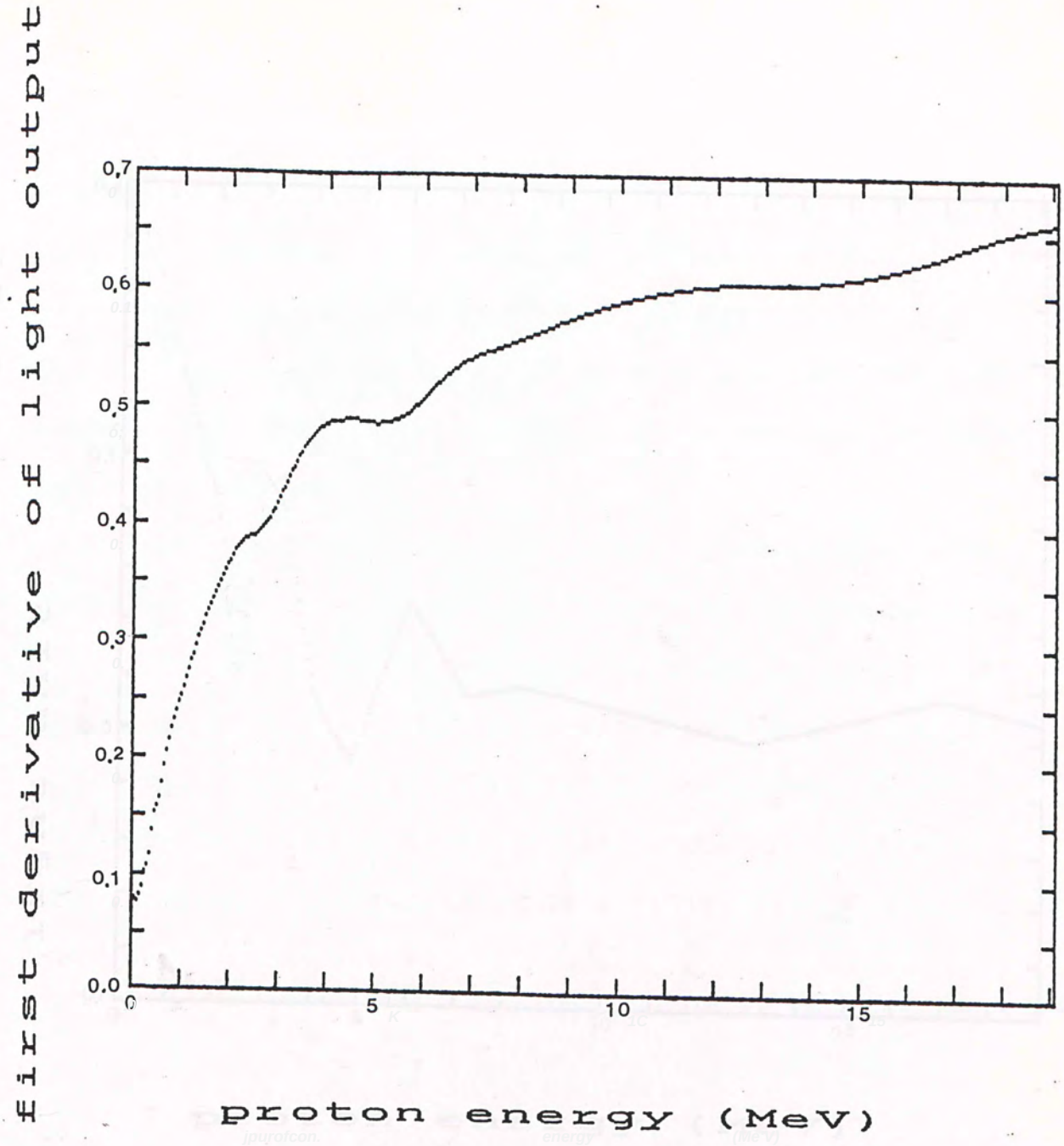

Figure 4.10b The first derivative of $L_p(E)$ ($L'_p(E)$) verus proton energy.

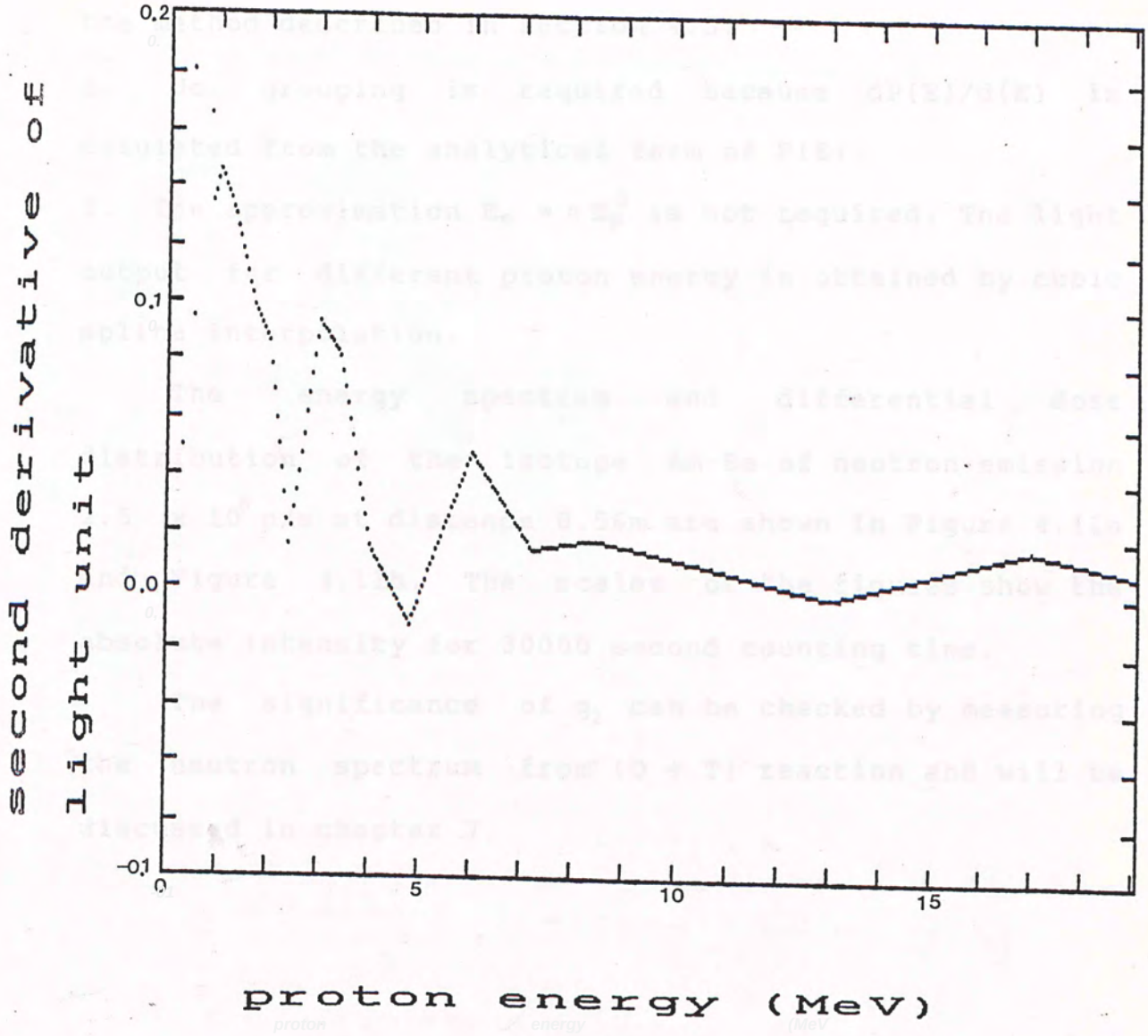

Figure 4.10c The second derivative of $L_p(E)$ ($L''_p(E)$) verus proton energy.

the method described in section 4.3:

1. No grouping is required because $dP(E)/d(E)$ is calulated from the analytical form of P(E).

2. The approximation $E_e = a E_p^{\beta}$ is not required. The light output for different proton energy is obtained by cubic spline interpolation.

The energy spectrum and differential dose distribution of the isotope Am-Be of neutron emission 2.5×10^6 n/s at distance 0.56m are shown in Figure 4.11a and Figure 4.11b. The scales of the figures show the absolute intensity for 30000 second counting time.

The significance of g_2 can be checked by measuring the neutron spectrum from (D + T) reaction and will be discussed in chapter 7.

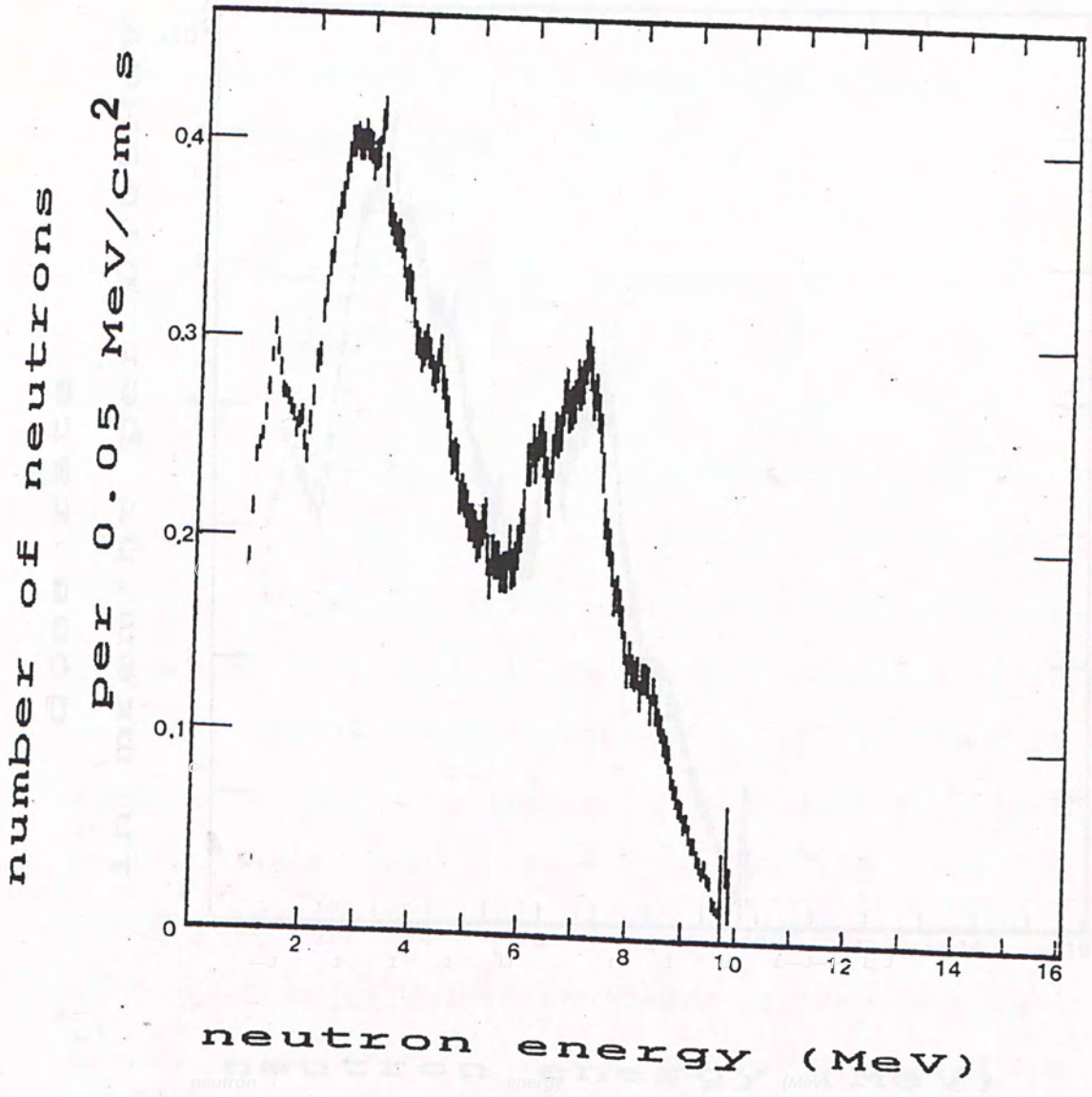

Figrue 4.11a The neutron spectrum of Am-Be source measured by NE213 liquid scintillation detector.

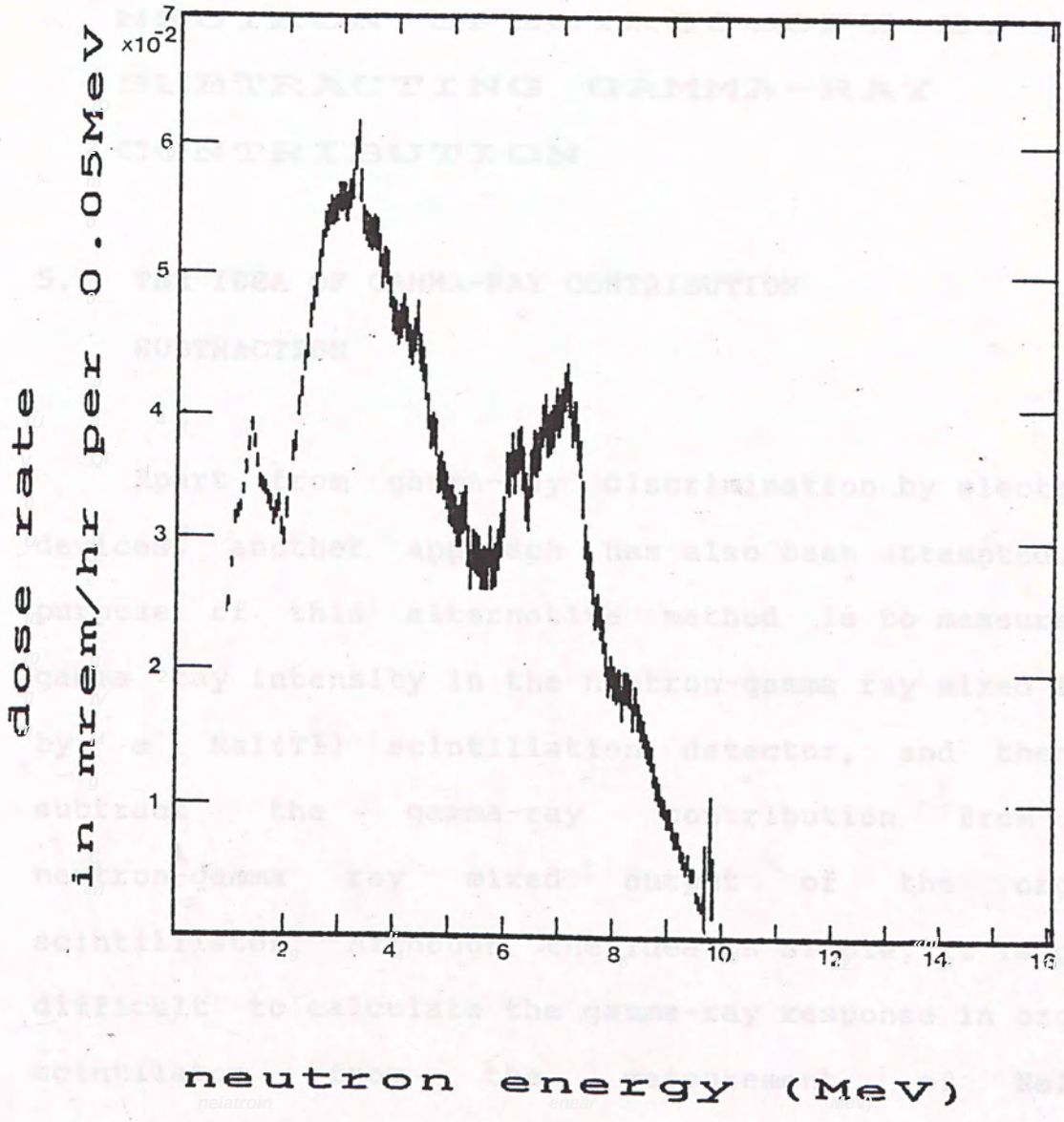

Figure 4.11b The differential dose-rate calculated from Figure 4.11a.

CHAPTER 5

NEUTRON SPECTROSCOPY BY SUBTRACTING GAMMA-RAY CONTRIBUTION

5.1 THE IDEA OF GAMMA-RAY CONTRIBUTION SUBTRACTION

Apart from gamma-ray discrimination by electronic devices, another approach has also been attempted. The purpose of this alternative method is to measure the gamma ray intensity in the neutron-gamma ray mixed field by a NaI(Tl) scintillation detector, and then to subtract the gamma-ray contribution from the neutron-gamma ray mixed output of the organic scintilllator. Although the idea is simple, it is quite difficult to calculate the gamma-ray response in organic scintilator from the measurement of NaI(Tl) scintillation detector.

Some investigators have studied the ability of organic scintillator in detecting the gamma-ray spectrum in a neutron-gamma ray mixed field.

N.A. Lurie, L. Harns,Jr and J.C. Young have calculated the gamma-ray response of a liquid organic scintillator (NE213).[51] They used the Monte

Carlo method to calculate the gamma-ray response and presented them in matrix form. The gamma spectrum can be calculated, in the same way as the neutron spectrum unfolding, from the raw output of NE213 by matrix-inversion method.

D.T. Ingersoll and B.W. Wehring have also constructed a gamma-ray response matrix to unfold the gamma-ray spectrum from raw data recorded by NE213.[52] They used an eletron accelerator combined with a bremsstrahlung monochromator to generate more than 100 monoenergetic gamma-rays within the energy range, 0.6 to 11.5MeV. However, matrix elements below 2MeV were constructed from the interpolation of the response functions from radioisopes.

Besides, P.K. Ray and E.S. Kenney have used a proton recoil counter to measure the neutron spectrum in a neutron-gamma ray mixed field by means of subtracting the gamma response.[53] They measured the response functions of five monoenegetic gamma-ray sources (namely, Au-198, Cs-137, Mn-54, Na-22 and Al-28). The reponse functions were used to interpolate 20 response functions for 20 gamma-ray enegries between 0.2755 and 2.0459MeV. Each response function was grouped into 20 channels. Hence, a 20x20 response matrix was constructed. The non-zero elements in the matrix are of triangular shape as shown in Figure 5.1. It is because

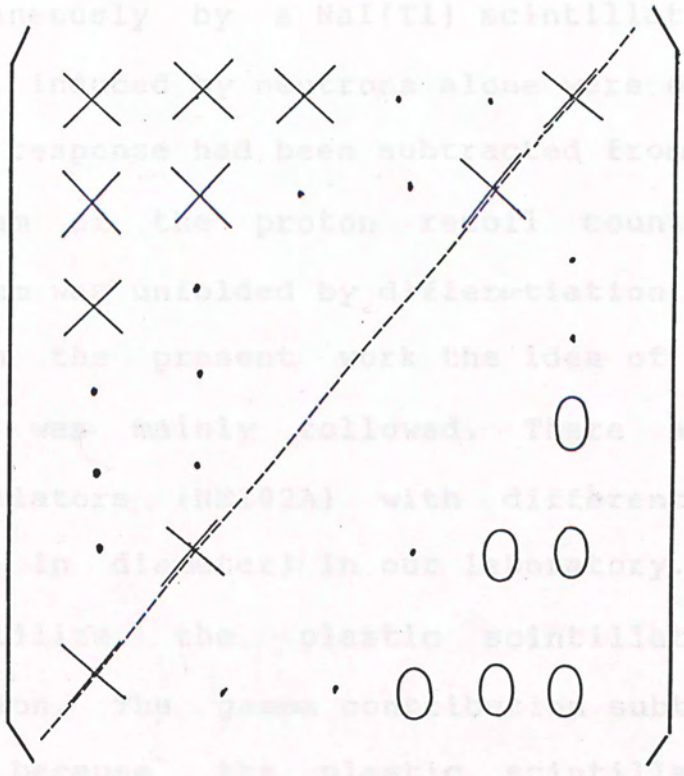

Figure. 5.1 The shape of nonzero elatments in the matrix formed by Ray and Kenney. (Ref 53)

low energy gamma-rays only produce counts in the low channel numbers. The gamma intensity was measured simultaneously by a NaI(Tl) scintillation detector. The events induced by neutrons alone were obtained after the gamma response had been subtracted from the pulse height spectrum of the proton recoil counter. The neutron spectrum was unfolded by differentiation method.

In the present work the idea of P.K. Ray and E.S. Kenney was mainly followed. There are many plastic scintillators (NE102A) with different sizes (from 12cm to 1m in diameter) in our laboratory. And it arouse me to utilize the plastic scintillatiors in neutron detection. The gamma contribution subtraction method is used because the plastic scintillator has no PSD property.

The gamma response function for a given energy can be calculated by interpolation. Since only limited number of monoenergetic gamma-ray sources are available, the technique of interpolation is critical. At the same time, the response functions doesn't need to be expressed in matrix form because gamma-ray spectroscopy using organic scintillator is not required.

Two schemes have been attempted to interpolate the gamma reponse functions for various gamma-ray energy. They are presented in section 5.2, some details of them would be further explained later on.

5.2 SCHEMES OF GAMMA-RAY RESPONSE CONSTRUCTION

The first scheme follows the following steps:

1. The gamma-ray output of several monoenergetic gamma-ray sources is taken by organic scintillator and then fitted by Tchebychev polynomials. Only the region between channels corresponding to electron energies AE_c and BE_c is considered. Where E_c is the energy of electron corresponding to the compton edge, A and B are constants and B is greater than A.

2. The gamma response function of each monoenergetic source is reproduced by the Tchebychev polynomials and is presented in 100 equal partition points. This procedure would smooth the response function. The total counts of the 100 points are normalized such that it would be equal to the total counts within AE and BE recorded by the organic scintillator in one second when the monoenergetic gamma-ray flux intensity can produce 10000 counts per second of photopeak area in the NaI(Tl) scintillation detector. The NaI(Tl) scintillator is placed at the side of the organic scintillator and detects the gamma-ray simultaneously. The details would be explained in section 5.5.

3. The gamma response functions of energy from 0.35MeV to 4.45MeV in 0.05MeV increment are interpolated between

the known monoenergetic gamma-ray response functions formed in step2. The channels are treated independently. The counts at channel i from gamma-ray of energy E (C(i,E)) is interpolated from the known counts produced by the monoenergetic gamma-ray sources in the same channel. For example, if there are S monoenergetic gamma response functions formed in step2, then there are S known points in the channel i. Let them be C(i,Ek) for k=1 to s. The value of C(i,E) is then interpolated from the values of C(i,E1) to C(i,Es). Cubic spline interpolation is used now.

4. The interpolated gamma response functions are fitted by Tcheychev polynomials again. The coefficients of Tchebychev polynomials are stored in floppy disc. Hence, 83 set data of the coefficients are stored.

5. When neutrons are detected in the neutron-gamma ray mixed field, the NaI(Tl) scintillator and the organic scintillator are placed together and are operated simultaneously. The energies of the detected gamma-ray are obtained from the pulse height spectrum recorded by NaI(Tl) scintillation detector. The pulse height spectrum is analysed by the method described in chapter 3. Then the coefficiencts of Tchebychev polynomials corresponding to the gamma-ray energies are read from floppy disc. The gamma-ray response in organic scintillator is then simulated by the Tchebychev

polynomials. Its total counts is nomalized to match the photopeak area in NaI(Tl) scintillation detector and the counting time of organic scintillation detector. The gamma-ray response for different gamma-ray energy is calculated independently and their summation gives the total gamma-ray response.

6. The resulting gamma-ray response is subtracted from the raw output of organic scintillation detector. The residue is considered to be the neutron induced counts and is unfolded by differetiation method.

This scheme is carried out by computer programs and is labelled as GSTI (Gamma contribution Subtraction using Tychebychev polynomials and Interpolation method) in the following text.

In fact, the coefficients of the Tchebychev polynomials is like a response matrix of which the elements in each row are parametized.

The second scheme is a simplified version of GSTI method. It includes the following steps:

1. The gamma-ray pulse height spectra of monoenegetic gamma-ray sources are recorded by the organic scintillation detector and are grouped into 100 channels between AE_c and BE_c without any fitting and smoothing.

2. Apply cubic spline interpolation between the gamma-ray responce functions grouped in step 1. Each channel consists of S known pairs if S monoenergetic

gamma-ray sources are used and the channels are treated independently like the treatment in the GSTI method. Each known point at the same channel is characterized by two quantities, namely, the gamma energy (E) and the counts (C(i,E)). These two quantities are treated as the independent variable (x) and dependent variable (f(x)) in the cubic spline interpolation. As explained in appendix A, after the slopes at the known points have been solved, the counts at gamma-ray energy (E) can be calculated from the values of slopes, counts and energies at the known points of the same channel. However, E must be within the energy bounded by the energies of the monoenergetic sources. Instead of storing the coefficients of Tchebychev polynomials, the values of slopes, counts and energies at the known points are stored in the floppy disc.

3. After neutron-gamma ray mixed output is recorded by the organic scintillation detector, the interpolated gamma contribution is subtracted from this output. The resulting pulse height is then unfolded by differentiation method. The intensity of the gamma-ray flux and the counting time of organic scintillator must be considered as descibed in the GSTI method.

This scheme is labelled as GSI (Gamma contribution Subtraction using Interpolation method) in the following text.

o

Figure 5.2 illustrates the interpolation scheme of GSI.

Some details of the interpolation method and gamma-ray contribution subtraction method are explained in section 5.3, 5.4 and 5.5. It includes : 1) the reason of limiting the energy range of each gamma-ray response function within AE_c and BE_c , 2) the reason of using Tchebychev polynomials to fit the gamma-ray response and 3) the procedure of normalizing the interpolated gamma-ray response in order to match the actual gamma-ray intensity.

5.3 SCALING OF COMPTON DISTRIBUTION

Gamma-rays of energy E can produce electrons by compton scattering from the atoms in organic scintillators. The electrons so produced have energy up to E_c which is expressed as:

$$E_c = E / (1+0.511/2E)$$

A continuous distribution in the output of the scintillation detector is formed below E_c and is called compton distribution. If the gain of the amplifier system is fixed, different shapes of compton distributions would be observed in the M.C.A. when gamma-rays of different energies are detected. Hence, direct interpolation between the raw pulse height

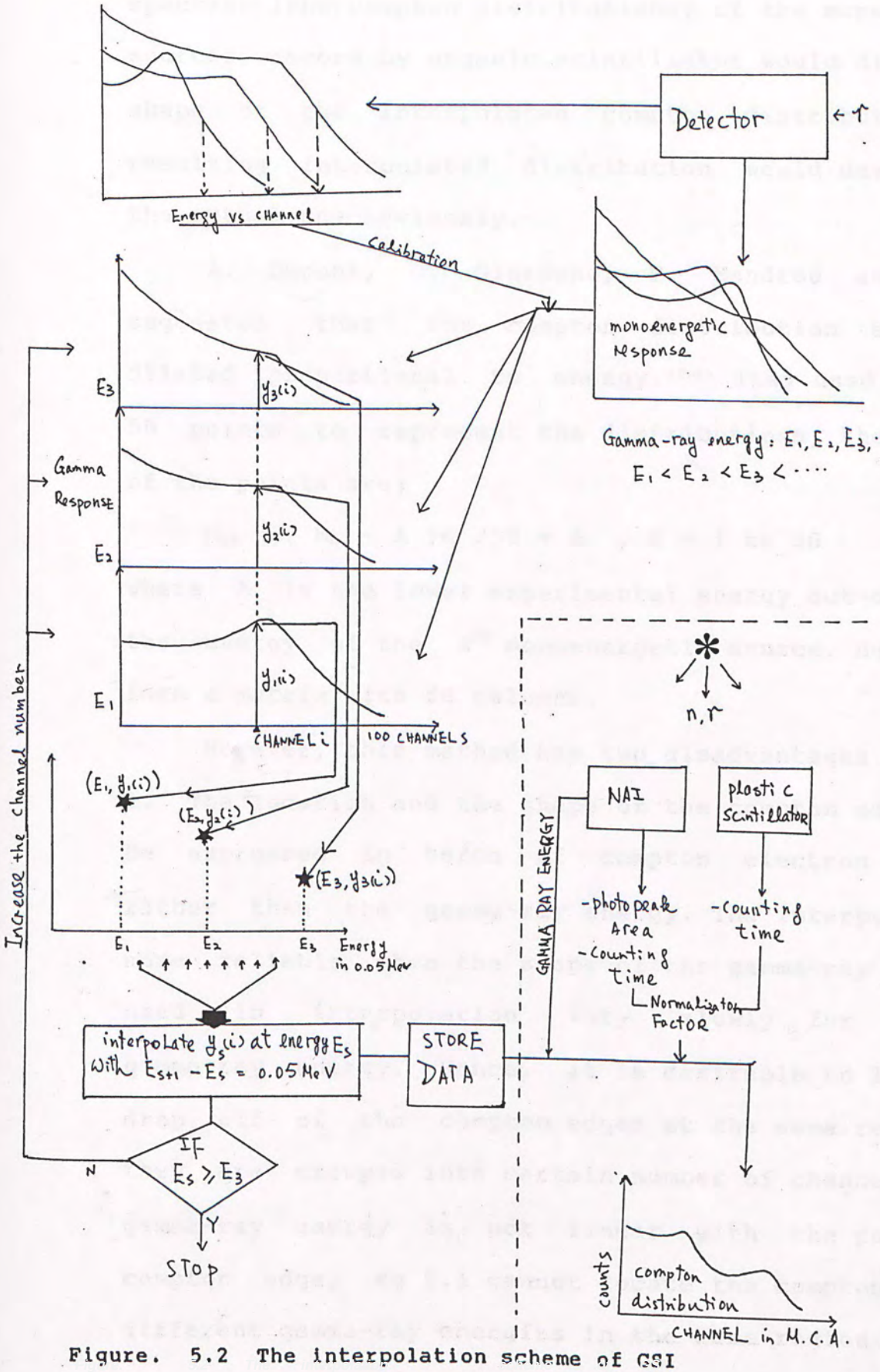

Figure. 5.2 The interpolation scheme of GSI

spectra (the compton distributions) of the monoenergetic sources record by organic scintillator would distort the shape of the interpolated compton distribution. The resulting interpolated distribution would deviate from the actual one seviously.

A. Dupont, G. Giordano, P. Mandrou and M. Niel suggested that the compton distribution should be dilated proportional to energy.[54] They used 50 points to represent the distributions, the energies of the points are:

$$E_{sk} = (E_s - A)K /50 + A \quad , K = 1 \text{ to } 50 \qquad (5.1)$$

Where A is the lower experimental energy cut-off. E_s is the energy of the S^{th} monoenergetic source. Hence, they form a matrix with 50 columns.

However, this method has two disadvantages.

1. The location and the shape of the compton edge should be expressed in terms of compton electron energy E_c rather than the gamma-ray energy. The interpolation is more reliable when the shape of the gamma-ray responses used in interpolation vary slowly for different gamma-ray energy. Hence, it is desirable to locate the drop off of the compton edges at the same region when they are grouped into certain number of channels. Since gamma-ray energy is not linear with the position of compton edge, eq 5.1 cannot locate the compton edges of different gamma-ray energies in the same region.

2. If a constant cut-off energy is set, different portions of the compton distribution for different gamma-ray energies would be selected. This effect is illustrated in Figure 5.3. The portions so selected have different shapes and make the results of interpolation unreliable.

Thus, the region AE_c to BE_c is selected in the present work. The pulse height spectrum within this energy range is grouped into 100 channels. The pulse height spectrum of each monoenergetic gamma-source is grouped in this way. The energy of the n^{th} channel is expressed as:

$$E_n = n(BE_c - AE_c)/100 + AE_c - (BE_c - AE_c)/100 \qquad (5.2)$$

The boundaries of this channel are

$$(n-1)(BE_c - AE_c)/100 + AE_c$$

and $$n(BE_c - AE_c)/100 + AE_c$$

Hence, the width of each channel is $(BE_c - AE_c)/100$, as expected.

The gamma ray responses of some monoenergetic sources were measured by NE213 and have been grouped into 100 channels. The results are shown in Figure 5.4. The performance of this method is satisfactory.

5.4 THE FITTING OF COMPTON DISTRIBUTION

Although some analytical formulae were suggested to

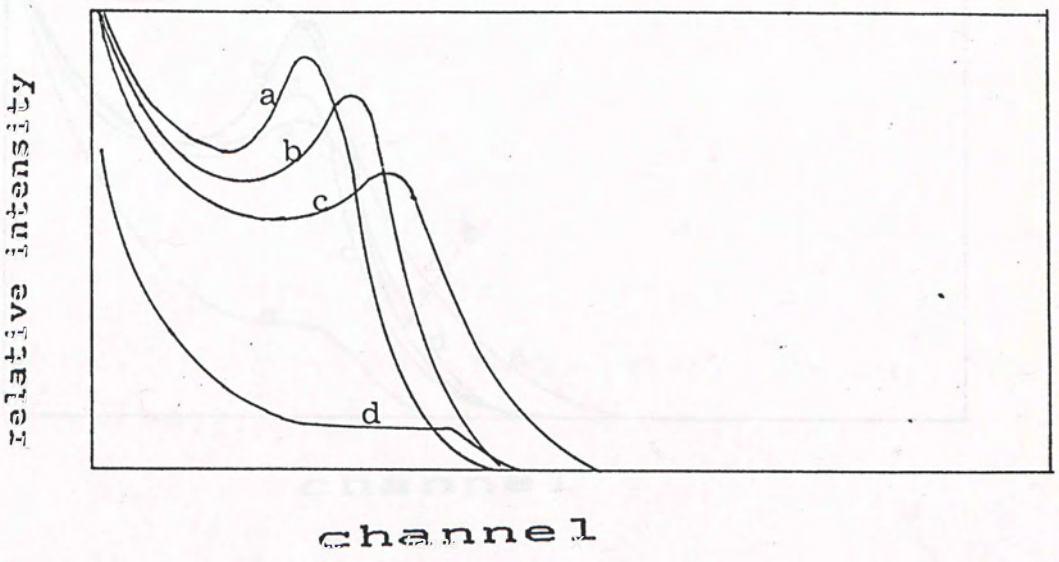

Figure. 5.3 The compton distributions after grouping. The constant cutoff energies are used. Curves a, b, c, d are produced by Cs-137, Mn-54, Co-60 and isotope Am-Be, respectively.

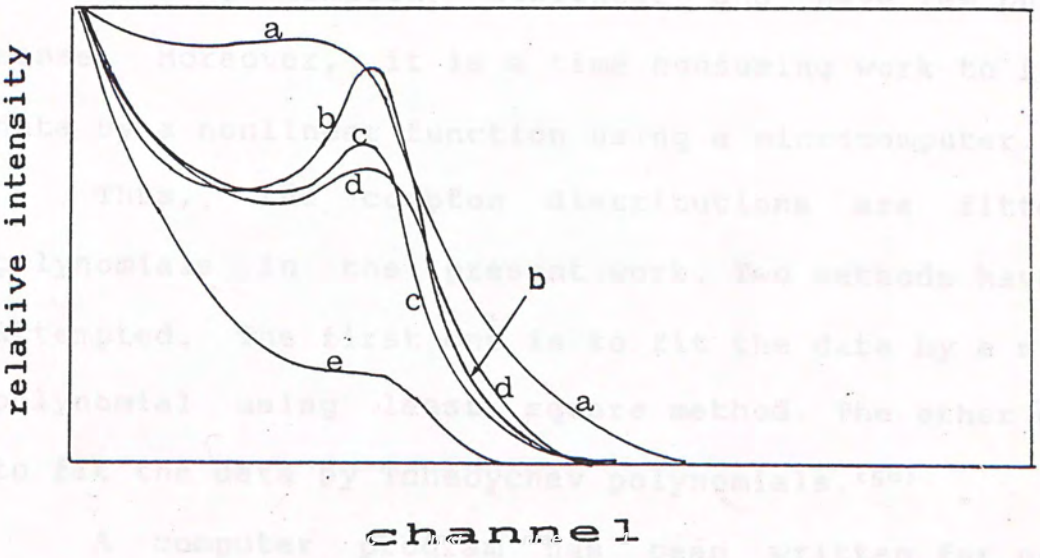

Figure. 5.4 The compton distributions after grouping. The cutoff energies are proportional to gamma -ray energies.
Curves a, b, c, d and e are produced by Ba-133, Co-60, Mn-54, Cs-137 and isotope Am-Be, respectively.

fit the gamma-ray induced pulse height spectrum, they are usually complex, nonlinear and have few physical sense. Moreover, it is a time consuming work to fit the data by a nonlinear function using a microcomputer.

Thus, the compton distributions are fitted by polynomials in the present work. Two methods have been attempted. The first one is to fit the data by a n-order polynomial using least square method. The other one is to fit the data by Tchebychev polynomials.[54]

A computer program has been written for n-order polynomial least square fitting. From 2-order up to 25-order polynomials have been tried. Figure 5.5 shows some results of the fitting. Instability in high orders can be observed in Figure 5.5. The unpredictabe oscillations may be caused by the singularity property of the matrix used in the calculating process.

Tchebychev polynomial, which is discussed in most text book about numberical method, is a optimized least square polynomial fitting and is commonly used. The undesirable oscillations can be avoided in the Tchebychev polynomial fitting. A computer program has been written to perform the fitting. The compton distribution of Cs-137 is fitted and the result is shown in Figure 5.6. The polynomials can fit the experimental data very well when 20 terms and 25 terms are used.

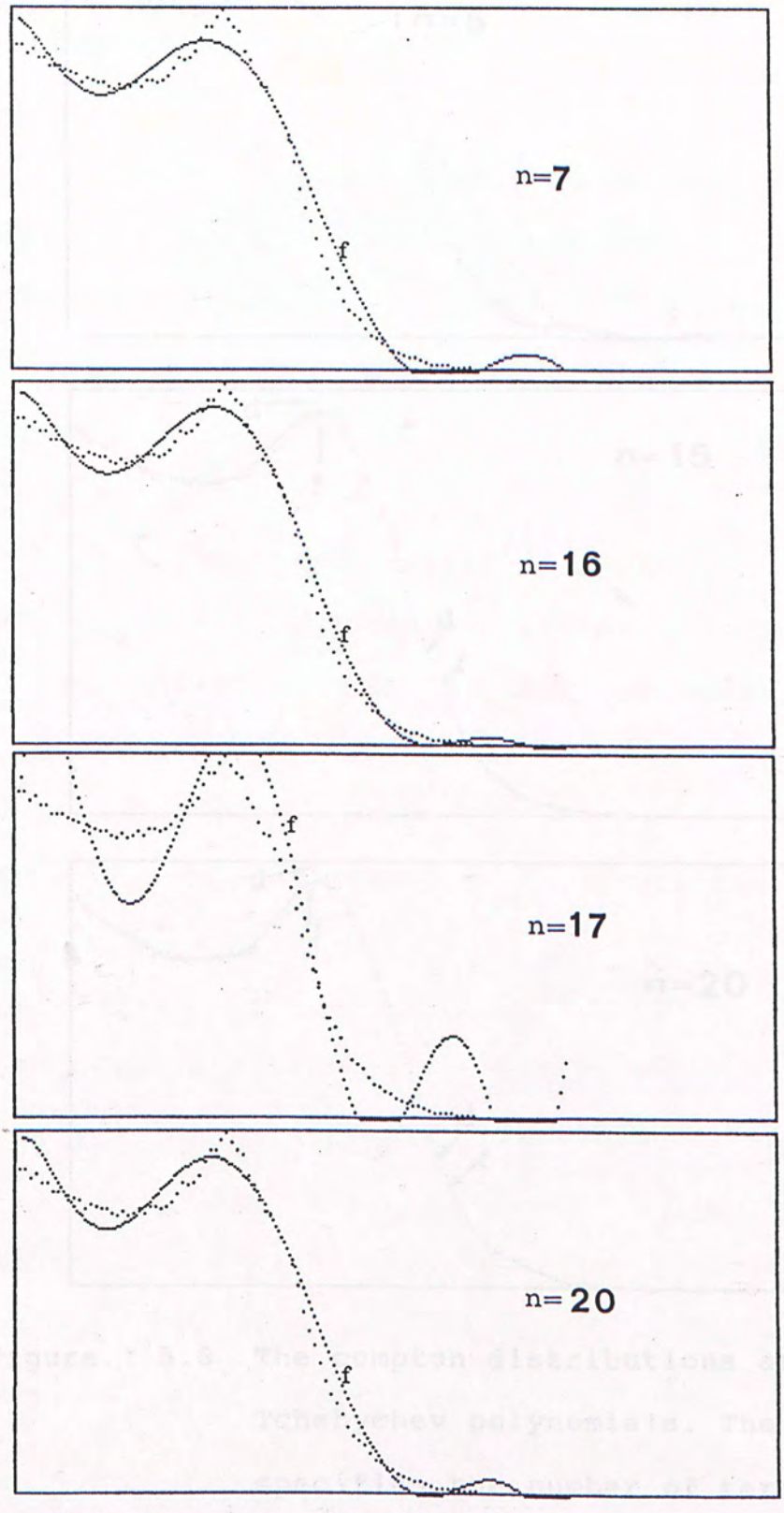

Figure. 5.5 The compton distributions are fitted by n-order polynomials. The values of n are given in each graph. The letter 'f' specifies the fitting curves.

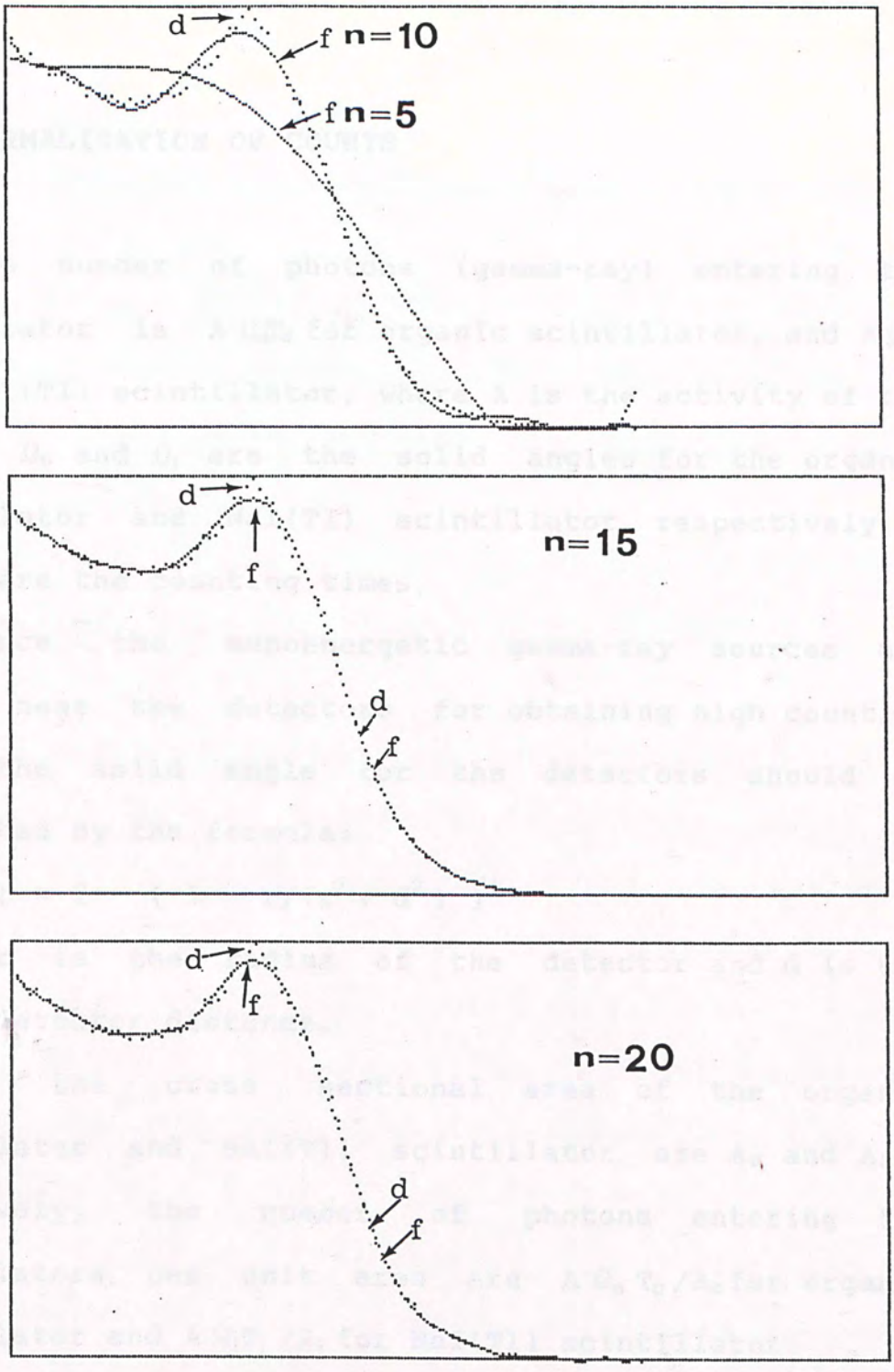

Figure. 5.6 The compton distributions are fitted by Tchebychev polynomials. The letter 'n' specifies the number of terms . 'f' and 'd' specify the fitting values and the raw data. The raw data and fitting values are nearly overlap when n=15 and 20.

5.5 NORMALIZATION OF COUNTS

The number of photons (gamma-ray) entering the scintillator is $A\,\Omega_o T_o$ for organic scintillator, and $A\,\Omega_i T_i$ for NaI(Tl) scintillator, where A is the activity of the source. Ω_o and Ω_i are the solid angles for the organic scintillator and NaI(Tl) scintillator, respectively. T_o and T_i are the counting times.

Since the monoenergetic gamma-ray sources are placed near the detectors for obtaining high counting rate, the solid angle for the detectors should be calculated by the formula:

$$\Omega = 2 \left(1 - r/(r^2 + d^2) \right)^{1/2}$$

where r is the radius of the detector and d is the source-detector distance.

If the cross sectional area of the organic scintillator and NaI(Tl) scintillator are A_o and A_i, repectively, the number of photons entering the scintillators per unit area are $A\,\Omega_o T_o / A_o$ for organic scintillator and $A\,\Omega_i T_i / A_i$ for NaI(Tl) scintillator.

After the pulse height spectra of the monoenergetic gamma-ray have been taken by the scintillation detectors, the photopeak area (in counts) from NaI(Tl) scintillation detector is multiplied by the following factor:

$$\left(A\,\Omega_o T_o / A_o \right) / \left(A\,\Omega_i T_i / A_i \right)$$

In other words,

New photopeak area = photopeak area x $\Omega_o T_o A_i / \Omega_i T_i A_o$

(5.3)

Eq 5.3 normalized the counts of NaI(Tl) scintillator such that the photon flux entering the organic scintillator and that entering the NaI(Tl) scintillator are equal.

Besides, the counts recorded by organic scintillator are also multiplied by the factor

$$\frac{10000}{T_n \text{(second)} \times \text{photopeak area after correction}}$$

This factor normalizes the counts rate recorded by the organic scintillator to the intensity of gamma-ray which produces 10000 counts photopeak area in the NaI(Tl) scintillation detector. In fact, this factor standardizes the intensity of monoenergetic gamma-rays which are used to interpolate the gamma-ray response at other energies.

The gamma-ray responses in the organic scintillation detector after normalization by above procedure are used in GSTI and GSI method described in section 5.2.

In the use of plastic scintillator for neutron monitoring in the neutron-gamma ray mixed field, the photopeak area recorded by the simultaneously operated NaI(Tl) scintillation detector is corrected by eq. 5.3.

The gamma-ray response in organic scintillator is interpolated according to the energies of gamma-ray. The gamma-ray response is simulated by Tchebychev polynomials if GSTI method is used. The resulting gamma-ray response is then multiplied by the factor

$$\frac{T_0 \text{ (second)} \times \text{photopeak area after correction}}{10000}$$

Hence, the interpolated gamma-ray response in organic scintillator can match the actual intensity of the gamma-ray and the counting time.

The advantage of such normalizing method is obvious. If the source is placed far from the detectors, the solid angles can be approximated by:

Counting area of scintillator/source-detector distance^2

and eq.5.3 can be simplified as :

New photopeak area = photopeak area x T_0/T_i

No geometical factors are involved.

The values of $\Omega_0 A_i / \Omega_i A_0$ is an indicator to evaluate whether the distance between the source and the detectors is 'far' or not.

If the radius of the organic scintillator and the NaI(Tl) scintillator are 6cm and 3.8 cm respectively, the values of $\Omega_0 A_i / \Omega_i A_0$ for various source-detector distances have been calculated and are plotted in Figure 5.7. Since the source-detectors distance is usually greater than 1m in the large area radiation monitoring,

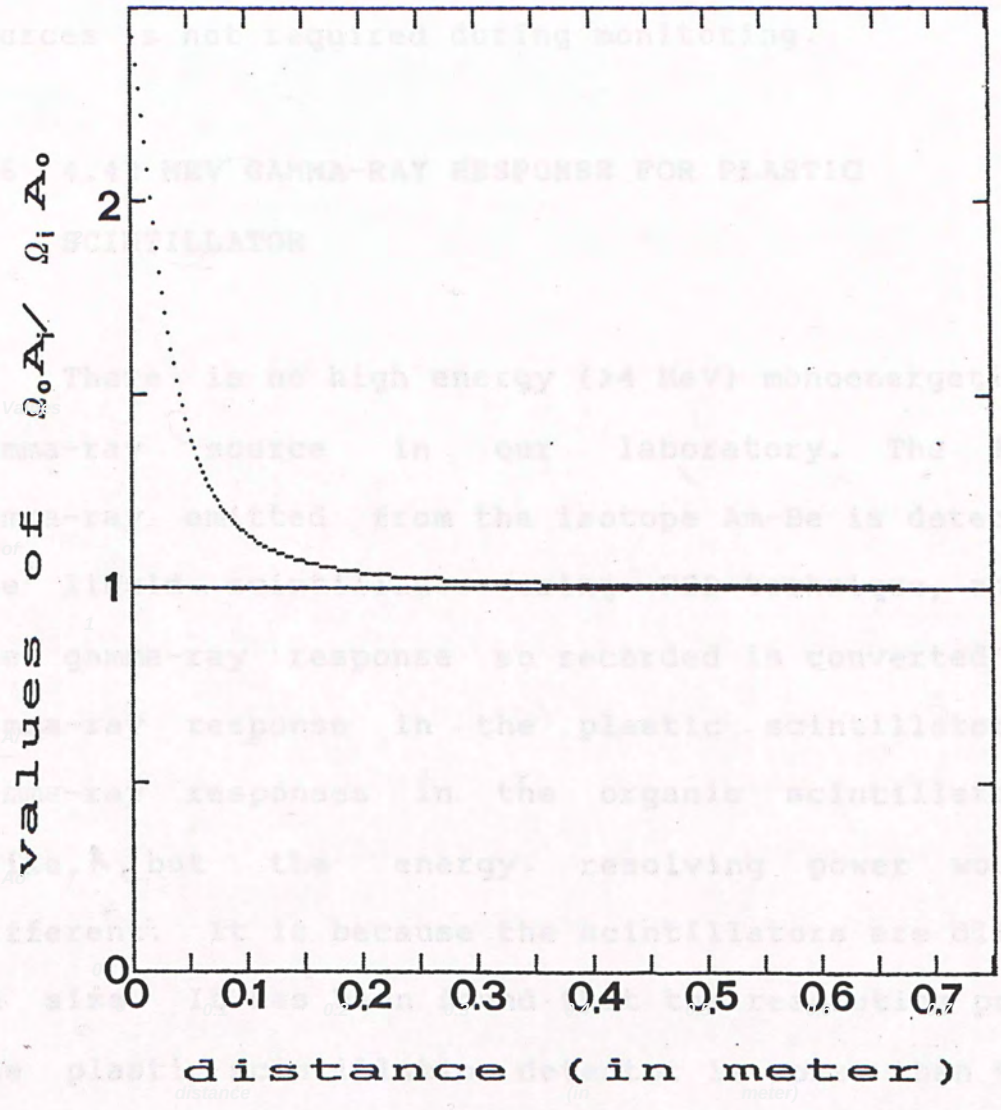

Figure. 5.7 Valus of $\Omega_o A_i / \Omega_i A_o$ for various distance.

the factor $\Omega_o A_i / \Omega_i A_o$ can be approximated by 1. It means that precise knowledge of the actual positions of the sources is not required during monitoring.

5.6 4.43 MEV GAMMA-RAY RESPONSE FOR PLASTIC SCINTILLATOR

There is no high energy (>4 MeV) monoenergetic pure gamma-ray source in our laboratory. The 4.43MeV gamma-ray emitted from the isotope Am-Be is detected by the liquid scintillator using PSD technique, and then the gamma-ray response so recorded is converted to the gamma-ray response in the plastic scintillator. The gamma-ray responses in the organic scintillators are alike, but the energy resolving power would be different. It is because the scintillators are different in size. It has been found that the resolution power of the plastic scintillation detector is worse than that of the liquid scintillation detector. Hence, the gamma-ray responses of the two scintillation detectors can be related in the form:

$$C_p(i) = \sum_{x=0}^{100} C_L(x) \sqrt{c/\pi} \exp(-c(i-x)^2) \qquad (5.4)$$

Where $C_p(i)$ is the counts in the plastic scintillation detector at channel i. $C_L(x)$ is the counts in the liquid scintillation detector at channel x. The gamma-ray responses have been grouped into 100 channels.

The effect of eq. 5.4 is to fold the gamma-ray response in liquid scintillation detector by gaussians. The FWHM of the gaussians need not be the same. We assume that the FWHM of the gaussians relates the channel number of the M.C.A. linearly.

Since $c = 4 \ln 2 / FWHM^2$, c can be expressed as:

$$c = 1 / (ax+b)^2$$

Where a and b are determined by minimizing the following quantity:

$$\sum_{i=5}^{95} \{ C_p'(i) - \sum_{x=0}^{100} C_L'(x) [\exp(-((i-x)/(ax+b))^2) / \sqrt{\pi}(ax+b)] \}^2$$

Where $C_p'(i)$ and $C_L'(x)$ are the counts of neutron-gamma ray mixed outputs in the plastic and the liquid scintillation detectors. In the present case, a and b are found to be -0.005243 and 2.2540, respectively.

Since the scintillations produced by proton in plastic scintillator and liquid scintillator are not the same, this method will slightly distort the 4.43MeV gamma-ray response in the plastic scintillator. The gamma-ray response construted in this way is used for interpolation.

5.7 THE PROGRAM OF GSI METHOD FOR PLASTIC SCINTILLATOR

Computer programs for GSTI and GSI methods have

been completed. These programs are tested for the NE213 liquid scintillator by measuring the neutron energy spectrum of an isotope Am-Be. The results are shown in Figure 5.8a and 5.8b. Although GSTI method can generate smoother gamma-ray response, the results of GSTI and GSI methods are nearly the same. Only GSI method is used on the plastic scintillator because the running time of GSTI method is longer than the running time of GSI method.

As mentioned previously, the 100 channel gamma-ray response function is calculated by the values of slopes, counts and energies at the known points. However, the resulting gamma-ray response function is not the actual compton distribution recorded by the M.C.A with 1024 channels. The actual compton distribution in the M.C.A output is obtained as following:

1. The total counts of the 100 channel gamma-ray response is corrected by multiplying the factor 'T_0 x photopeak area in NaI(Tl) scintillator/10000'. Let the total counts after correction be TC.
2. The electron energy-channel relation is calibrated by gamma-ray sources as described in chapter 4.
3. The channel numbers corresponding to AE_c and BE_c are calculated and labelled as CA and CB, respectivly . Negative channels and channels beyond 1023 are also used.

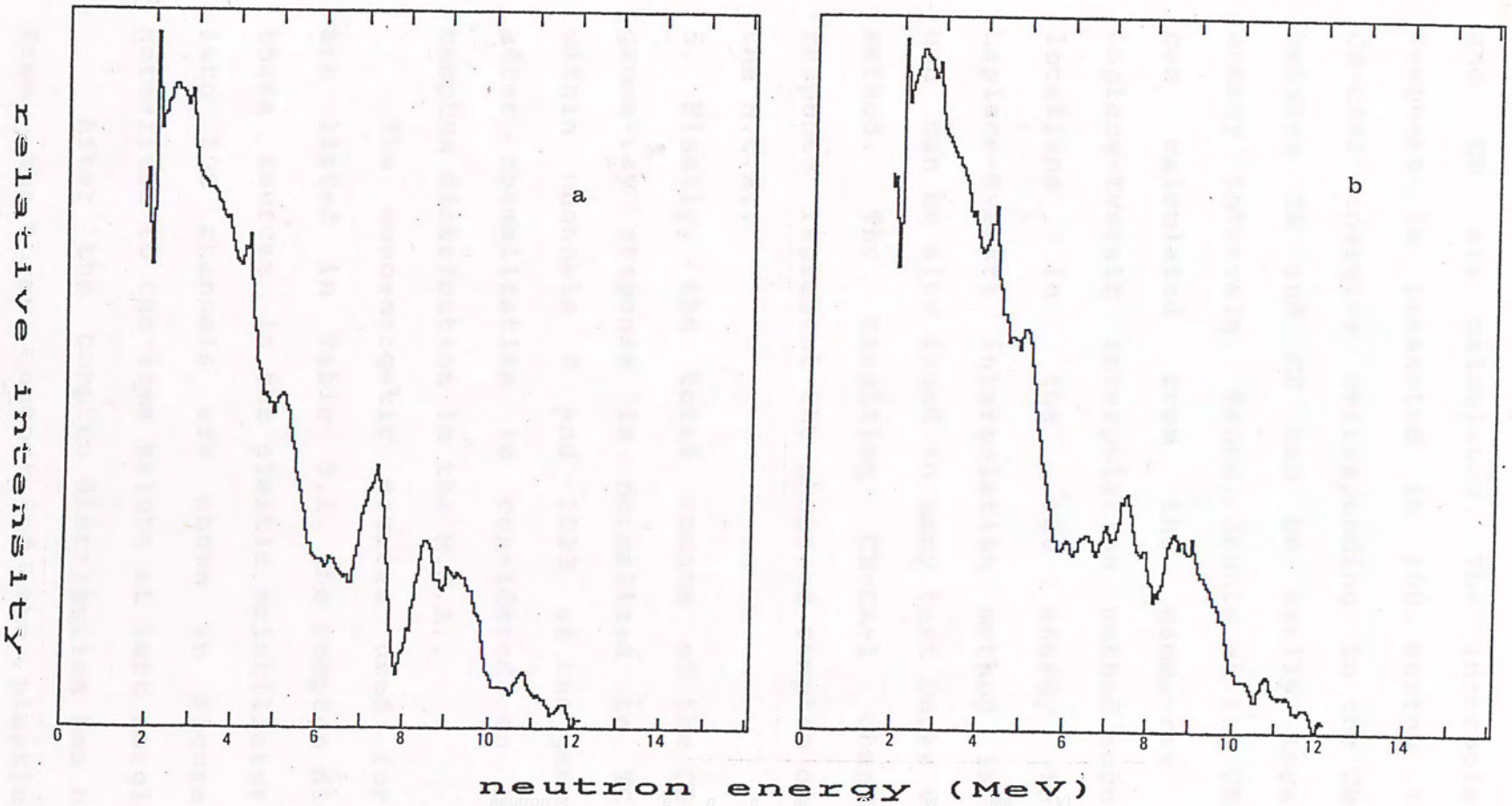

Figure. 5.8 The neutron spectrum of isotope Am-Be.
Figure a is the result given by GSTI and
figure b is the result given by GSI.

4. The energies correponding to each channel between CA and CB are calculated. The interpolated gamma-ray response is presented in 100 energy intervals. The CB-CA+1 energies corresponding to the CB-CA+1 channels between CA and CB can be easily located in the 100 energy intervals. Hence, counts at the CB-CA+1 energies can calculated from the gamma-ray response by Laplace-Everett interpolation method according to their locations in the 100 energy intervals. The Laplace-Everett interpolation method is commonly used and can be also found in many text books about numerical method. The resulting CB-CA+1 channels gamma-ray response represent the shape of compton dis t ribution in the M.C.A..

5. Finally, the total counts of the CB-CA+1 channels gamma-ray response is normalized to TC. The region within channels 0 and 1023 of the gamma-ray response after normalization is considered to be the actual compton distribution in the M.C.A..

The monoenergetic sources used for interpolation are listed in Table 5.1. The compton distributions of these sources in the plastic scintillator after grouped into 100 channels are shown in Figure 5.9. They are normalized to the same height at left margin.

After the compton distribution has been subtracted from the raw output of the plastic scintllation

TABLE 5.1 THE GAMMA-RAY SOURCES USED IN CSI

Sources	Energy (MeV)	Energy at compton edge (MeV)
Ba-133	0.356	0.207
Cs-137	0.662	0.477
Mn-54	0.835	0.639
Co-60	1.30	1.12
Am-Be	4.43	4.19

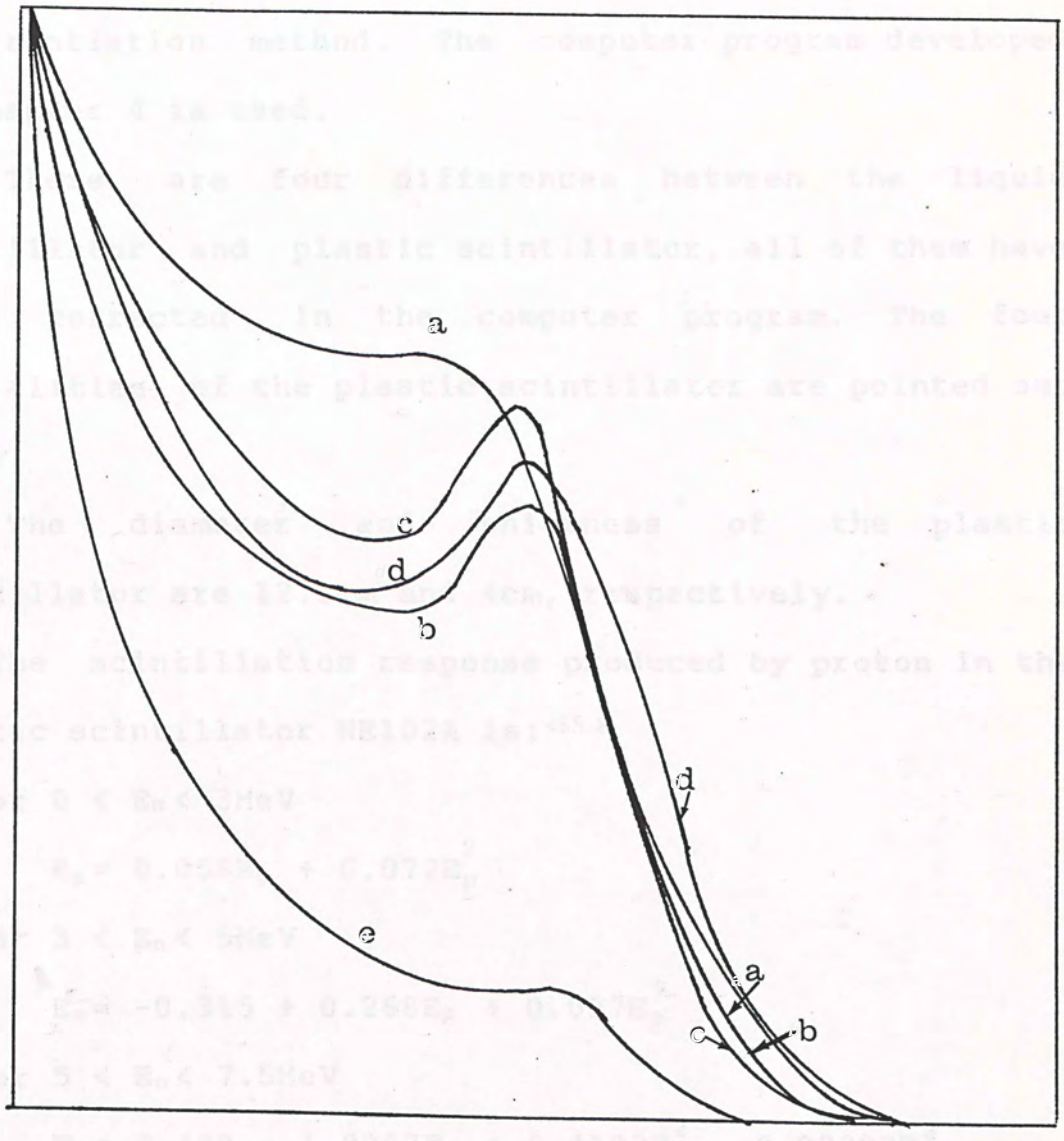

Figure. 5.9 The compton distribution of monoenegetic gamma-ray sources used in GSI. curves a, b, c, d and e are produced by Ba-133, Cs-137, Mn-54, Co-60 and isotope Am-Be, respectively.

detector, the neutron spectrum is unfolded by differentiation method. The computer program developed in chapter 4 is used.

There are four differences between the liquid scintillator and plastic scintillator, all of them have been corrected in the computer program. The four specialities of the plastic scintillator are pointed out below.

1. The diameter and thickness of the plastic scintillator are 12.2cm and 4cm, respectively.
2. The scintillation response produced by proton in the plastic scintillator NE102A is:[55]

for $0 < E_n < 3MeV$

$$E_e = 0.058E_p + 0.072E_p^2$$

for $3 < E_n < 5MeV$

$$E_e = -0.315 + 0.268E_p + 0.037E_p^2$$

for $5 < E_n < 7.5MeV$

$$E_e = 3.488 - 1.8287E_p + 0.4193E_p^2 - 0.02302E_p^3$$

for $7.5 < E_n < 30MeV$

$$E_e = 0.0424 + 2.3604 \times \sqrt{(1.0+0.10432(E_p-3.9255))^2}$$

Where E_p is the recoil proton energy, E_e is the equivalent electron energy in MeV which produces the equal light output as proton of energy E_p. E_n is the energy of neutrons which produce recoil protons.

The scintillation response of NE102A is shown in figure 5.10 taken from ref. [55]. The solid curve in the

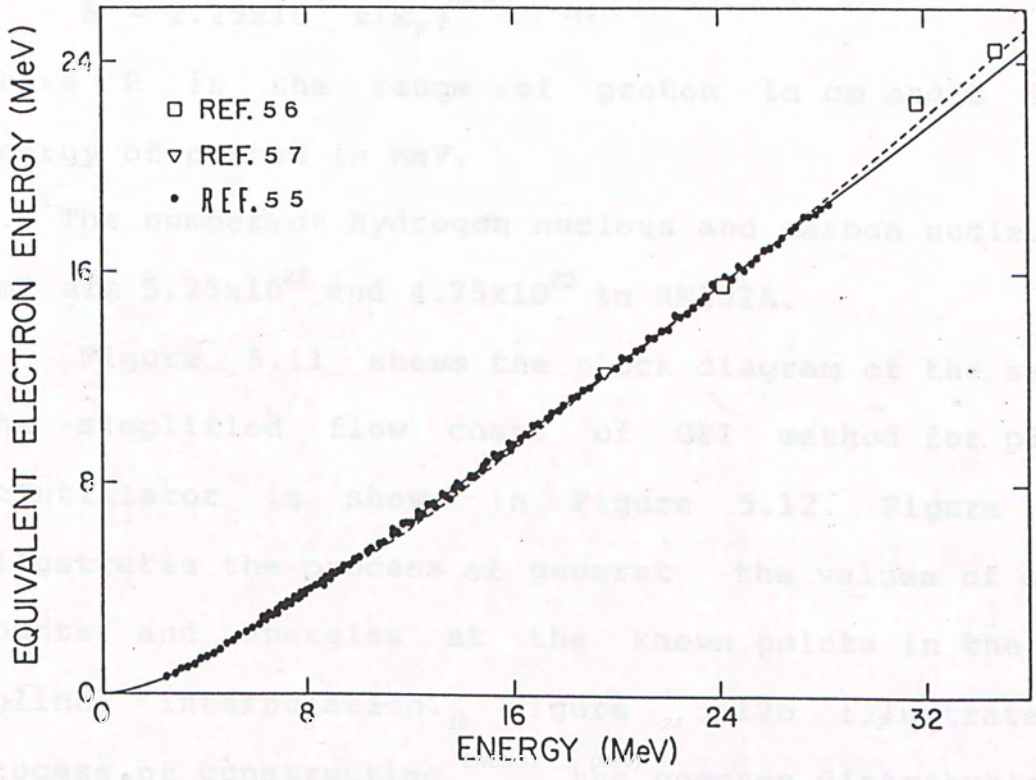

Figure. 5.10 The scintillation response of NE102A taken from ref.(55).

figure is given by the above formulae.

3. The range of proton (R) is required in eq. 4.7. The value of R in NE102A is given by the formula:

$$R = 2.25 \times 10^{-3} \times (E_p)^{1.76} \quad (5.8)$$

where R is the range of proton in cm and E is the energy of proton in MeV.

4. The numbers of hydrogen nucleus and carbon nucleus per cm^3 are 5.25×10^{22} and 4.75×10^{22} in NE102A.

Figure 5.11 shows the block diagram of the set up. The simplified flow chart of GSI method for plastic scintillator is shown in Figure 5.12. Figure 5.12a illustrates the process of generat the values of slopes, counts and energies at the known points in the cubic spline interpolation. Figure 5.12b illustrates the process of constructing the compton distribution in NE102A.

The performance of this method would be evaluated in chapter 7.

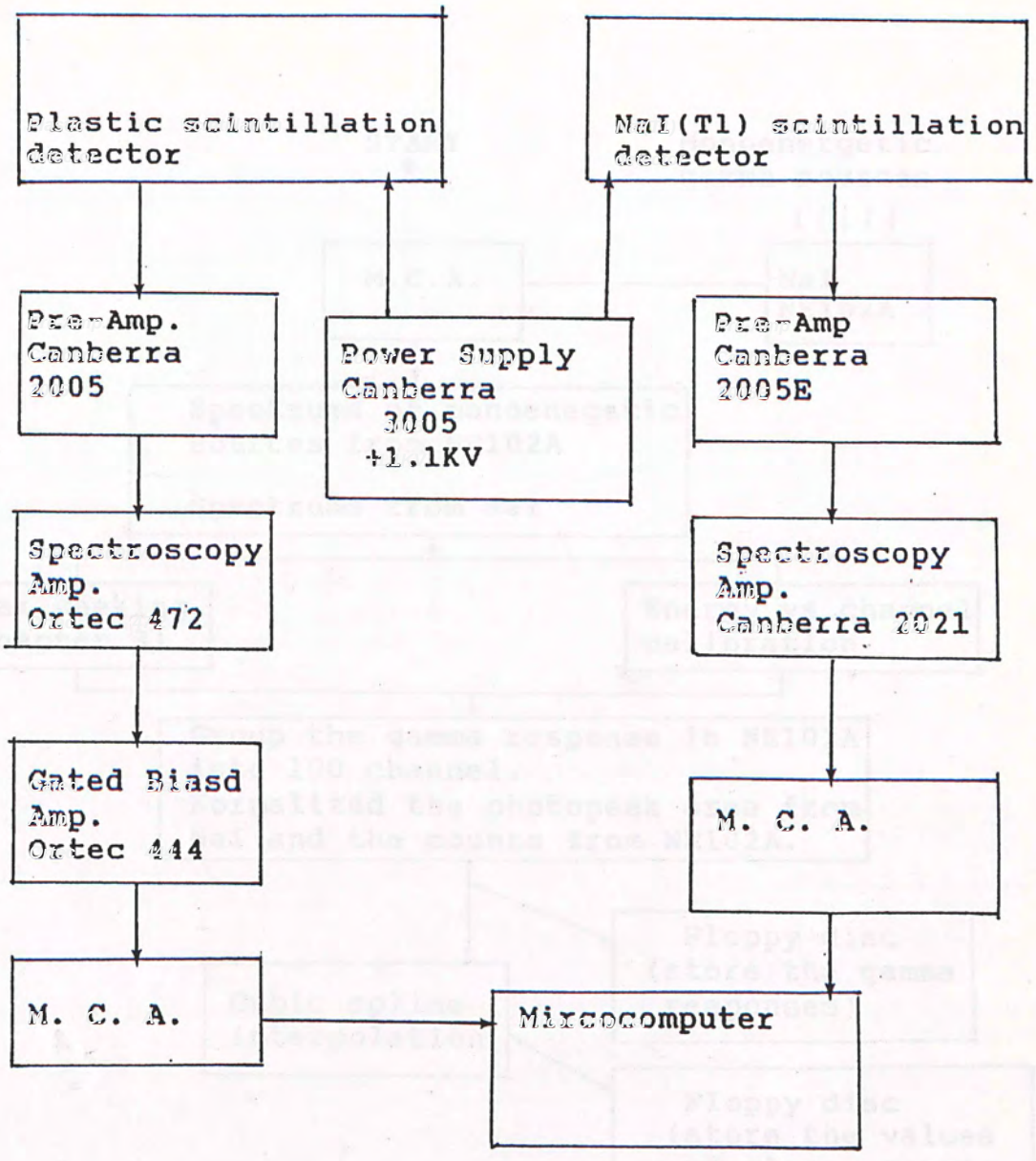

Figure 5.11 The block diagram of GSI system.

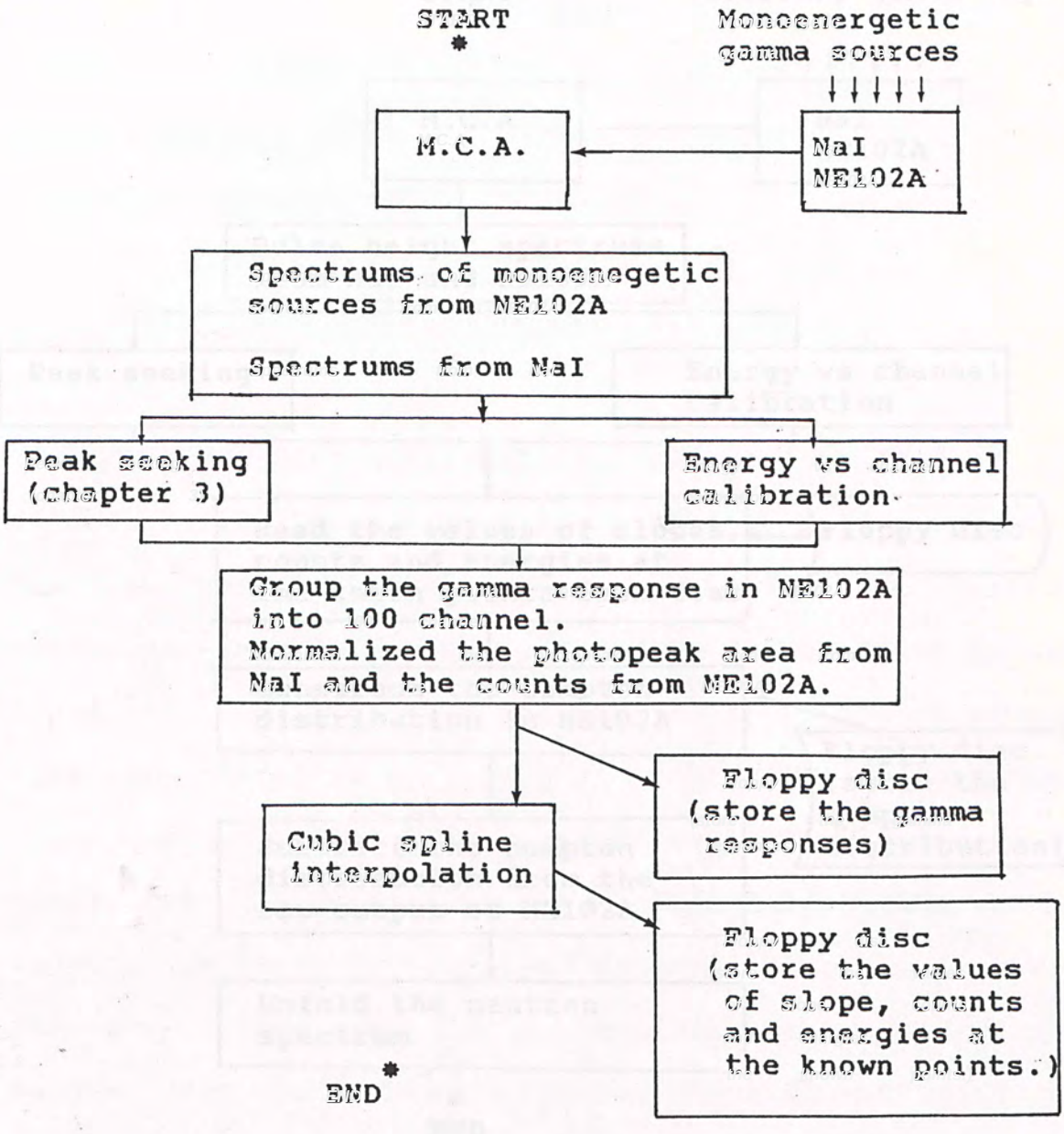

Figure. 5.12a The process of generating the values of slopes, counts and energies at known points in GSI.

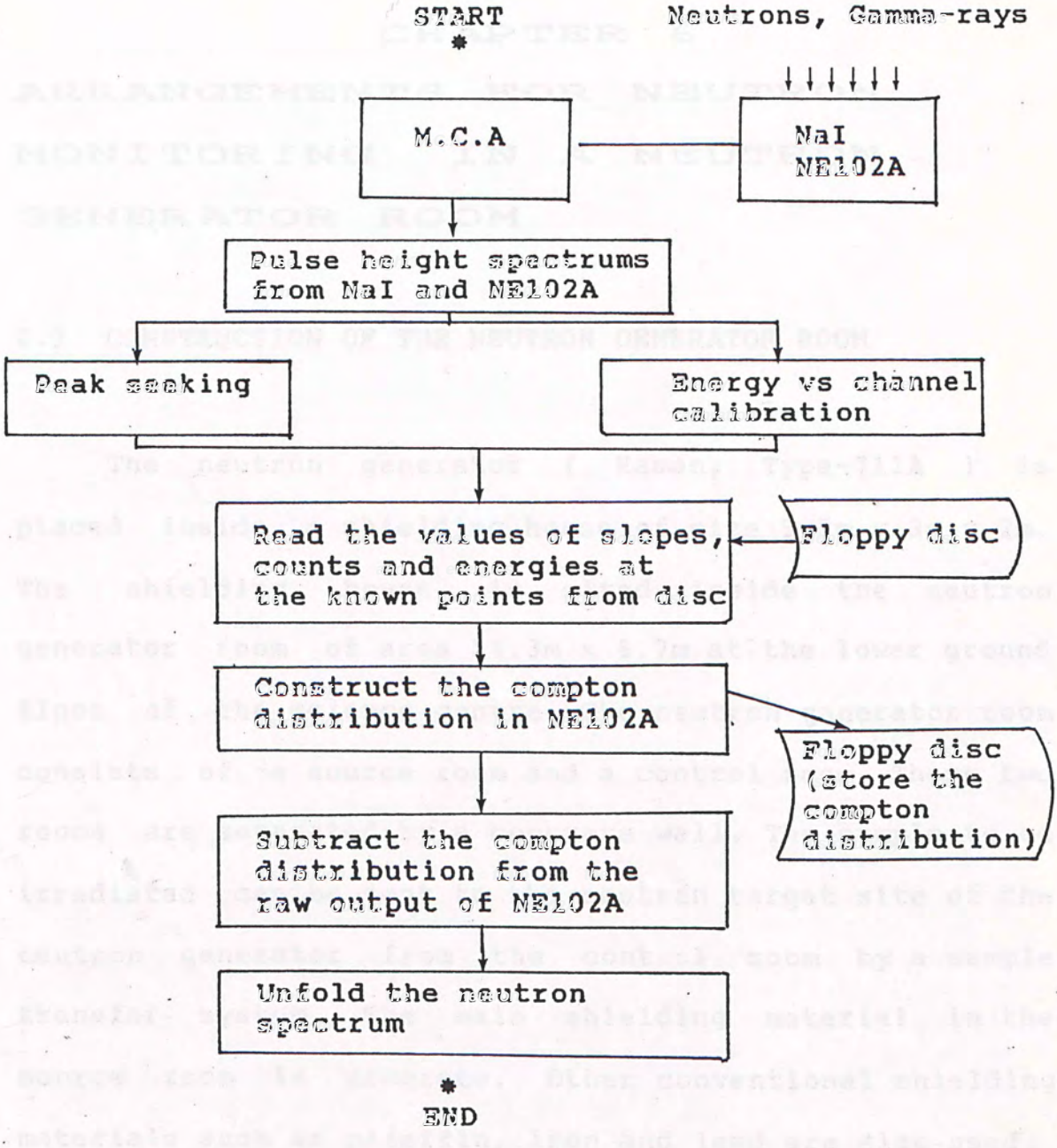

Figure. 5.12b The process of constructing compton distribution in NE102A in GSI.

CHAPTER 6

ARRANGEMENTS FOR NEUTRON MONITORING IN A NEUTRON GENERATOR ROOM

6.1 CONSTRUCTION OF THE NEUTRON GENERATOR ROOM

The neutron generator (Kaman, Type-711A) is placed inside a shielding house of size 9.3m x 3m x 2m. The shielding house is sited inside the neutron generator room of area 14.3m x 8.7m at the lower ground floor of the science centre. The neutron generator room consists of a source room and a control room. These two rooms are separated by a concrete wall. The sample to be irradiated can be sent to the neutron target site of the neutron generator from the control room by a sample transfer system. The main shielding material in the source room is concrete. Other conventional shielding materials such as paraffin, iron and lead are also used.

In addition to the neutron generator, an isotope Am-Be is also placed in the source room. The isotope is stored in a cyclindrical container which is filled of paraffin.

The construction of the neutron generator room in views of plan, longitudinal and transverse section are

shown in Figure 6.1 to 6.3. The graphs are obtained from ref.(59).

The isotope Am-Be is stored at location A and is sited 1.05m above ground at the location B marked in Figure 6.1 when it is in use.

6.2 THE BF_3 FLUX MONITOR

A BF_3 counter of dimension 2.5cm diameter x 12cm active length (20th Century Electronic Limited, Type 12EB20), which is surrounded by 6cm paraffin, is used as a total neutron flux counter. The counter is a type of moderator detector. Its structure is shown in Figure 6.4. The relative count-rate of a paraffin covered BF_3 counter depends on the thickness of the paraffin and the energy of neutrons detected. Figure 6.5 shows the energy dependence of the relative count-rate of a paraffin covered BF_3 counter for different paraffin thickness.[60]

As estimated in Figure 6.5, the neutron energy dependence of the count-rate would be considerably flat when the BF_3 counter is covered by 6cm paraffin. Hence, it is suitable to be used as a flux counter.

The absolute efficiency of this flux counter is calibrated by the isotope Am-Be. The neutrons scattered from the surroundings are minimized by placing the

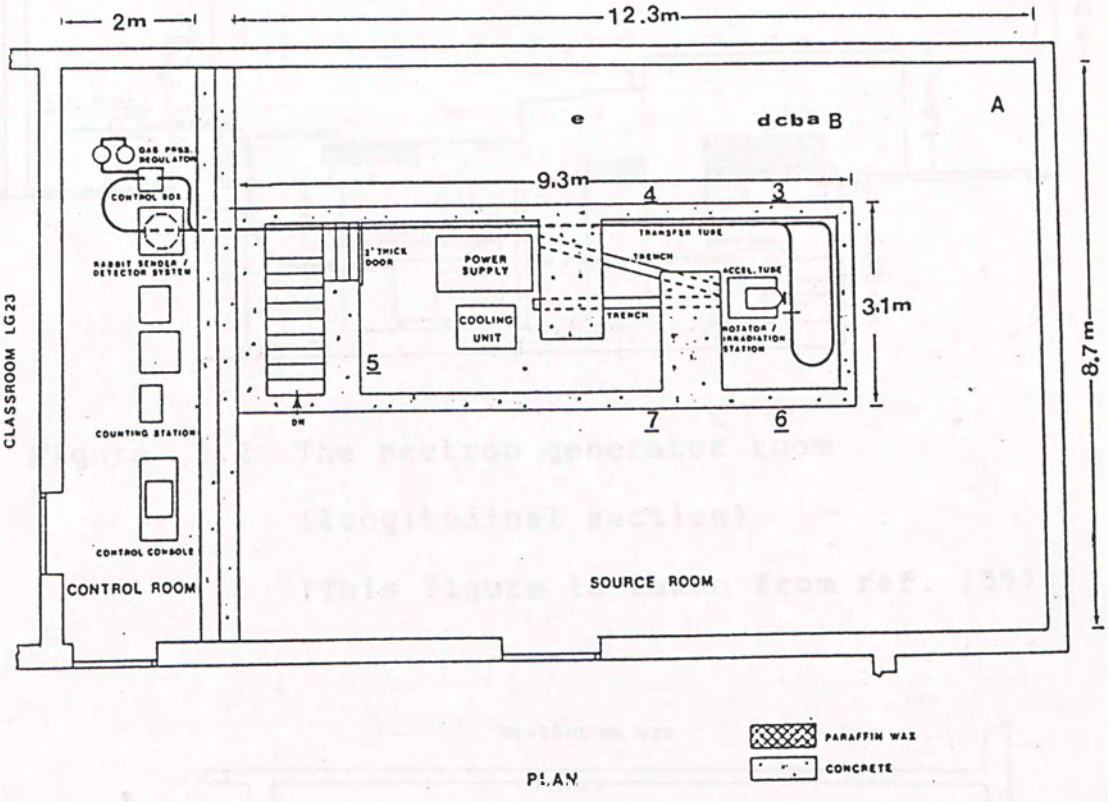

Figure 6.1 The neutron generator room

(plan view)

(This figure is taken from ref. (59))

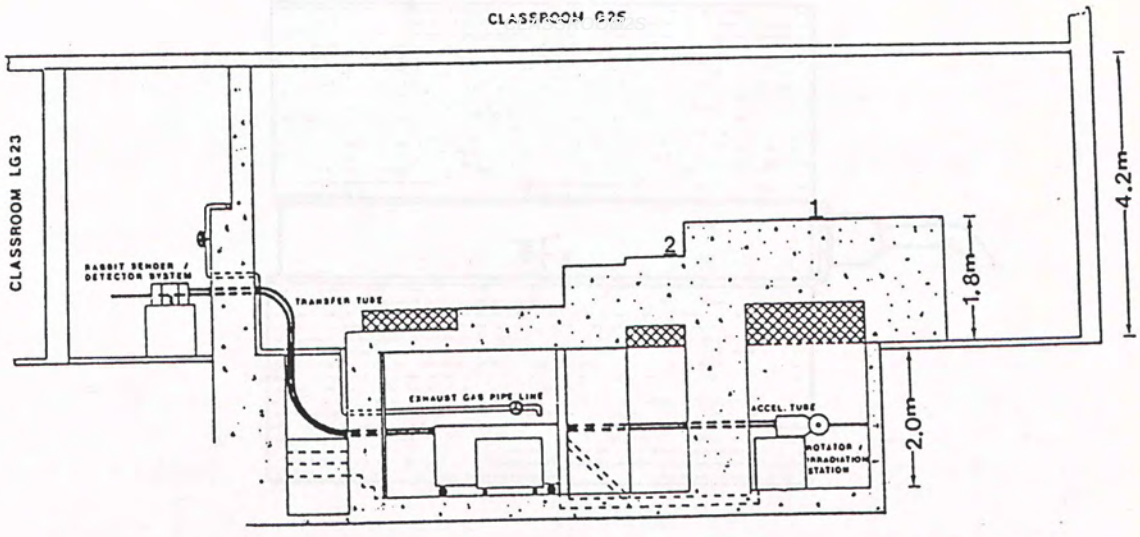

Figure 6.2 The neutron generator room
(longitudinal section)
(This figure is taken from ref. (59))

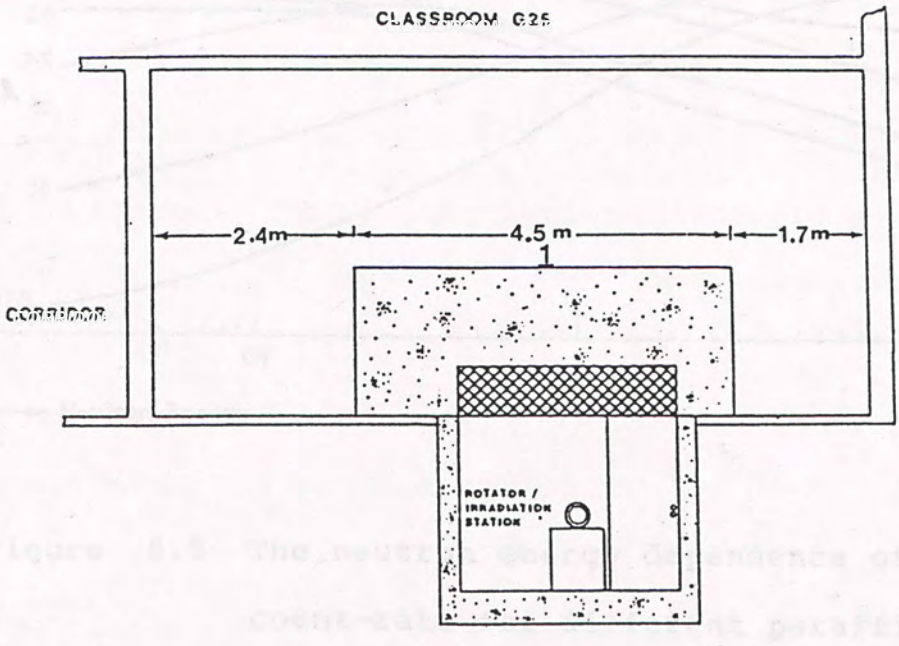

Figure 6.3 The neutron generator room
(transverse section)
(This figure is taken from ref. (59))

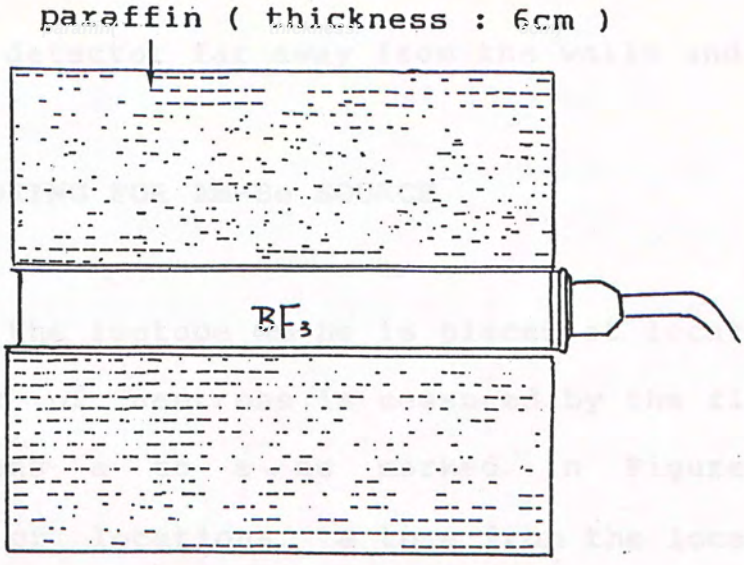

Figure 6.4 The structure of the flux-counter

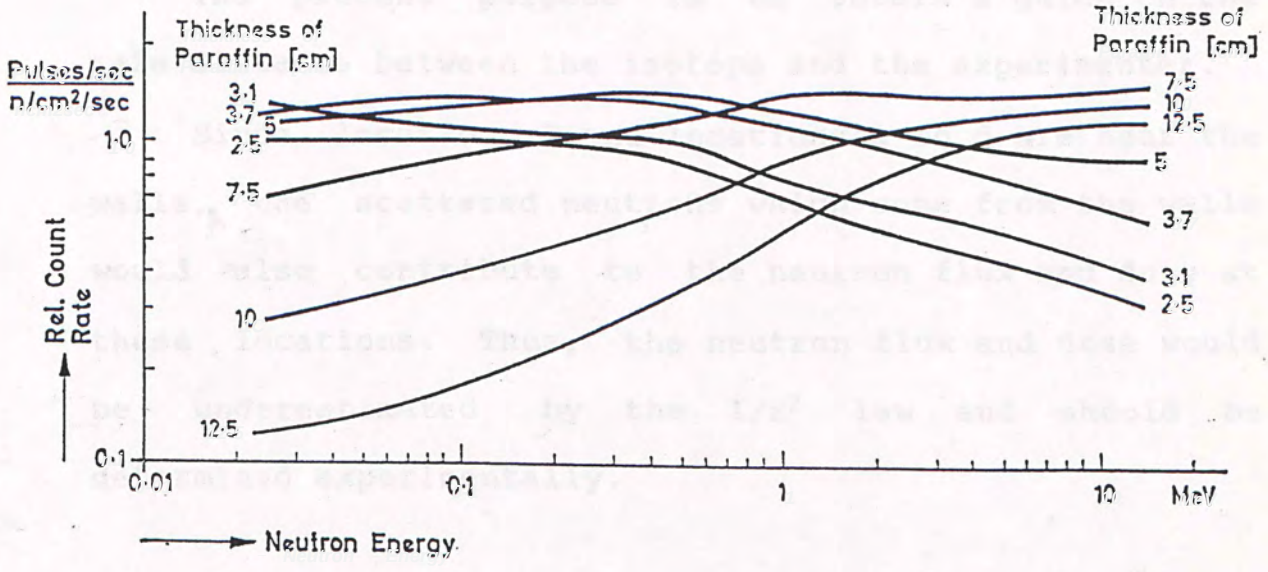

Figure 6.5 The neutron energy dependence of the count-rate for different paraffin thickness. (Taken from ref. (60))

source and detector far away from the walls and floor.

6.3 MONITORING FOR Am-Be SOURCE

When the isotope Am-Be is placed at location B, the total flux of neutrons is measured by the flux counter at locations a to e as marked in Figure 6.1. The distances of locations a to e from the location B are 0.3, 0.5, 0.7, 1.5 and 4.0 meters, respectively. The fast neutron flux and dose are also measured by a liquid scintillation detector (NE213) at locations a to d.

The present purpose is to obtain a guide on the safe distance between the isotope and the experimenter.

Since location B and locations a to d are near the walls, the scattered neutrons which come from the walls would also contribute to the neutron flux and dose at these locations. Thus, the neutron flux and dose would be underestimated by the $1/r^2$ law and should be determined experimentally.

6.4 MONITORING FOR NEUTRON GENERATOR

The total neutron flux is measured at locations 1 to 7, as is marked in Figures 6.1 and 6.2, by the flux counter when the neutron generator is in operation.

Besides, the fast neutron flux and dose at

locations 1 to 5 are also measured by the plastic scintillation detector developed in chapter 5.

The first aim of these measurements is to roughly estimate the flux and dose distribution in the source room during the neutron generator is in operation. The second aim is to study the possibility of monitoring the fast neutron flux and dose in the source room by the plastic scintillator.

The results of above work are presented and discussed in chapter 7.

CHAPTER 7

RESULTS AND DISCUSSION

7.1 PERFORMANCE OF LIQUID SCINTILLATION DETECTOR

Two computer programs, named NEUD (NEutron Spectrum Unfolding by Differentiation) and NEUMD (NEutron Spectrum Unfolding by Modified Differentiation), have been written to unfold the neutron spectrum. The first one uses the equation $E_e = \alpha E_p^{\beta}$ to approximate the light output produced by proton of energy E_p, and unfolds and spectrum by eq. 4.8. The second one uses a modified differentiation method and unfolds the spectrum following the process described in section 4.4.

Figure 7.1a and 7.1b show the neutron spectra of isotope Am-Be unfolded by NEUD and NEUMD, respectively. The raw data were taken by a liquid scintillation detector (NE213). The unfolded spectra are compared with the measurement from Lorch[48] as shown in the figures. The measurement from Kluge, Weise and Zill is also shown in Figure 7.2 for reference.[51]

The result given by NEUMD is better than the result given by NEUD. Since the proton energy dependence of light output is obtained by cubic spline interpolation in NEUMD, the approximation $E_e = E_p^{\beta}$ is not required.

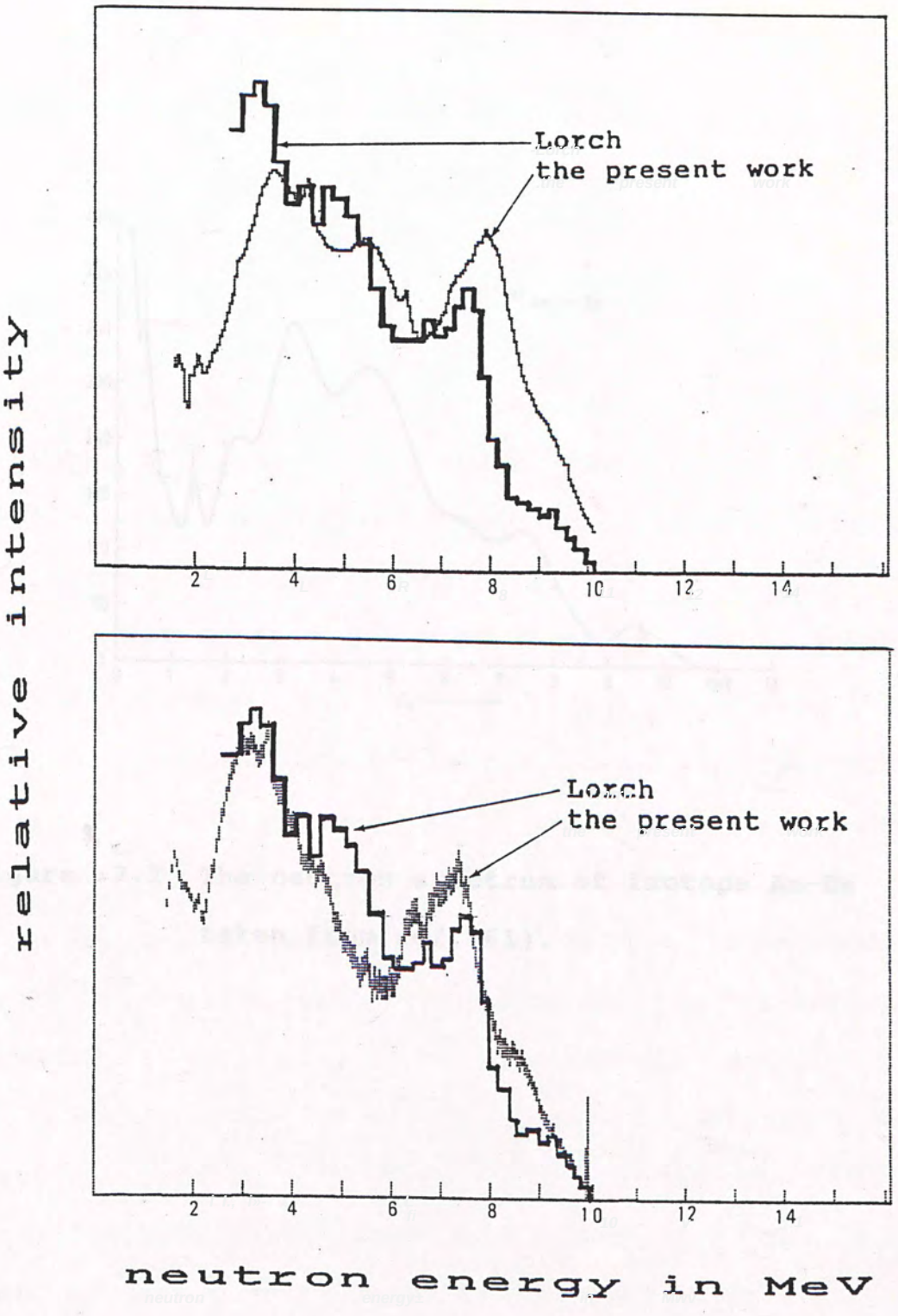

Figure 7.1 The neutron spectrum of isotope Am-Be. Figure a and b are given by NEUD and NEUMD respectively. The measurement of Lorch (ref. (48)) is also shown.

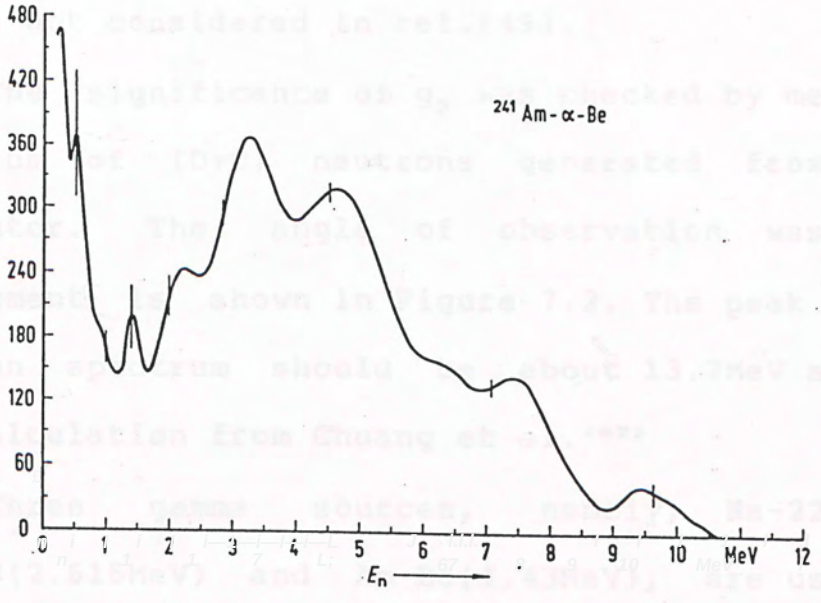

Figure 7.2 The neutron spectrum of isotope Am-Be taken from ref.(61).

Thus, the better performance of NEUMD is expected.

In NEUMD, the detector pulse height (x) is expressed in terms of light output (L_p) by eq 4.9.

$$x = g_0 + g_1 L_p(E) + g_2 L_p(E)^2 \qquad (4.9)$$

g_2 was not considered in ref.(49).

The significance of g_2 was checked by measuring the spectrum of (D+T) neutrons generated from a neutron generator. The angle of observation was 135°. The arrangment is shown in Figure 7.3. The peak position of neutron spectrum should be about 13.7MeV according to the calculation from Chuang et al.[47]

Three gamma sources, namely, Na-22(1.275MeV), Th-228(2.615MeV) and Am-Be(4.43MeV), are used in pulse height verus light output calibration. The electron energies corresponding to the compton edge are converted to light output, and then the values of g_0, g_1 and g_2 can be calculated by eq.4.9. When g_2 is assumed to be zero, g_0 and g_1 are obtained by fitting the data to the equation $x = g_0 + g_1 L_p(E)$ by least square method.

The result for $g_2 = 0$ is shown in Figure 7.4a. The neutron spectrum is greatly distorted and the peak position shifts to the high energy region. When g is not set to zero, the result is improved a lot and is shown in Figure 7.4b. The peak position is 13.45MeV.

In fact, the significance of g_2 can be estimated from eq. 4.14.

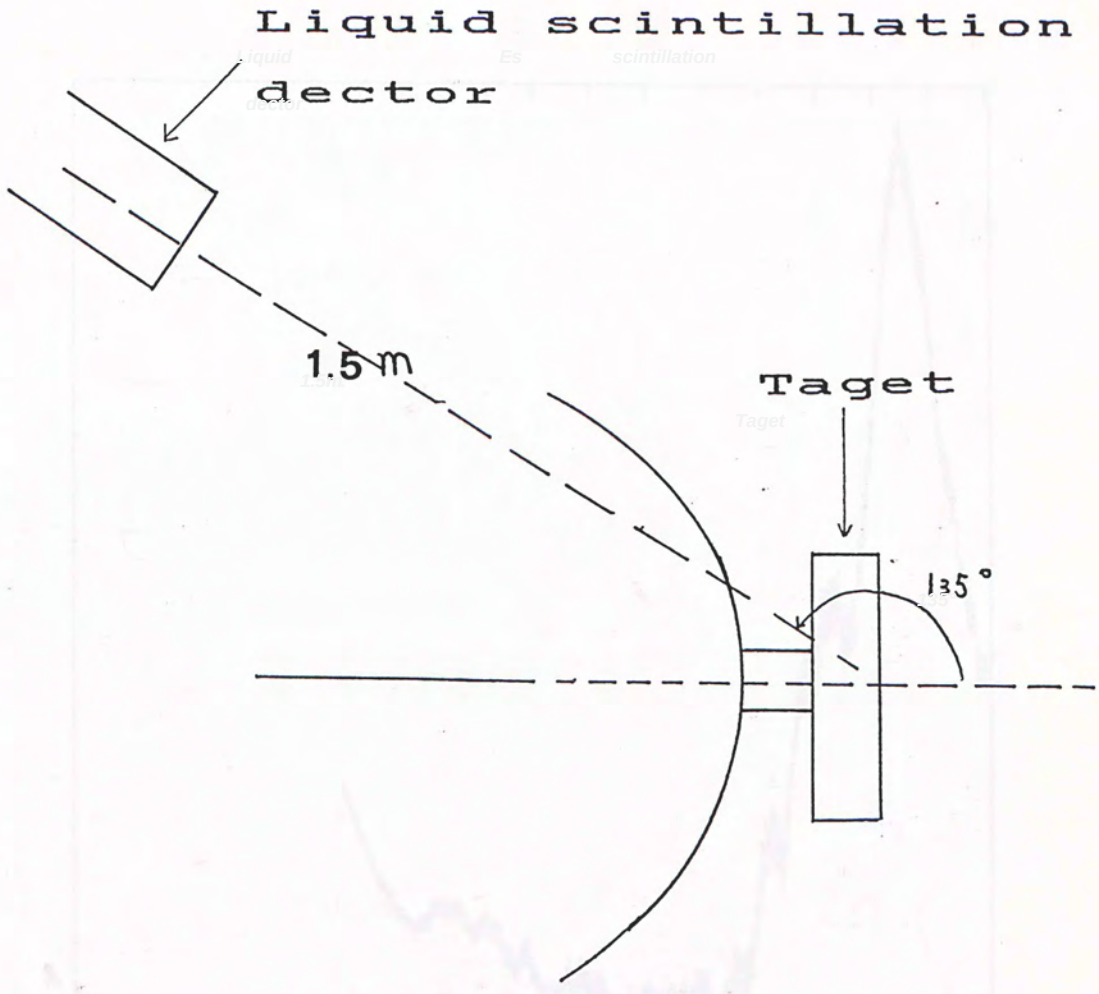

Figure 7.3 The arrangment for measuring the neutron spectrum of the neutron generator.

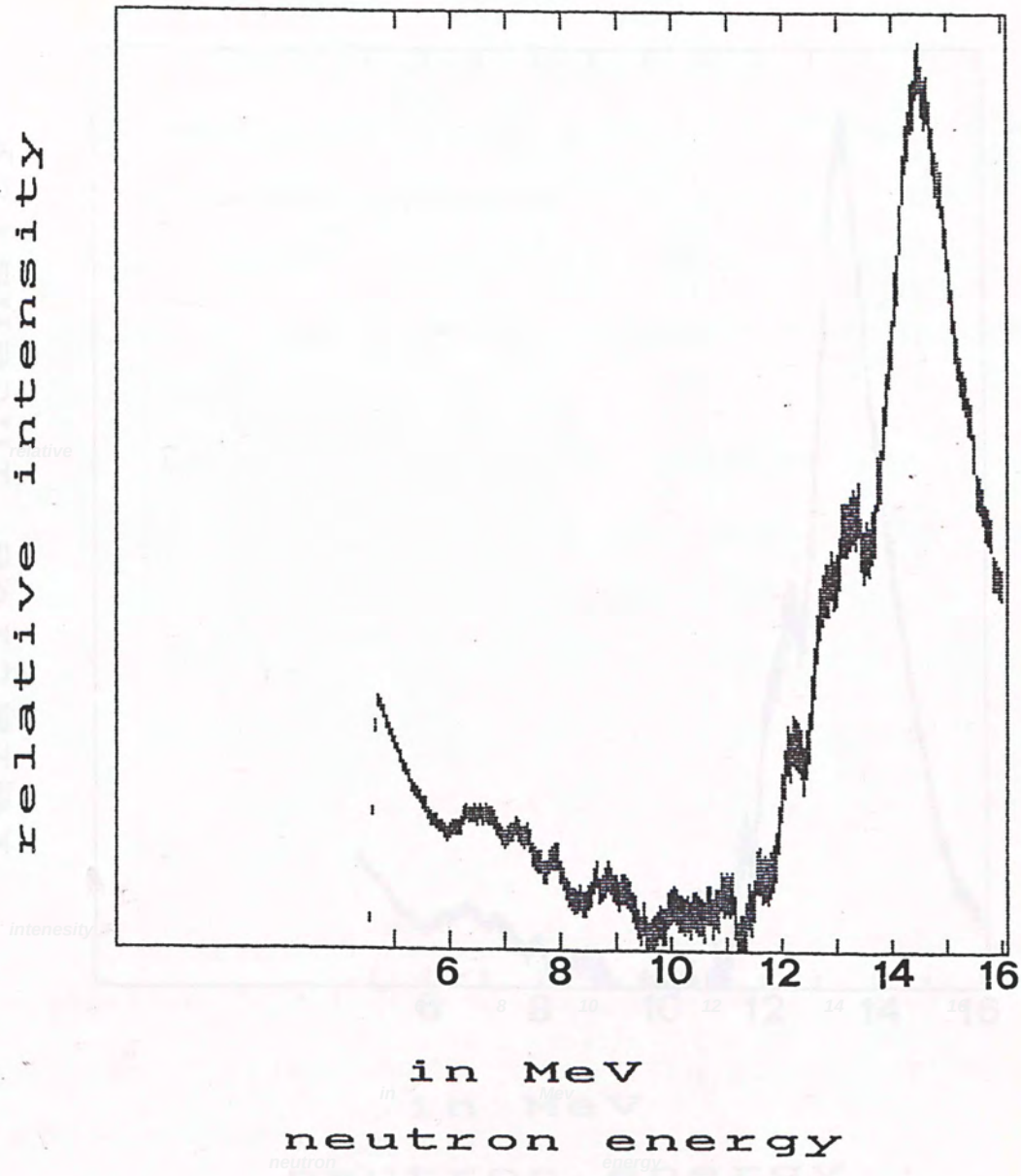

Figure 7.4a The (D+T) neutron spectrum unfolded by NEUMD when q_2 is assumed to zero.

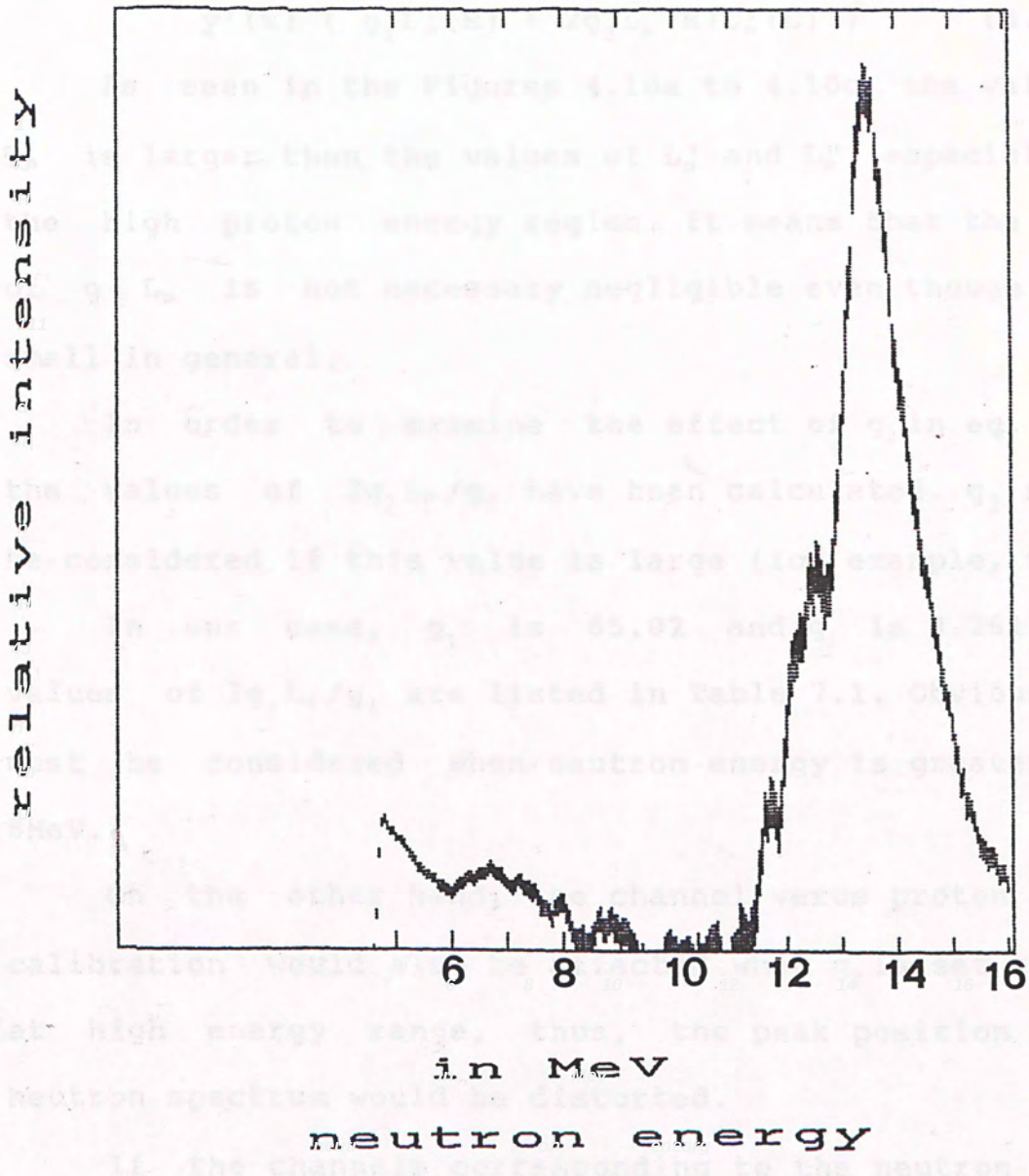

Figure 7.4b The (D+T) neutron spectrum unfolded by NEUMD when g_2 is also considered.

$$\Phi(E) = -E/(A\,S(E)\,\epsilon(E,L))\,[\,y(x)\,(g_1 L_p''(E) + 2g_2 L_p'(E) + 2g_2 L_p(E)L_p''(E)) + y'(x)\,(g_1 L_p'(E) + 2g_2 L_p(E)L_p'(E))^2\,] \quad (4.14)$$

As seen in the Figures 4.10a to 4.10c, the value of L_p is larger than the values of L_p' and L_p'', especially in the high proton energy region. It means that the value of $g_2 L_p$ is not necessary negligible even though g_2 is small in general.

In order to examine the effect of g_2 in eq. 4.14, the values of $2g_2 L_p/g_1$ have been calculated. g_2 should be considered if this value is large (for example, 0.5).

In our case, g_1 is 65.02 and g_2 is 3.261. Some values of $2g_2 L_p/g_1$ are listed in Table 7.1. Obviously, g_2 must be considered when neutron energy is greater than 9MeV.

On the other hand, the channel verus proton energy calibration would also be affected when g_2 is set to zero at high energy range, thus, the peak position of the neutron spectrum would be distorted.

If the channels corresponding to the neutron energy range are covered by the energy range of the calibration gamma-ray sources, the distortion caused by setting g_2 = 0 would be smaller. However, there is no calibration gamma-ray source can fullfill this requirment when the spectrum of (D+T) neutrons is measured. It is because the proton of energy 14MeV can produce light output

TABLE 7.1 THE VALUE OF $2g_2 L_p(E)/g_1$ FOR DIFFERENT PROTON ENERGIES

ENERGY (MeV)	$L_p(E)$ (in light unit)	$2g_2 L_p(E)/g_1$
2	0.4725	0.047
4	1.327	0.133
6	2.310	0.232
8	3.394	0.340
10	4.550	0.456
12	5.752	0.577
14	6.968	0.699
16	8.199	0.822

equivalent to that produced by 7MeV electrons approximatly.

The relation between the light output and the electron energy is linear in theory. When g_2 is not equal to zero, it means that the pulse height does not linearly relate to the light output of the scintillator. This nonlinearity may be caused by the space charge which affects the trajectories of the electrons near the last dynode of the photomultiplier tube. The space charge would be produced when large pulse is recorded.

However, the actual reason have not been known. Further studies on the anode voltage dependence of the nonlinear effect may be helpful.

7.2 THE PERFORMANCE OF PLASTIC SCINTILLATION DETECTOR

The gamma contribution subtraction method GSI is used for plastic scintillator. In order to evaluate the reliability of this method, two measurements have been taken.

The first one was to compare the compton distribution interpolated by GSI with the experimental result.

Gamma source Na-22 was detected by the plastic scintillation detector ar the ılse eight spectrum

recorded by a M.C.A. is shown in Figure 7.5. The interpolated result is also shown in the same figure. The interpolated spectrum shows a good agreement with the experimental one.

The second one was to measure the neutron spectrum of the isotope Am-Be which was surrounded by paraffin as shown in Figure 7.6. The neutrons emitted from the isotope would be slowed down by the hydrogen nuclei in paraffin. The slow neutrons can be absorbed through the reaction $^{1}H(n,\gamma)^{2}D$ and 2.2MeV gamma-ray can be produced. Figure 7.7 shows the gamma-ray spectrum taken by a 3'x3' NaI(Tl) scintillation detector. The ability to subtract the 4.43MeV and 2.2MeV gamma-rays contribution in the output of the plastic scintillation detector indicates the performance of GSI. The result of the unfolded neutron spectrum of isotope Am-Be is shown in Figure 7.9. Although the result is not quite good, it can give an approximation of the neutron spectrum. The dose rate measured in this case is 1.76 mrem/hour. This value is in agreement with the results given by liquid scintillation detector.

However, the neutron spectrum unfolded by GSI is only an approximation. Since the compton distributions from monoenergetic gamma-rays would be slightly smoothed when they are grouped into 100 channels, so the interpolated gamma-ray [illegible] be slightly flatter

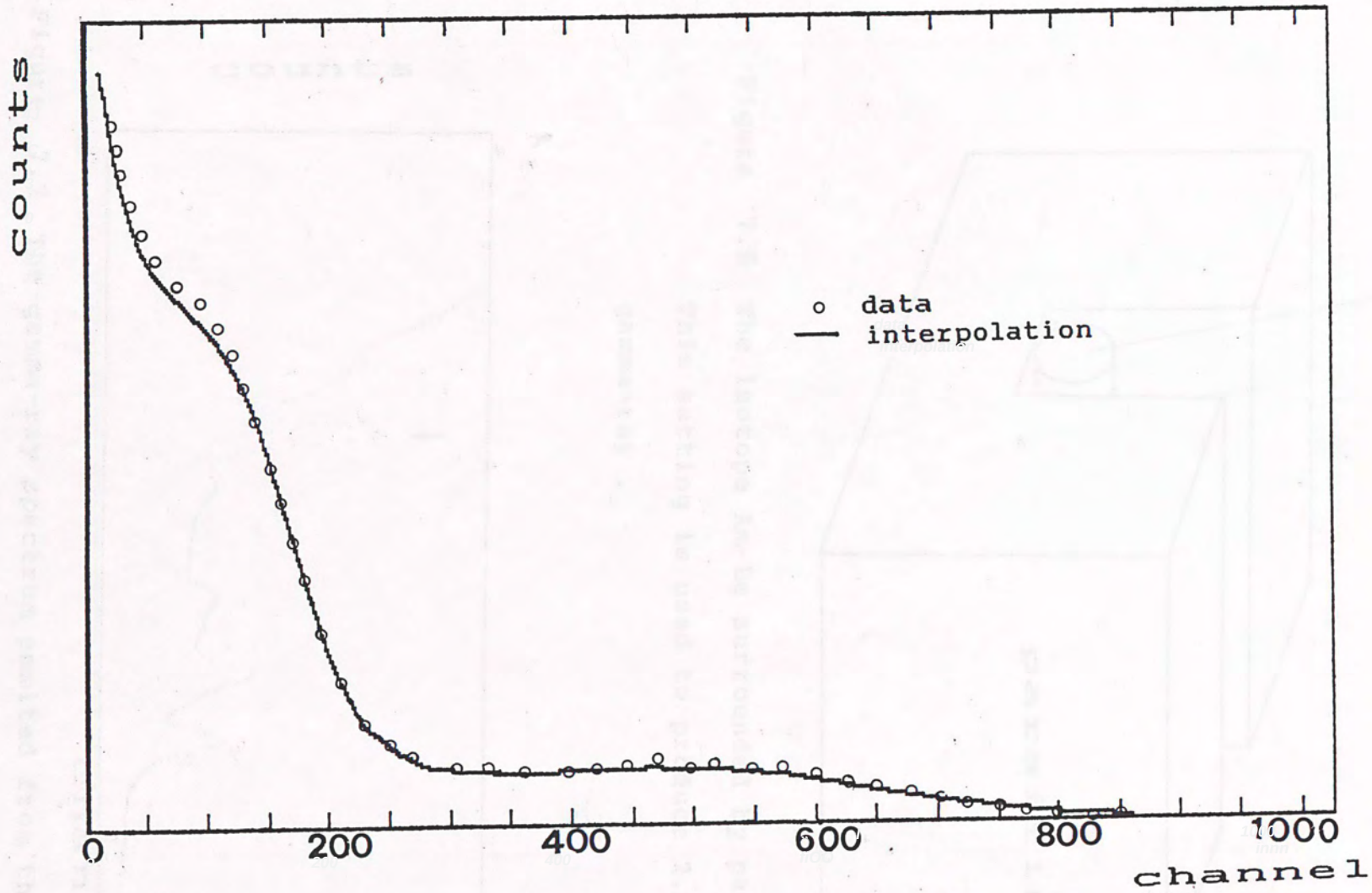

Figure 7.5 The compton distribution of Na-22 recorded by plastic scintillator. The black curve is the compton distribution interpolated by GSI.

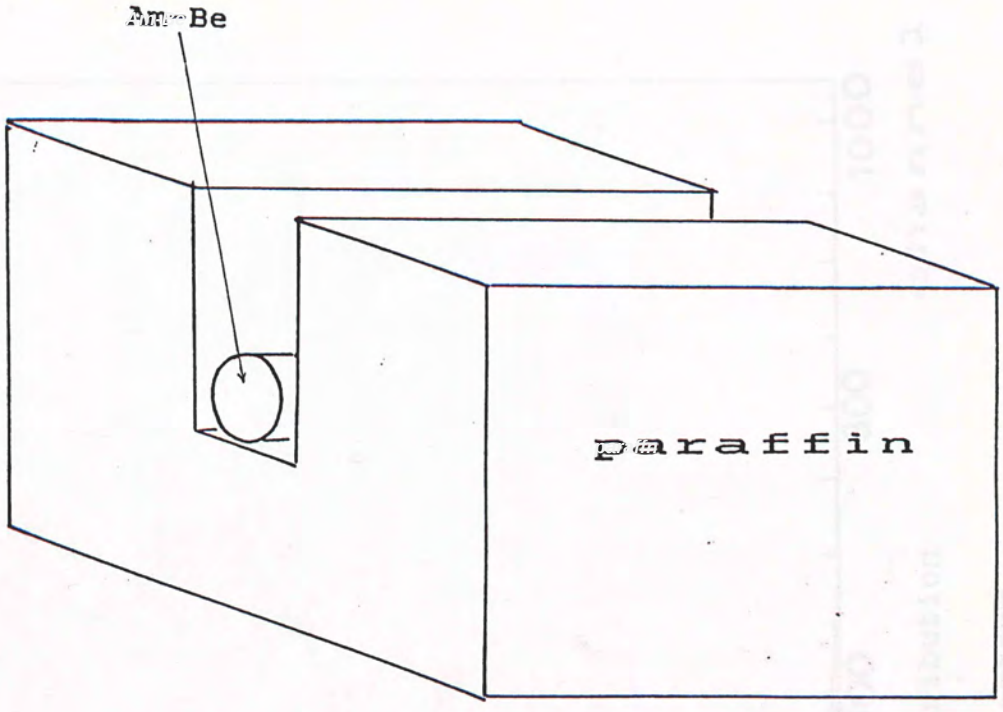

Figure 7.6 The isotope Am-Be surrounded by paraffin. This setting is used to produce 2.2 MeV gamma-ray .

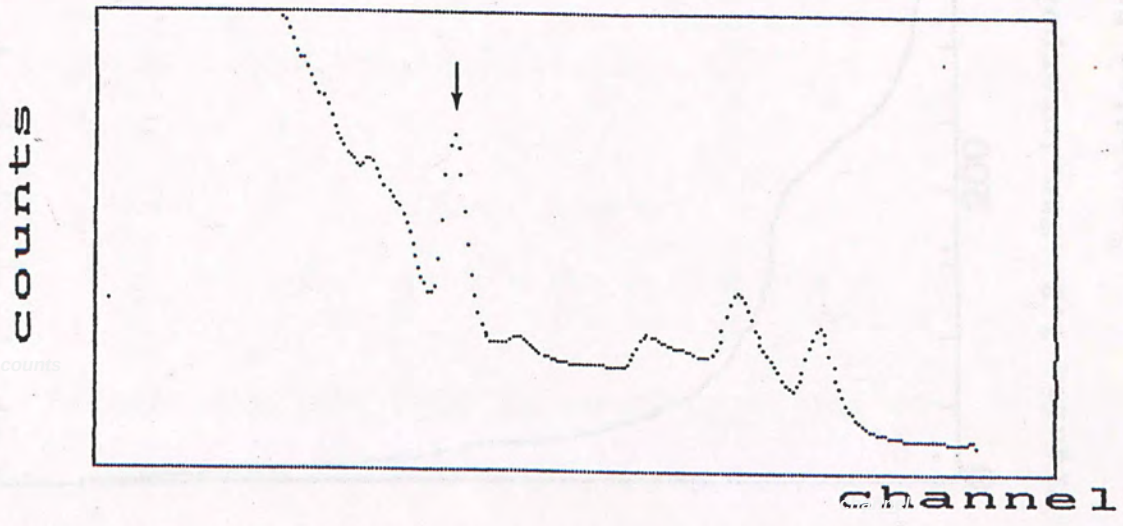

Figure 7.7 The gamma-ray spectrum emmited from the paraffin surrounded Am-Be source. It is detected by a NaI(Tl) scintillation detector. The arrow specifies the 2.2 MeV gamma-ray photopeak.

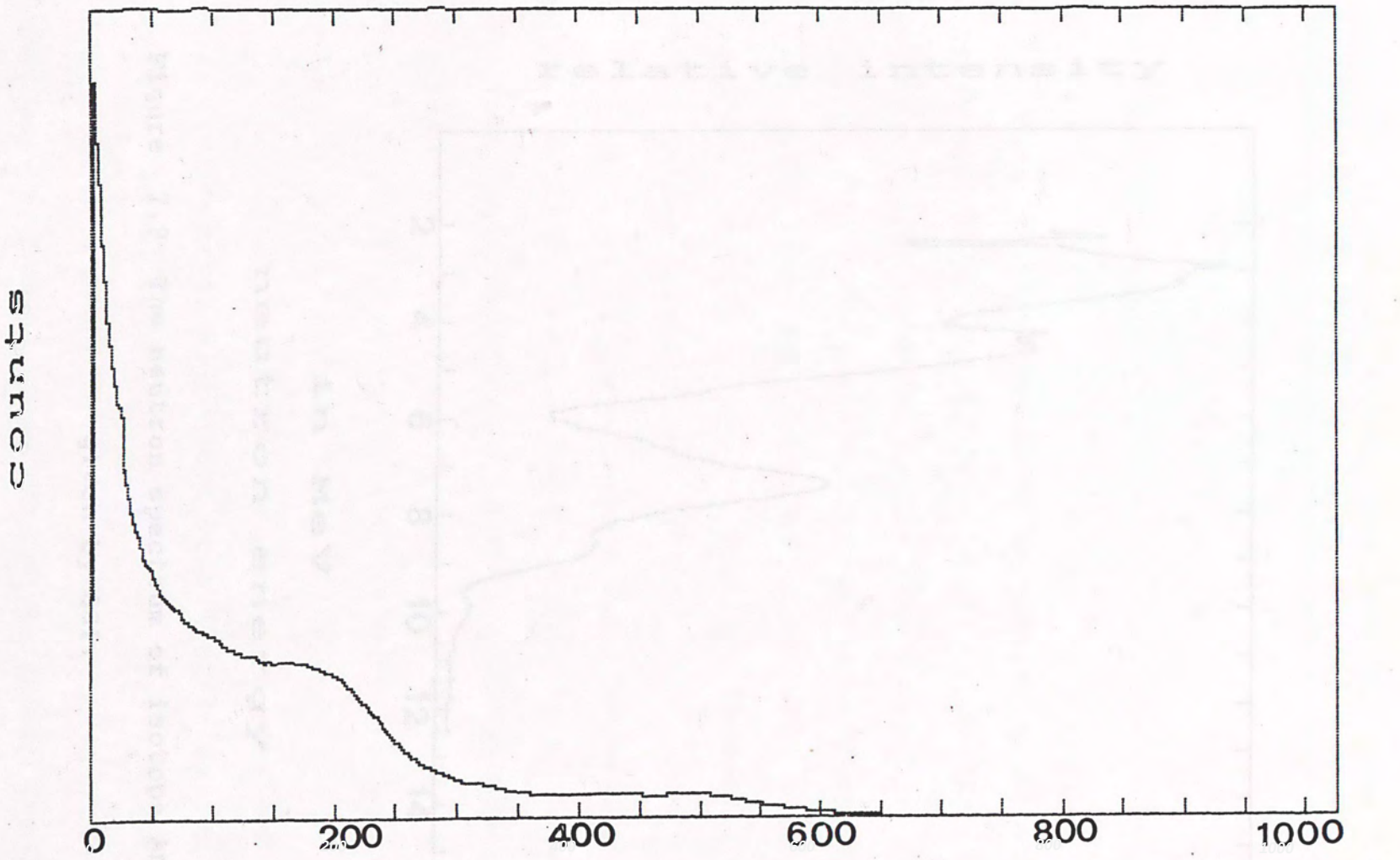

Figure 7.8 The interpolated compton distribution according to the gamma-ray spectrum presented in figure 7.7.

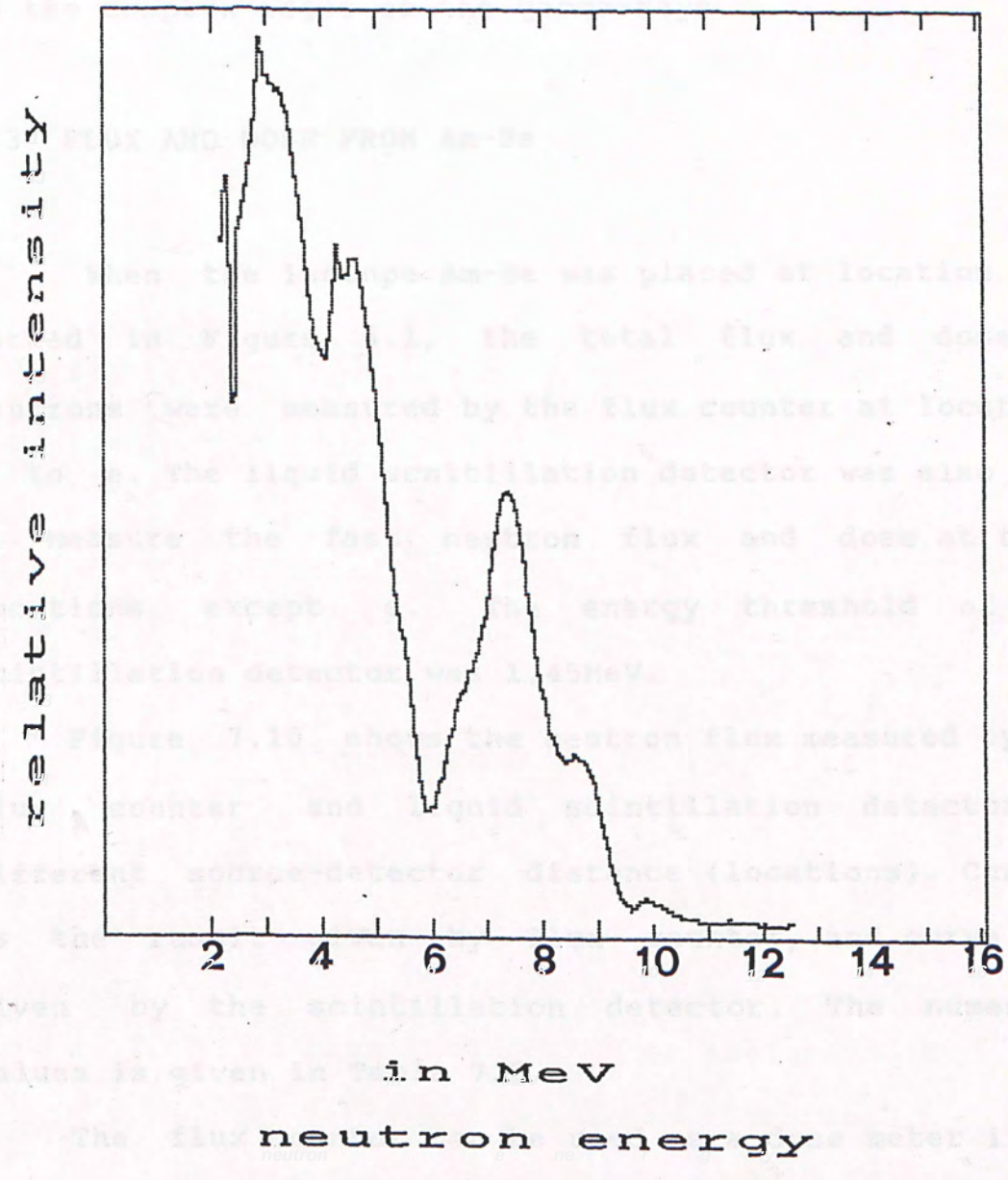

Figure 7.9 The neutron spectrum of isotope Am-Be given by GSI.

than the actual one. Thus, there are pertubations on the unfolded neutron spectrum at the positions corresponding to the compton edges of the gamma-rays.

7.3 FLUX AND DOSE FROM Am-Be

When the isotope Am-Be was placed at location B as marked in Figure 6.1, the total flux and dose of neutrons were measured by the flux counter at locations a to e. The liquid scnitillation detector was also used to measure the fast neutron flux and dose at these locations except e. The energy threshold of the scintillation detector was 1.45MeV.

Figure 7.10 shows the neutron flux measured by the flux counter and liquid scintillation detector at different source-detector distance (locations). Curve a is the result given by flux counter, and curve b is given by the scintillation detector. The numerical values is given in Table 7.2.

The flux counter can be used as a dose meter if the mean flux-dose equivalent convertion factor of the neutron field is known. This factor for isotope Am-Be is about 4×10^{-8} rem cm^2.[61] The total dose-rate is obtained by multiplying the total flux by the flux-dose equivalent convertion factor. The total dose-rate obtained in such a way at different distance is plotted

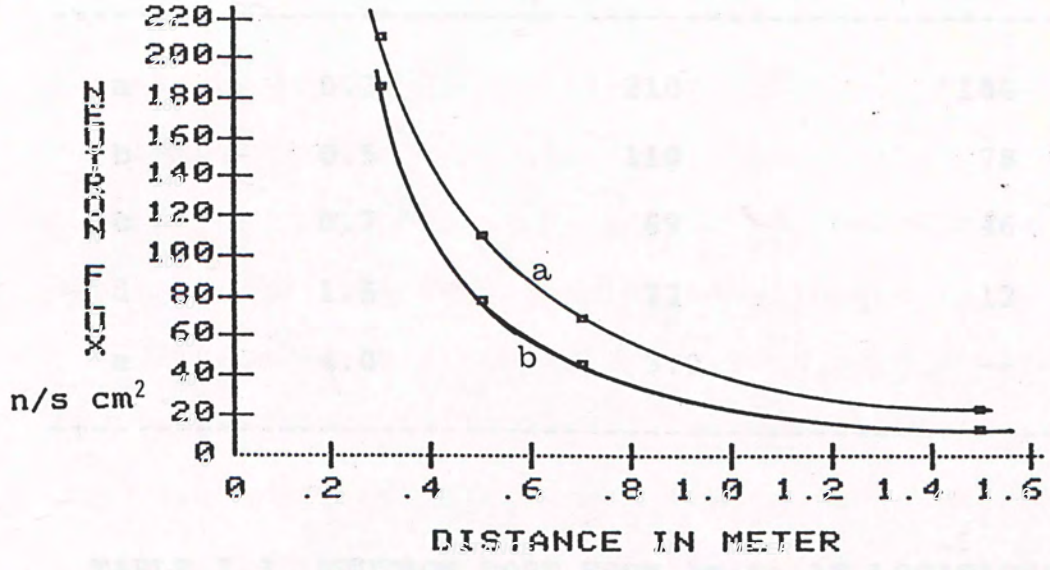

Figure 7.10 Neutron flux due to an isotope Am-Be at different distances (locatios). Curve a is given by the NE213 liquid scintillation detector. Curve b is given by the paraffin covered BF_3 counter.

TABLE 7.2 NEUTRON FLUX FROM Am-Be AT LOCATIONS a TO e

LOCATION	DISTANCE (in meter)	FLUX (in neutron/second cm^2)	
		FLUX COUNTER	NE213
a	0.3	210	186
b	0.5	110	78
c	0.7	69	46
d	1.5	23	12
e	4.0	3.0	--

TABLE 7.3 NEUTRON DOSE FROM Am-Be AT LOCATIONS a TO e

LOCATION	DISTANCE (in meter)	DOSE (in mrem/hour)	
		FLUX COUNTER	NE213
a	0.3	30.2	26.3
b	0.5	15.7	10.8
c	0.7	9.93	6.4
d	1.5	3.37	1.7
e	4.0	0.436	---

in Figure 7.11. At the same time, the fast neutron dose measured by the liquid scintillation detector is also shown in Figure 7.12 in same scale.

In order to compare the measured neutron flux to the 1/distance^2 law, the graph flux verus 1/distance^2 is plotted in Figure 7.13. The flux is detected by the flux counter in this case. The straight line is given by (total neutron output)/distance^2. The difference between the experimental results and the straight line may be caused by the neutrons scattered from the walls. This confirms that the experimental measurement is necessary.

The numerical values of neutron dose at locations a to e are given in Table 7.3. As mentioned in chapter 1, the maximum permissible dose for radiation workers are 5 rem/year. Hence, the occupational maximum permissible dose rate is 2.5 mrem/hour. When the isotope Am-Be is placed at location B , the dose rate at locations a to d would excess the maximum permissible value. Although the 1/distance^2 law gives 1.27mrem/hour at location d, the experimental result is much higher. However, if the exposed time is below 10 hours per week, the dose-rate at locations c to e are still permissible.

7.4 THE NEUTRON FLUX AND FAST NEUTRON DOSE IN SOURCE ROOM WHEN NEUTRON GENERATOR IS IN OPERATION.

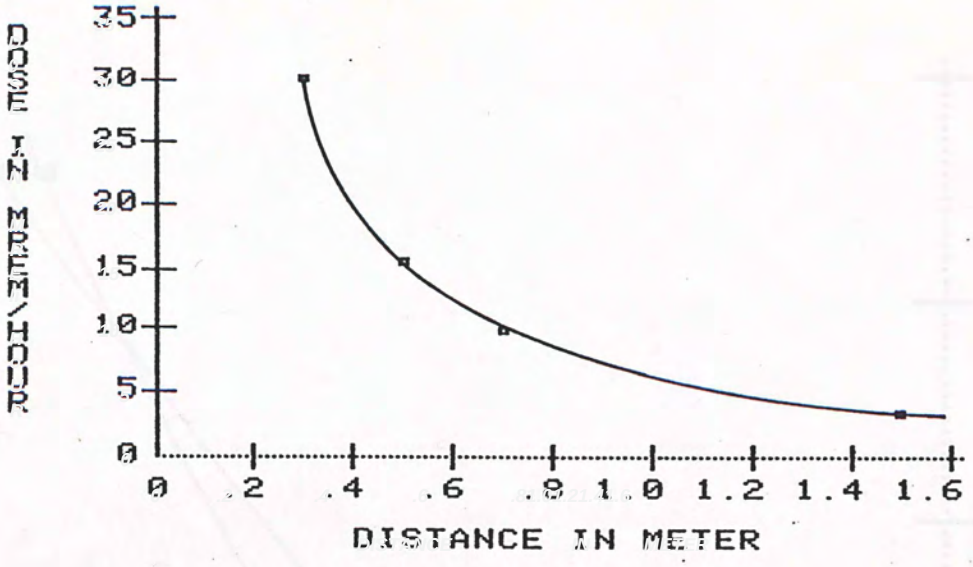

Figure 7.11 The neutron dose-rate due to an isotope Am-Be at various distance measured by the paraffin covered BF_3 counter.

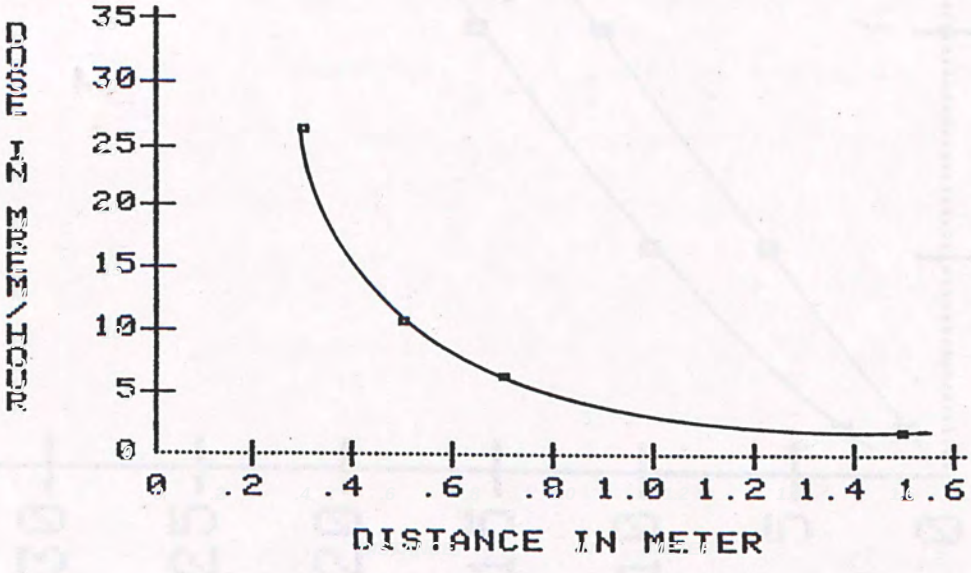

Figure 7.12 The neutron dose-rate due to an isotope Am-Be at various distance measured by the liquid scintillation detector.

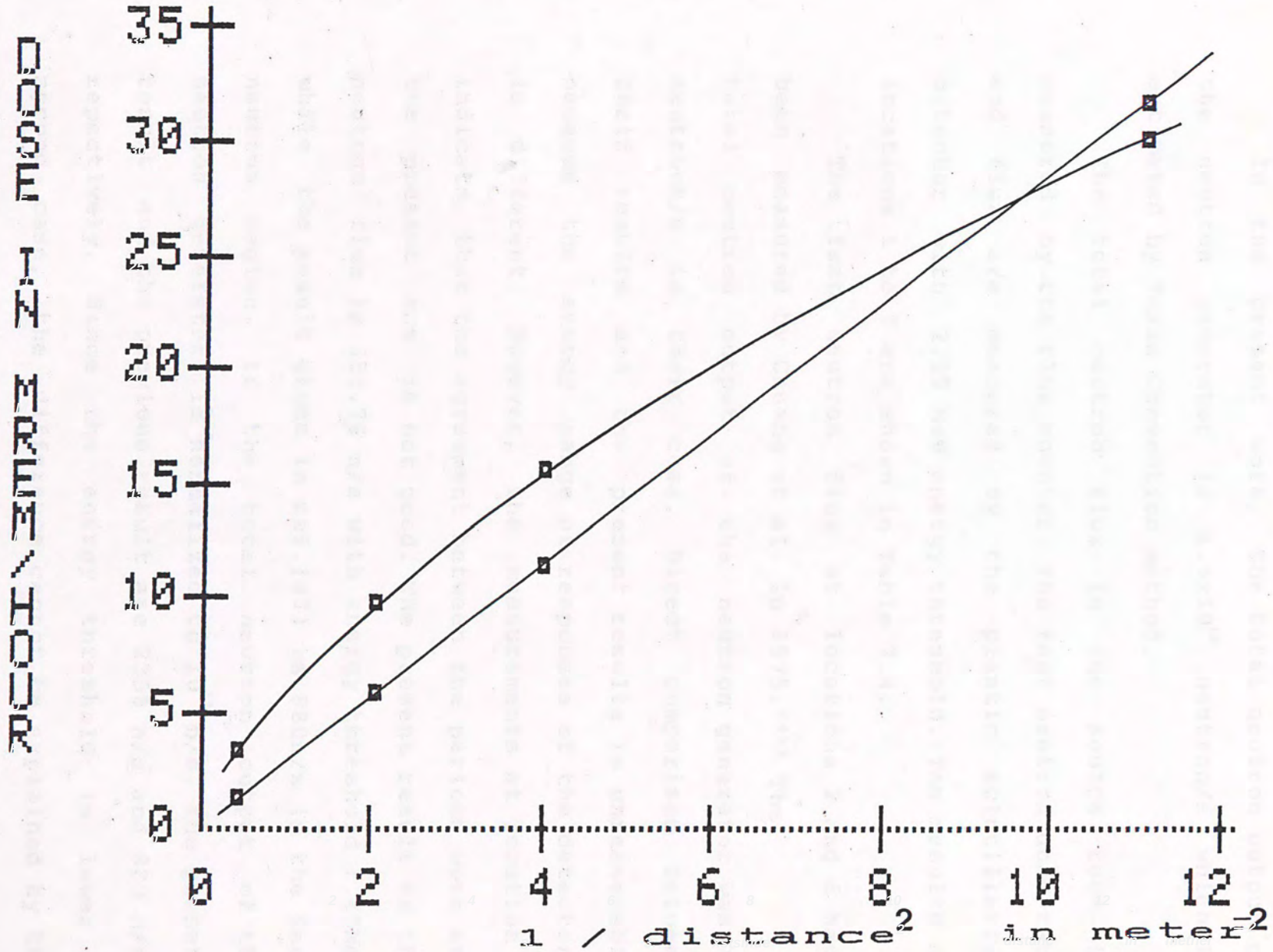

Figure 7.13 The dose-rate measurement of the paraffin covered BF_3 counter as a function of (1/source-detector distance)^2. The neutron source is an isotope Am-Be. The straight line shows the result given by 1/distance^2 law.

In the present work, the total neutron output of the neutron generator is 1.5×10^{10} neutron/s which is estimated by Texas Convention method.

The total neutron flux in the source room is measured by the flux counter. The fast neutron dose-rate and flux are measured by the plastic scintillation detector with 2.15 MeV energy threshold. The results at locations 1 to 7 are shown in Table 7.4.

The fast neutron flux at locations 2 and 6 have been measured by Chuang et al. in 1975.[47] The total neutron output of the neutron generator was 10 neutrons/s in their case. Direct comparison between their results and the present results is unreasonable because the energy range of responses of the detectors is different. However, the measurements at location 2 indicate that the agreement between the perious work and the present one is not good. The present result of the neutron flux is 353.76 n/s with energy threshold 1.45MeV while the result given in ref.(47) is 880n/s in the fast neutron region. If the total neutron output of the neutron generator is normalized to 10^{11} n/s, the present result and the previous result are 2358 n/s and 880 n/s, repectively. Since the energy threshold is lower in second case, the difference cannot be explained by the different energy of these two measuremnts. However, the actual reason has not been investigated.

TABLE 7.4 NEUTRON FLUX AND DOSE AT LOCATIONS 1 TO 7 WHEN NEUTRON GENERATOR IS IN OPERATION

LOCATION	FLUX MEASURED BY FLUX COUNTER (mrem/hour)	RESULTS FROM NE213 FLUX (n/s·cm^2)	RESULTS FROM NE213 DOSE (mrem/hour)
1	2.57	2.17	0.2732
2	638	353	51.27
3	110	86.4	12.34
4	0.874	0.871	0.1238
5	259	128	18.37
6	58	---	---
7	0.947	---	---

CHAPTER 8
CONCLUSION

The program NEUMD described in chapter 4 was applied to NE213 liquid scintillator. The preformance of this system has been checked by an isotope Am-Be and the (D+T) 14MeV neutrons, the results are satisfactory. The neutron spectra in both cases can be correctly unfolded. The nonlinearity between the light output of the scintillator and the pulse height output of the photomultiplier tube should be considered at high neutron energy range, e.g., 8MeV.

A computer program called GSI was used to subtract the gamma-ray contribution from the neutron-gamme-ray mixed output of the plastic scintillation detector. After the gamma-ray contribution has been subtracted, the neutron spectrum can be unfolded from the resulting pulse height spectrum by differentiation method. This system can give an approximation of the fast neutron spectrum and dose rate. The result shows that it is possible to eliminate the gamma-ray contribution by constructing the gamma-ray response using interpolation method.

Besides, a BF_3 counter covered with paraffin of 6cm thickness was also used as flux counter.

When the isotope Am-Be with 2.5×10^6 n/s neutron output was placed at location B shown in Figure 6.1, the neutron flux at locations a to d was larger than the values given by $1/\text{distance}^2$ law. The difference might be caused by the neutrons scattered from the surroundings. The dose-rates at locations a to d (within 1.5m from the isotope) were beyond the maximum permissible level if the exposure time was 40 hours/week.

In fact, the exposure time for the experimenters is much shorter than 40 hours/week in our laboratory. Hence, the dose-rate is at the safe level even the distance is 0.5m from the Am-Be source only.

When the neutron generator was in operation, the dose distribution in the source room was very heterogeneous. Moreover, high dose-rate was recorded at locations 2 and 3. It is dangerous to stay inside the source room during the neutron generator is in operation, although it may be safe at some locations.

APPENDIX A
CUBIC SPLINE INTERPOLATION

Given n+1 points (x_i, f_i) $i=0,1,2,...n$

and assume $a = x_0 < x_1 ..... < x_n = b.$

Our intention is to find a function F(x) such that

1. $F(x_i) = f$
2. $F(x_i - 0) = F(x_i + 0)$
3. $F'(x_i - 0) = F'(x_i + 0)$, and
4. $F''(x_i - 0) = F''(x_i + 0)$

Conditions 3 and 4 mean that the first derivative and second derivative of F(x) are continuous for $x \in [a,b]$.

Such conditions can be satisfied by fitting cubics between each two successive points. If so, there are four parameters for each cubic, hence, there are 4n parameters to be determined.

Condition 1 and Condition 2 give n+1 equations and n-1 equations, repectively. Conditions 3 and 4 also give 2(n-1) equations. It means that only 4n-2 equations are available, so two boundary conditions are required.

Let $F''(x_i) = M_i$, $i = 0,1,2,...n$ (A.1)

then

$$F''(x) = \frac{x_{i+1} - x}{h_i} M_i + \frac{x - x_i}{h_i} M_{i+1} \qquad (A.2)$$

Where $h_i = x_{i+1} - x_i$, $x_i \quad x \leqslant x_i$, $i = ,$ $2...n-1$

Integrate eq A.2 twice and use $F(x_i) = f_i$ and $F(x_i + 1) = f_{i+1}$, we can obtain:

$$F(x) = \frac{(x_{i+1} - x)^3}{6h_i} M_i + \frac{(x - x_i)}{6h_i} M_{i+1}$$

$$+ (x_{i+1} - x)\left(\frac{f_i}{h_i} - \frac{h_i M_i}{6}\right)$$

$$+ (x - x_i)\left(\frac{f_{i+1}}{h_i} - \frac{h_i M_{i+1}}{6}\right) \qquad \text{(A.3)}$$

There are still n+1 unknowns $M_0, M_1, \ldots M_n$ in eq. A.3.

Since $F'(x_i - 0) = F'(x_i + 0)$, hence

$$h_{i-1} M_{i-1} + 2(h_{i-1} + h_i) M_i + h_i M_{i+1} = 6\left[\frac{f_{i+1} - f_i}{h_i} - \frac{f_i - f_{i-1}}{h_{i-1}}\right]$$

$$i = 1, 2, 3, \ldots . n-1 \qquad \text{(A.4)}$$

Eq. A.4 contains n-1 equations only, it is not enought to solve the n+1 unknowns M_i.

If two boundary conditions are imposed to M_0 and M_n, eq A.4 can be rewritten in a matrix form:

$$\begin{bmatrix} b_0 & c_0 & & & & \\ a_1 & b_1 & c_1 & & 0 & \\ & & \ddots & \ddots & \ddots & \\ & 0 & & a_{n-1} & b_{n-1} & c_{n-1} \\ & & & & a_n & b_n \end{bmatrix} \begin{pmatrix} M_0 \\ M_1 \\ \vdots \\ M_{n-1} \\ M_n \end{pmatrix} = \begin{pmatrix} d_0 \\ d_1 \\ \vdots \\ d_{n-1} \\ d_n \end{pmatrix} \qquad \text{(A.5)}$$

Where $a_i = h_{i-1}$, $b_i = 2(h_{i-1} + h_i)$, $c_i = h_i$, and

$$d_i = 6\left(\frac{f_{i+1} - f_i}{h_i} - \frac{f_i - f_{i-1}}{h_{i-1}}\right), \quad i = 1, 2, \ldots n-1$$

If the boundary conditions are $M_0 = M_1$ and $M_n = M_{n-1}$, eq. A.5 can be simplified as:

$$\begin{bmatrix} a_1+b_1 & c_1 & & & 0 \\ a_2 & b_2 & c_2 & & \\ & \ddots & \ddots & \ddots & \\ & & a_{n-2} & b_{n-2} & c_{n-2} \\ 0 & & & a_{n-1} & b_{n-1}+c_{n-1} \end{bmatrix} \begin{bmatrix} M_1 \\ M_2 \\ \vdots \\ M_{n-2} \\ M_{n-1} \end{bmatrix} = \begin{bmatrix} d_1 \\ d_2 \\ \vdots \\ d_{n-2} \\ d_{n-1} \end{bmatrix} \qquad (A.6)$$

The first derivative and second derivative of $F(x)$ at x $(x \in [a,b])$ can be calculated by eq. A.3, they are expressed as:

$$F'(x) = -\frac{(x_{i+1}-x)^2}{2h_i} M_i + \frac{(x-x_i)^2}{2h_i} M_{i+1} + \frac{f_{i+1}-f_i}{h_i} + \frac{h_i}{6}(M_i - M_{i+1}) \qquad (A.7)$$

and

$$F''(x) = \frac{(x_{i+1}-x)}{h_i} M_i + \frac{(x-x_i)}{h_i} M_{i+1} \qquad (A.8)$$

Relevant information can be found in ref.(62) and ref.(63).

<REFERENCE>

1. Nicholas Tsoulfanidis, Measurement and Detection of Radiation, p.486, Hemisphere Publishing Corporation, 1983.

2. A. Edward Profio, Radiation Shielding and Dosimetry, p.311, John Wiley & Sons, 1979.

3. P. A. H. Saunders, B. O. Wade, Radiation and its control, Nuclear Power Technology, V.3, Nuclear Radiation, p.9, Clarendon Press, 1983.

4. Marcel Barbier, Induced Radioactivity, p.33, 1969.

5. International Commission on Radiological Units and Measurements, Nation Bureau of Standards (USA), ICRU Report II, Radiation Quantities and Units, 1968.

6. H. Dertinger and H. Jung, Molecular Radiation Biology, Springer, New York, 1970.

7. Ref. (1), p.503.

8. Ref. (2), p.327.

9. Neutron and Gamma-ray Flux-to-Dose Rate Factor, American National Standard, ANSI/ANS6.11-1977.

10. Nuclear Regulation Commission, Title 10, chap.1, part 20, Code of Federal Regulations (10 CFR 20), 1978.

11. F. W. K. Firk, Neutron time-of-flight spectrometers, Nucl. Instr. and Meth., 162, (1979), p.539.

12. Hans Kiefer and Rupprecht Maushart, Radiation Protection Measurement, p.56-68, Pergamon Press, 1972.

13. K. Verghese, J. R. Bohannon and A. D. Kowalczuk, Response of BF_3 counters to neutrons in moderate gamma fields, Nucl. Instr. and Meth., 74, (1969), p.355.

14. Glenn F. Knoll, Radiation Detection and Measurement, p.523, John Wiley & Sons, 1979.

15. Ref. 14, p.533, p.567.

16. A. Sayres and M. Coppola, Rev. Sci. Instr., 35, p.469, (1964).

17. S. Izumi and Y. Murata, Nucl. Instr. and Meth., 94, (1971), p.141.

18. T. Tojo and Y. Nakajima, Preparation of thermal neutron scintillators based on a mixture of ZnS(Ag), ^{6}LiF and polyethylene, Nucl. Instr. and Meth., 53, (1967), p.163.

19. F. Mantler-Niederatatter, F. Bensch and F. Grass, An extremely thin scintillation detector for thermal neutrons, Nucl. Instr. and Meth., 142, (1977), p.463.

20. D. R. Johnson, J. H. Thorngate and P. T. Perdue, A sensitive spectrometer for fast neutrons using ^{6}LiI(Eu), Nucl. Instr. and Meth., 75, (1969), p.61.

21. Catalogue for scintillators, semiconductor detectors, nucleonic instruments of Nuclear Enterprises

(G.B) Ltd. 1967

22. J. B. Birks, The Theory and Practice of Scintillation Counting, Pergamon Press, London, 1964.

23. F. D. Brooks, Development of organic scintillators, Nucl. Instr. and Meth., 162, (1979), p.477.

24. J. A. Havey, N. W. Hill, Scintillation detectors for neutron physics research, Nucl. Instr. and Meth., 162, (1979), p.507.

25. Jean Kleior, Elementary mechanism in liquid scintillation counting, Nucl. Instr. and Meth., 112, (1973), p.117.

26. R. L. Craun and D. L. Smith, Analysis of response data for several organic scintillators, Nucl. Instr. and Meth., 80, (1970), p.239.

27. P. B. Lyons, Time response of plastic scintillators, Nucl. Instr. and Meth., 114, (1974), p.313.

28. B. Bengtson and M. Moszywski, Energy-transfer and light-collection characteristics for different types of plastic scintillators, Nucl. Instr. and Meth., 117, (1974), p.227.

29. Ref. (14) , p.246.

30. V. V. Verbinski, W. R. Burrus, T. A. Love, W. Zobel and N. W. Hill, Calibration of an organic scintillator for neutron spectrometry, Nucl. Instr. and Meth., 65, (1968), p.8.

31. M. W. Mcnaughton, F. P. Brady, W. B. Broste, A. L.

Sagle and S. W. Johnson, An investigation of the neutron detection efficiency of a plastic scintillation detector in the energy range 6 to 41MeV, Nucl. Instr. and Meth., 116, (1974), p.25.

32. P. Leleux, P. C. Macq, J. P. Meucders and C. Pirart, Neutron-detector efficiency measurement from 7 to 14MeV, Nucl. Instr. and Meth., 116, (1974), p.41.

33. K. Gul, A study of neutron detection efficiency of an organic scintillation detector through simulation of detection processes, Nucl. Instr. and Meth., 176, (1980), p.549.

34. Victor Fajer and Lilliam Alvarez, Organic scintillator efficiency using a Monte Carlo code, Nucl. Instr. and Meth., 184, (1981), p.515.

35. D. B. Gayther, Flux measurement techniques for white neutron sources, Nuclear Standard Reference Data, IAEA-TECDOC-335, 1985.

36. Ortec catalogue and brochunes (1976 and 1979).

37. Abraham Savitzky and Marcel J. E. Golay, Smoothing and differentiation of data by simplified least squares procedures, Analytical chemistry, Vol36, no.8, p.1627, (1964).

38. Herbert P. Yule, Data convolution and peak location, peak area, and peak energys measurements in scintillation spectrometry, Analytical chemistry, Vol38, no.1, (1966).

39. P. Quittner, Gamma-ray spectroscopy, Adam Hilger Ltd., London, 1972.

40. Wilbert N. Hubin, Basic Programming For Scientists and Engineers, p.82, Preutice-Hall, Inc., 1978.

41. L. M. Bollinger and G. E. Thomas, Measurement of time dependence of scintillation intensity by a delay-coincidence method, The Review of Scientific Instruments, v.32, p.1044, (1969)

42. W. R. Burrus and V. V. Verbinski, fast neutron spectroscopy with thick organic scintillators, Nucl. Instr. and Meth., 67, (1969), p.181.

43. H. W. Broek and C. E. Anderson, The stilbene scintillation crystal as a spectrometer for continuous fast-neutron spectra, The Review of Scientific Instruments, v.31, p.1063, (1960).

44. D. W. Jones and M. E. Toms, A neutron spectrometer using organic scintillators, NRL Report 7324 (1971).

45. J. R. Stehn, M. D. Goldbery, B. A. Magurno, and R. Wiener-Chasman, Neutron Cross Section, BNL325, second edition, supplement2, vol.1, 1964.

46. C. D. Swartz, G. E. Owen and O. Ames, The stilbene scintillation crystal as a neutron spectrometer, AEC Report NYO-2053. (1957).

47. L. S. Chuang, H. K. Wong and K. C. Wong, Absolute

determination of 14MeV neutron spectrum by means of liquid-scintillation spectrometer and threshold foil-detectors, Nucl. Instr. and Meth., 160, (1979), p.487.

48. Edgar A. Lorch, Neutron spectra of $^{241}Am/B$, $^{241}Am/Be$, $^{241}Am/F$, $^{242}Cm/Be$, $^{238}Pu/^{13}C$ and ^{252}Cf isotopic neutron sources, International Journal of Applied Radiation and Isotopes, 24, p.585, (1973).

49. J. Devos, R. Van De Vyver, E. Van Camp, R. Carchon and H. Ferdinande, An absolute recoil-proton photoneutron spectrometer using a Monte Carlo calculated efficiency, Nucl. Instr. and Meth., 135, (1976), p.395.

50. D. Slaughter and R. Strout, II, FLYSPEC : A simple method of unfolding neutron energy spectra measured with NE213 and stilbene spectrometers, Nucl. Instr. and Meth., 198, (1982), p.349.

51. N. A. Lurie, L. Harris, Jr. and J. C. Young, Calculation of gamma-ray response matrix for 5cm NE213 organic scintillation detector, Nucl. Instr. and Meth., 129, (1975), p.543.

52. D. T. Ingersoll and B. W. Wehring, Gamma-ray pulse-height response of an NE213 scintillation detector, Nucl. Instr. and Meth., 147, (1977), p.551.

53. Pradosh K. Ray and Edward S. Kenney, calculation of the gamma ray contribution to proportional recoil counter data

in a mixed neutron-gamma ray field, Nucl. Instr. and Meth., 144, p.579.

54. A. Dupont, G. Giordano, P. Maudrou and M. Neil, Gamma ray scintillator response and unscrambling of pulse height spectra, Nucl. Instr. and Meth., 151, (1978), p.233.

55. S. D. Martin, JR., H. L. Woolverton, R. L. York, S. Nath, K. K. Sekhanran, J. C. Hiebert and L. C. Northcliefe, Measurement and parameterization of the response of NE102 to fast neutrons, Nucl. Instr. and Meth., 185, (1981), p.287.

56. T. J. Gooding and H. G. Pugh, Nucl. Instr. and Meth., 7, (1960), p.189.

57. R. Madey, F. M. Waterman, A. R. Baldwin, J. N. Knudson, J. D. Carlson and J. Rappaport, The response of NE-228A, NE-228, NE-224, and NE-102 scintillators to protons from 2.43 to 19.55 MeV, Nucl. Instr. and Meth., 151, (1978), p.445.

58. J. W. Watson, Finite-size effects in neutron detectors, Nucl. Instr. and Meth., 117, (1974), p.541.

59. L. S. Chuang, K. C. Wong and W. Y. Chiu, Shielding of neutrons generated by a 14 MeV neutron generator installed in the Chinese University of Hong Kong, Journal of Chinese University of Hong Kong, vol.III, No.2, (1975).

60. Wallace, R. et al., The dosimetry of high-energy neutrons produced by 6.2 Bev protons accelerated in the Bevatron, UCRL-9214, (1960). (Figure 6.5 is obtained from ref.(12))

61. H. Kluge, K. Weise, H. W. Zill, Measurement of the spectral distributions of neutrons from radioactive sources and Uranium-235 fission, and the resulting fluence-dose conversion factors, Neutron Monitoring for Radiation Protection Purposes, Vol.1, p.13, IAEA, 1973.

62. 鴻康等編, <数値計算方法>, 国防工業出版社, 1978.

63. E. K. Blum, Numberical Analysis and Computation : Theory and Practice, Addison-Wesley Publishing Company, 1972.

64. Irving Allen Dodes, Numerical Analysis for Computer Science, North-Holland, 1978.